

ABSTRACT

PROCTOR, WILLIAM CYRUS. Elements of High-Order Predictive Model Calibration Algorithms with Applications to Large-Scale Reactor Physics Systems. (Under the direction of Dan Cacuci and Yousry Azmy.)

The inevitable discrepancies between experimental and computational results provide the basic motivation for performing quantitative model verification, validation, and predictive estimation. Loosely speaking, “code verification” addresses the question “are you solving the mathematical model correctly?”, while model validation addresses the question “does the model represent reality?” Ultimately, one aims at obtaining a probabilistic description of possible future outcomes based on all recognized errors and uncertainties, from all steps in the sequence of modeling and simulation processes that leads to a prediction using a computational model. Achieving this goal requires the combination (“assimilation”) of computational and experimental results in order to adjust (“calibrate”) the model parameters for predicting results (“responses”) more accurately – the so-called “best-estimate” results, with smaller uncertainties. The mathematical frameworks for combining experimental and computational quantities are customarily called “data adjustment” (for time-independent reactor physics applications) or “data assimilation” (for time-dependent geophysical applications). Notably, the current state-of-the-art procedures for data adjustment and/or assimilation are restricted to the use of second-order uncertainties (i.e., covariance matrices), and do not have provisions for incorporating response derivatives higher than first-order (in data adjustment procedures) or second-order (in some limited-scope research-versions of data assimilation procedures). Furthermore, neither the data adjustment nor the data assimilation procedures are currently able of computing higher-order moments (e.g., skewness and kurtosis) of the response distribution. In the absence of these higher-order moments of the response distribution, the predicted response distribution must implicitly be assumed as being Gaussian, since it is not possible to quantify the departures, if any, of the predicted responses from the assumed Gaussian distribution.

An important aspect of the novel contributions presented in this dissertation is the de-

velopment of highly parallel and scalable algorithms for application of data adjustment and assimilation to large (peta)-scale systems, thereby significantly extending the practical feasibility and applicability of predictive model calibration activities. These new algorithms also include mathematical verification procedures for identifying non-physical covariance matrices, as well as quantifying the consistency of computational and experimental information. Furthermore, the dissertation presents expressions for computing the skewness and kurtosis of response distributions, to be used for quantifying non-Gaussian features of computed response distributions. A novel method, using adjoint functions, for computing very efficiently second-order mixed derivatives of responses to parameters, is also presented in this work.

The significant impact of the above algorithmic advances is demonstrated by using the neutron transport code Denovo, a highly parallel (one the order of tens of thousands of processors) code that runs on ORNL's leadership-class computer Jaguar, in conjunction with experimental results from the Lady Godiva and Jezebel benchmarks, as well as the "LEU-COMP-THERM-008" (shorthand: LCT) assembly. We recall here that the Lady Godiva benchmark is a bare sphere containing 94 wt% ^{235}U , Jezebel is a critical assembly containing ^{239}Pu , and the LCT assembly models a 3×3 array of Pressurized Water Reactor fuel assemblies comprising 4808 fuel rods and 153 water holes. Noteworthy new results in this dissertation are also obtained by using the remarkable efficiency of the "adjoint sensitivity analysis procedure for operator-type responses", originally developed by Cacuci in 1981, to compute the sensitivities (derivatives) of the spatially dependent (as opposed to point-values of) neutron fluxes to cross sections.

The results obtained in this work represent first-of-a-kind computations of response skewness and kurtosis, thus enabling a quantitative assessment of non-Gaussian features of predicted responses (results). In particular, the illustrative results presented for the Godiva, Jezebel, and LCT benchmarks show that the response skewness and kurtosis are relatively small, thus quantitatively confirming the intuitive feeling (based on the presumed applicability of the central limit theorem) that simple reactor physics problems involving small cross section uncertainties tend to produce reaction rate responses that are nearly normally distributed. Finally, yet

importantly, the algorithmic advances and results presented in this dissertation represent a fundamental first step towards developing a high-order predictive model calibration procedure capable of Bayesian combination of non-Gaussian model parameter features with non-Gaussian experimental distributions. Such developments are currently underway, and their successful completion is expected to enable more accurate predictions of “best-estimate results” including corresponding predicted non-Gaussian features, for large (peta- and exa-) scale systems.

© Copyright 2012 by William Cyrus Proctor

All Rights Reserved

Elements of High-Order Predictive Model Calibration
Algorithms with Applications to Large-Scale
Reactor Physics Systems

by
William Cyrus Proctor

A dissertation submitted to the Graduate Faculty of
North Carolina State University
in partial fulfillment of the
requirements for the Degree of
Doctor of Philosophy

Nuclear Engineering

Raleigh, North Carolina

2012

APPROVED BY:

Paul Turinsky

Ralph Smith

Dan Cacuci
Co-chair of Advisory Committee

Yousry Azmy
Co-chair of Advisory Committee

DEDICATION

“Trust yourself. You know more than you think.”

–Fortune Cookie

BIOGRAPHY

William Cyrus Proctor was born July 9, 1985 in Asheville, North Carolina to Bill Proctor and Debby Smith. He attended A. C. Reynolds Middle and High School until 2003 where he moved to North Carolina State University to pursue an undergraduate career in Nuclear Engineering and Physics. Upon graduation in 2007 he continued on, obtaining a Nuclear Engineering Master of Science degree in 2010.

ACKNOWLEDGEMENTS

It is to you, the reader, which I give my first acknowledgements to. For, it is because of the few who continue to read on that truly makes this composition worthwhile. May you find some small measure of meaning from the collection of words and numbers written below.

I am very grateful to have crossed paths with you Dr. Cacuci. Your guidance and direction have made these years a pleasure. I look forward our future endeavours together.

To Drs. Azmy, Mattingly, Smith and Turinsky; who have graciously taken time out of their schedules to read, review and solidify this work, your thoughts and inputs are greatly appreciated.

To Todd and Christine, you all were the ones down in the trenches with me. It's always been a pleasure working as a group and I owe both of you thanks for your time and efforts making this work possible.

To my friends and colleagues, I give collective thanks. Without sounding boards for thoughts and ideas or without those times to distract me, this work would not be what it is. I'm going to miss my time here in Raleigh with you all but I will never forget the memories.

To my parents, thank you. It is because of both you that I am here today. You give me strength and wisdom in ways you cannot know. I am very grateful to be able to share this moment with both of you.

TABLE OF CONTENTS

List of Tables	vii
List of Figures	viii
Chapter 1 Introduction	1
Chapter 2 A Priori Covariance Verification Steps for First-Order Predictive Model Calibration	10
2.1 Background	10
2.2 Necessary Conditions for Bona Fide Covariance Matrices	18
2.2.1 Definitions	18
2.2.2 Symmetric Positive Definiteness	18
2.2.3 Physical Correlations	19
2.3 Parameter Covariance Consistency Verification	20
2.4 Evaluation of SCALE Covariance Matrices	21
2.4.1 Covariance Data Hierarchy	21
2.4.2 Specific Tests Conducted on Covariance Matrices	23
2.4.2.1 Symmetry	23
2.4.2.2 Non-physical Correlations	23
2.4.2.3 Relative Standard Deviation Consistency	23
2.4.2.4 Positive Definiteness	24
2.4.2.5 Singular Value Decomposition	24
2.4.3 Summary of Results	24
Chapter 3 Optimized Responses & Parameters Following Data Assimilation	27
3.1 Computational Framework	27
3.1.1 Denovo	27
3.1.1.1 Overview	27
3.1.1.2 Adjoint Sensitivity Analysis	29
3.1.2 best_pred	33
3.1.2.1 Overview	33
3.1.2.2 Code Inputs	34
3.1.2.3 Computed Matrices/Vectors	35
3.1.3 Lemon	35
3.1.3.1 Overview	35
3.2 Applications	36
3.2.1 Godiva	36
3.2.1.1 Benchmark Description	36
3.2.1.2 Computation of the Space-Dependent Neutron Flux Sensitivities	39
3.2.1.3 Sensitivities of the Normalized Space-Dependent Flux	43
3.2.1.4 Calibration Results	48

3.2.2	Jezebel	52
3.2.2.1	Benchmark Description	52
3.2.2.2	Calibration Results	55
3.2.3	LEU-COMP-THERM-008	59
3.2.3.1	Benchmark Description	59
3.2.3.2	Calibration Results	64
Chapter 4 Higher-Order Moments for Quantifying Non-Gaussian Response		
	Features	74
4.1	Mathematical Expressions	74
4.1.1	Expectation Value	75
4.1.2	Variance-Covariance	76
4.1.3	Skewness	80
4.1.4	Kurtosis	81
4.2	Higher-Order Computed Response Moments: Applications	83
4.2.1	Computational Framework	83
4.2.2	Results	86
4.2.2.1	Partial Standard Deviations and Sensitivities	86
4.2.2.2	Higher-Order Moments	96
Chapter 5 Conclusions & Outlook		109
References		114
Appendices		117
Appendix A KENO Input Specifications		118
A.1	Godiva	118
A.2	Jezebel	120
A.3	LEU-THERM-COMP-008	122
Appendix B Detailed Higher Order Derivations		135
B.1	Third Central Moment	135
B.2	Fourth Central Moment	146

LIST OF TABLES

Table 2.1	Experimental Benchmarks Input Parameter Covariance Matrix Dimensions	26
Table 3.1	Godiva Composition	37
Table 3.2	Godiva Experimentally Measured Results	39
Table 3.3	Godiva Best-Estimate Results	49
Table 3.4	Jezebel Composition	52
Table 3.5	Jezebel Atomic Densities	54
Table 3.6	Jezebel Experimentally Measured Results	54
Table 3.7	Jezebel Best-Estimate Results	56
Table 3.8	LCT Atom Densities	62
Table 3.9	LCT Best-Estimate Results	71
Table 4.1	Godiva c_{ii}^k Rankings	90
Table 4.2	Godiva c_{ii}^k Rankings	90
Table 4.3	Jezebel c_{ii}^k Rankings	91
Table 4.4	Jezebel c_{ii}^k Rankings	91
Table 4.5	Godiva $\mathbf{r}_{(U233)}$ First- and Second-Order Sensitivities	92
Table 4.6	Godiva $\mathbf{r}_{(U238)}$ First- and Second-Order Sensitivities	92
Table 4.7	Godiva $\mathbf{r}_{(Np237)}$ First- and Second-Order Sensitivities	93
Table 4.8	Godiva $\mathbf{r}_{(Pu239)}$ First- and Second-Order Sensitivities	93
Table 4.9	Jezebel $\mathbf{r}_{(U233)}$ First- and Second-Order Sensitivities	94
Table 4.10	Jezebel $\mathbf{r}_{(U238)}$ First- and Second-Order Sensitivities	94
Table 4.11	Jezebel $\mathbf{r}_{(Np237)}$ First- and Second-Order Sensitivities	95
Table 4.12	Jezebel $\mathbf{r}_{(Pu239)}$ First- and Second-Order Sensitivities	95
Table 4.13	Number (\mathbf{n}_α) of Second-Order Derivatives Computed	97
Table 4.14	Godiva Computed Responses and Expectation Values	97
Table 4.15	Jezebel Computed Responses and Expectation Values	98
Table 4.16	Godiva First-Order Computed Response Covariance Matrix	98
Table 4.17	Godiva Second-Order Computed Response Covariance Matrix	98
Table 4.18	Jezebel First-Order Computed Response Covariance Matrix	99
Table 4.19	Jezebel Second-Order Computed Response Covariance Matrix	99
Table 4.20	Godiva Skewness and Excess Kurtosis Values	99
Table 4.21	Jezebel Skewness and Excess Kurtosis Values	99

LIST OF FIGURES

Figure 3.1	^{235}U Godiva Assembly	38
Figure 3.2	Godiva Representative Operator-Type Response Result	46
Figure 3.3	Godiva Representative Operator-Type Response Error	47
Figure 3.4	Godiva First-Order Optimization Results	50
Figure 3.5	Godiva First-Order Relative Sensitivities	51
Figure 3.6	^{239}Pu Jezebel Assembly	53
Figure 3.7	Jezebel First-Order Optimization Results	57
Figure 3.8	Jezebel First-Order Relative Sensitivities	58
Figure 3.9	LCT Core Configuration.	60
Figure 3.10	LCT Axial Dimensions	61
Figure 3.11	LCT Central Assembly Pin Numbering	63
Figure 3.12	LCT Central Assembly Experimental Measurements	64
Figure 3.13	LCT Axial $z = 0$ Normalized Fission Reaction Rate	66
Figure 3.14	LCT Axial $z = 0$ Relative Rod-by-Rod Power Densities	67
Figure 3.15	LCT Computed vs. Measured Responses	68
Figure 3.16	LCT Denovo Computed vs. MCNP Computed Responses	69
Figure 3.17	LCT First-Order Optimization Results	72
Figure 3.18	LCT First-Order Relative Sensitivities	73
Figure 4.1	Skewness	80
Figure 4.2	Kurtosis	82
Figure 4.3	Godiva and Jezebel c_{ii}^k Rankings	88
Figure 4.4	Godiva and Jezebel c_{ii}^k Rankings (Zoom)	89
Figure 4.5	Godiva Normalized Expectation Values	101
Figure 4.6	Jezebel Normalized Expectation Values	102
Figure 4.7	Godiva Normalized Variances	103
Figure 4.8	Jezebel Normalized Variances	104
Figure 4.9	Godiva Skewness	105
Figure 4.10	Jezebel Skewness	106
Figure 4.11	Godiva Excess Kurtosis	107
Figure 4.12	Jezebel Excess Kurtosis	108

Chapter 1

Introduction

Repeated measurements of the same physical quantity yield values that differ from each other, as well as from the true but unknown value of that quantity. Such variations in results stem from a variety of causes, including experimental errors, imperfect instruments, and imperfectly known calibration standards. Hence, around any reported experimental value, there always exists a range of values that may also be plausibly representative of the true value. Thus, since the true value of physical quantities cannot be measured exactly, nominally measured values are insufficient by themselves for applications; the quantitative uncertainties accompanying the measurements are also needed, along with the respective nominal values.

Models of complex physical systems usually involve two distinct sources of uncertainties, namely: (i) stochastic uncertainty, which arises because the system under investigation can behave in many different ways, and (ii) subjective or epistemic uncertainty, which arises from the inability to specify an exact value for a parameter that is assumed to have a constant value in the respective investigation. Epistemic (or subjective) uncertainties characterize a degree of belief regarding the location of the appropriate value of each parameter. In turn, these subjective uncertainties lead to subjective uncertainties for the response, thus reflecting a corresponding degree of belief regarding the location of the appropriate response values as the outcome of analyzing the model under consideration. A typical example of a complex

system that involves both stochastic and epistemic uncertainties is a nuclear reactor power plant: in a typical risk analysis of a nuclear power plant, stochastic uncertainty arises due to the hypothetical accident scenarios which are considered in the respective risk analysis, while epistemic uncertainties arise because of uncertain parameters that underlie the estimation of the probabilities and consequences of the respective hypothetical accident scenarios.

Quantifying uncertainties in experimental and/or computational results is the goal of uncertainty analysis. Achieving this goal requires a weighted propagation of the uncertainties afflicting the parameters that influence the result (or response) of interest. This influence is quantitatively measured by the so called sensitivities of the results (or response) to the respective parameters. The procedures for quantifying response sensitivities to parameters fall within the scope of sensitivity analysis. Sensitivity and uncertainty analysis procedures can be either local or global in scope. The objective of local analysis is to analyze the behavior of the system response locally around a chosen point (for static systems) or chosen trajectory (for dynamical systems) in the combined phase space of parameters and state variables. On the other hand, the objective of global analysis is to determine all of the system's critical points (bifurcations, turning points, response maxima, minima, and/or saddle points) in the combined phase space formed by the parameters and dependent (state) variables, and subsequently analyze these critical points by local sensitivity and uncertainty analysis. The methods for sensitivity and uncertainty analysis are based on either statistical or deterministic procedures. In principle, both types of procedures can be used for either local or for global sensitivity and uncertainty analysis, although, in practice, deterministic methods are used mostly for local analysis while statistical methods are used for both local and global analysis.

Sensitivity and uncertainty analysis are becoming increasingly widespread in many fields of engineering and sciences, as diverse as nuclear and chemical engineering, econometric modeling, electrical engineering, atmospheric and geophysical sciences, encompassing practically all of the experimental data processing activities as well as many computational modeling and process simulation activities. There are many methods, based either on deterministic or statistical

concepts, for performing sensitivity and uncertainty analysis. However, despite this variety of methods, or perhaps because of it, a precise, unified terminology, across all methods, does not seem to exist yet, even though many of the same words are used by the practitioners of the various methods. For example, even the word sensitivity as used by analysts employing statistical methods may not necessarily mean or refer to the same quantity as would be described by the same word, sensitivity, when used by analysts employing deterministic methods. Care must be therefore exercised, since identical words may not necessarily describe identical quantities, particularly when comparing deterministic to statistical methods. Furthermore, conflicting and contradictory claims are often made about the relative strengths and weaknesses of the various methods.

Extracting “best-estimate” values together with “best-estimate” uncertainties from often sparse, incomplete, error-afflicted, and occasionally discrepant experimental data requires a wide range of probability-theory concepts and tools, from deductive statistics involving mainly frequencies and sample tallies to inductive inference for assimilating non-frequency data and a priori knowledge. In general, the uncertainties in computational results arise from several distinct causes, the most usual being: (i) the adequacy or inadequacy of the mathematical equations to model the actual phenomenon may give rise modeling uncertainties; (ii) the numerical methods used to solve the model’s equation also give rise to uncertainties and (iii) the data and parameters in a model give rise to parameter uncertainties.

The discrepancies between experimental and computational results provide the basic motivation for performing quantitative model verification, validation, qualification and predictive estimation. Loosely speaking, “code verification” means “are you solving the mathematical model correctly?” Code verification involves activities that are related to software quality assurance (SQA) practices and to activities directed toward finding and removing deficiencies in numerical algorithms used to solve partial differential equations (PDEs). SQA procedures are needed during software development and modification, as well as during production computing. SQA procedures are well developed in general, but areas of improvement are needed with regard

to software operating on massively parallel computer systems. Numerical algorithm verification addresses the software reliability of the implementation of all the numerical algorithms that affect the numerical accuracy of solutions produced by the code. Numerical algorithm verification is conducted by comparing computational solutions with benchmark solutions: analytical solutions, manufactured solutions, and highly accurate numerical solutions. Solution verification, also called numerical error estimation, deals with the quantitative estimation of the numerical accuracy obtained when PDEs are solved using discretization methods. The primary goal in solution verification is the estimation of the numerical accuracy of all of the solution quantities of interest in a given simulation. Solution verification is related to the topic of adaptive mesh refinement (AMR), although the goals of AMR are more restrictive than those of solution verification. The discretization errors must be quantified in order to separate them, in principle, from other error and uncertainty sources, such as physics modeling errors and variability in physical properties. Two major shortcomings affect current verification methods, namely: (i) estimating discretization errors using solutions on multiple mesh resolutions is a computationally expensive process, and (ii) current methods for complex physics simulations are not robust.

Loosely speaking, model validation means “does the model represent reality?” Model validation emphasizes the quantitative assessment of computational model accuracy by comparison with high-quality validation experiments; that is, experiments that are well characterized in terms of measurement and documentation of all the input quantities needed for the computational model, as well as carefully estimated and documented experimental measurement uncertainty. These validation experiments can be conducted on hardware that represents any level of simplification or disassembly of the actual, or complete, system of interest (for example, even experiments conducted on simple geometries with only one element of physics occurring). The state-of-the-art in model validation addresses issues of (a) assessing model accuracy when several system response quantities have been measured and compared; and (b) comparing system response quantities from multiple realizations of the experiment with computational results

that are characterized by probability distributions.

Predictive estimation (PE) aims at providing a probabilistic description of possible future outcomes based on all recognized errors and uncertainties, from all steps in the sequence of modeling and simulation processes that leads to a prediction using a computational model. Typical uncertainties include: (a) data error or uncertainty (input data such as cross sections, model parameters such as reaction-rate coefficients, initial conditions, boundary conditions, and forcing functions such as external loading), (b) numerical discretization error, and (c) uncertainty (e.g., lack of knowledge) in physics processes being modeled. The result of the PE analysis is a probabilistic description of possible future outcomes based on all recognized errors and uncertainties. Predictive estimation for computer experiments has three key elements; namely model calibration, model extrapolation, and estimation of the validation domain. Model calibration addresses the integration of experimental data for the purpose of updating the data of the computer model. Important components include the estimation of discrepancies in the data, and more important, estimation of the biases between model predictions and experimental data. The mathematical framework for model calibration is provided by the data adjustment and data assimilation procedures, which encompass the propagation of all relevant uncertainties, including: (i) data uncertainties (in input data, model parameters, initial and boundary conditions, forcing functions, etc.); (ii) numerical discretization errors; (iii) discrepancies within the experimental data and/or discrepancies between data and model predictions; (iv) uncertainties in the physics of the modeled processes (e.g., due to incomplete knowledge). The state-of-the-art of calibration of models is fairly well developed, but current methods are still hampered in practice by the significant computational effort required; alternative methods for reducing the computational effort are of great interest, and methods based on adjoint models show great promise in this regard.

Model extrapolation addresses the prediction uncertainty in new environments or conditions of interest, including both untested parts of the parameter space and higher levels of system complexity in the validation hierarchy. Extrapolation of models and the resulting increase of

uncertainty are poorly understood, particularly the estimation of uncertainty that results from nonlinear coupling of two or more physical phenomena that were not coupled in the existing validation database.

Perhaps the earliest systematic activities on data assimilation were initiated in Europe by Cecchini et al. [12], in Israel by Humi et al. [23], and in the former Soviet Union by Usachhev [36], in the course of evaluating neutron cross sections by using time-independent reactor physics experiments for measuring “integral quantities” (also called “system responses”) such as reaction rates and multiplication factors. A decade later, these activities had reached conceptual maturity under the name of “cross-section adjustment” (see, e.g. Refs. [34] and [19]), which essentially amounted to using a weighted least-square procedure (with response sensitivities as weighting functions) for combining uncertainties in the model parameters with uncertainties in the experimental data, subject to the constraint imposed by the linearized model. The resulting “adjusted” parameters and their “adjusted” uncertainties were then employed in the respective core neutronics model to predict better results (reaction rates, multiplication factors, Doppler coefficients) in an extended application domain (e.g., a new or improved reactor core design). By the late-1970s, the first-order response sensitivities, which appeared as weighting functions in the least squares adjustment procedure, were efficiently computed using adjoint neutron fluxes, as typified by the works of Kuroi and Mitani [26], Dragt et al [14], and Weisbin et al. [37]. It is important to note that all of these works dealt with the time-independent linear neutron transport or diffusion equation, as encountered in reactor physics and shielding, for which the corresponding adjoint equations were already known and readily available. For nonlinear, time-dependent or stationary problems, the adjoint method for computing efficiently sensitivities was generally formulated in 1981 by Cacuci [6, 7], while the first general formulation of a data adjustment methodology for time-dependent nonlinear problems was presented in 1982 by Barhen et al. [2]. Regrettably, this advanced (for its time) data adjustment methodology stagnated in the field of nuclear engineering since 1982 and apparently failed to influence other scientific fields.

In the late 1980s and during the 1990s, the fundamental concepts underlying “data adjustment” seem to have been rediscovered while developing the so-called “data assimilation” procedure in the geophysical sciences, in that the concepts underlying data assimilation are the same as those underlying the (much older) “data adjustment” procedure. Since then, well over a thousand works on data assimilation have been published in the geophysical sciences alone, obviously too numerous to cite extensively here; representative works can be found cited in the books by Lewis et al. [29], Lahoz et al. [27], and Cacuci et al. [11].

Cacuci and Ionescu-Bujor [10] have recently published a comprehensive mathematical methodology for best-estimate predictions following the assimilation of experimental data and simultaneous calibration of model parameters and responses, for large-scale nonlinear time-dependent systems. This methodology generalizes and significantly extends the results customarily used in nuclear engineering as well as those underlying the so-called 4D- VAR data assimilation procedures in the geophysical sciences [29, 27, 11].

This methodology also provides a quantitative indicator constructed from sensitivity and covariance matrices for determining the consistency (agreement or disagreement) among the a priori computational and experimental data (parameters and responses). Once the inconsistent data, if any, is discarded, the methodology by Cacuci and Ionescu-Bujor [10] yields best-estimate values for parameters and predicted responses, as well as best-estimate reduced uncertainties (i.e., “smaller” values for the variance-covariance matrices) for the predicted best-estimate parameters and responses.

The dissertation is structured into five main chapters, including two appendices. Chapter 2 presents the mathematical framework for data assimilation and simultaneous calibration of model parameters and responses, for a time-independent physical system. All theory in this chapter is based on the NS&E article by Cacuci and Ionescu-Bujor [10] which is generalized for a time-dependent physical system. The data assimilation and best-estimate model calibration methodology presented in Chapter 2 also includes quantitative indicator (based on uncertainties and sensitivities) for determining the degree of agreement (or disagreement) relevant to the

assimilation and best-estimate adjustment of parameters and responses, of computations and experiments. Following the mathematical framework, the main features of a systematic procedure for verifying the consistency for any general covariance matrix are outlined. A matrix must be symmetric positive definite to truly be considered a physically meaningful variance-covariance matrix. It is a corollary of the Cauchy-Schwarz inequality that the correlation between any two quantities cannot exceed 1 in absolute value. Lastly, a specific evaluation is carried out and reported for the model parameter covariance matrices, which utilize ORNL's SCALE cross section information, that are relevant to the work presented in later chapters.

Chapter 3 begins with the introduction of several of the computational tools used throughout this work. Attention is given to the leadership-class code Denovo [16] and the recently implemented sensitivity analysis module by R. T. Evans [15] from which this work is possible. Two other tools, developed in-house, specifically for the demonstration of the mathematical frameworks presented in Chapters 2 and 4, are described for use with massively parallel computer architectures including ORNL's Jaguar. Applications of best-estimate model calibration, including the exercise of the previously described quantitative indicator are demonstrated with three different benchmark systems from the International Handbook of Evaluated Criticality Safety Benchmark Experiments [4]; namely the Lady Godiva, Jezebel and LEU-THERM-COMP-008 benchmarks. Each system is thoroughly detailed before individual model calibration results are presented along with representative first-order sensitivity information. Furthermore, the Lady Godiva benchmark was used as demonstration for the efficient computation of spatially-dependent sensitivities via the "adjoint sensitivity analysis procedure for operator-type responses" as discussed in [8].

Chapter 4, entitled "Higher-Order Moments for Quantifying non-Gaussian Response Features", commences with the derivation of expressions for the response skewness and kurtosis, taking into account the second-order mixed-derivatives of the response with respect to parameters, as well as the first four parameter moments. Skewness is a measure of the asymmetry of a probability distribution, while the kurtosis measures the "peakedness" of a probability dis-

tribution when compared with the corresponding Normal distribution. To efficiently compute the second-order mixed-derivatives, a novel method by Cacuci is presented utilizing adjoint functions. This method reduces the number of computations from the previous methods (see [18, 20]) which are on the order of the number of parameters squared, to on the order of the number of parameters, or less, depending on the nonlinearity of the system. Next, the benchmark systems, Godiva and Jezebel are exercised with this new framework. Results for the higher-order moments confirm the expectation that these models should behave nearly linear with respect to the chosen responses.

Lastly, Chapter 5 offers concluding remarks, addressing further work needed to alleviate the current limitations of the best-estimate predictive methodology presented in this work.

Chapter 2

A Priori Covariance Verification Steps for First-Order Predictive Model Calibration

2.1 Background

All theory in this chapter is based on the Nuclear Science and Engineering article by Cacuci and Ionescu-Bujor [10].

A physical system where indirect experimental measurements may be taken can be modeled in terms of

- a system of linear and/or nonlinear equations that relate the system's independent and dependent variables
- (in)equality constraints that bound the range of the system's parameters
- usually several output responses of interest computed by the model
- experimentally measured responses (mean and covariances)

In general, this mathematical framework can and has been written for time-dependent systems. In this work, only time-independent systems have been considered such that the following notation will be simplified to reflect this.

The time-independent physical system to be analyzed in this chapter comprises of N_α model parameters and N_r distinct responses. Hence, the column vector $\boldsymbol{\alpha}$ of system parameters and the vector \boldsymbol{r}^m of experimentally measured responses may be shown in component form as

$$\begin{aligned}\boldsymbol{\alpha} &\equiv (\alpha_1, \alpha_2, \dots, \alpha_i, \dots, \alpha_{N_\alpha})^T, \\ \boldsymbol{r} &\equiv (r_1, r_2, \dots, r_k, \dots, r_{N_r})^T.\end{aligned}\tag{2.1}$$

The system parameters are considered variates with mean values $\boldsymbol{\alpha}^0$. The covariance between two parameters α_i and α_j are written as

$$(\mathbf{C}_\alpha)_{ij} \equiv E([\alpha_i - \alpha_i^0][\alpha_j - \alpha_j^0]),\tag{2.2}$$

where $E(\cdot)$ denotes the expectation value. These covariances constitute elements of the symmetric covariance matrix of the form

$$\mathbf{C}_\alpha \equiv E([\boldsymbol{\alpha} - \boldsymbol{\alpha}^0][\boldsymbol{\alpha} - \boldsymbol{\alpha}^0]^T) = \mathbf{C}_\alpha^T.\tag{2.3}$$

In a similar fashion, the measured responses are characterized by mean values \boldsymbol{r}^m and by the symmetric covariance matrix

$$\mathbf{C}_m \equiv E([\boldsymbol{r} - \boldsymbol{r}^m][\boldsymbol{r} - \boldsymbol{r}^m]^T) = \mathbf{C}_m^T.\tag{2.4}$$

Generally speaking, the measured responses may be correlated to the input parameters by the (often rectangular) response-parameter uncertainty matrix

$$\mathbf{C}_{\alpha r} \equiv E([\boldsymbol{\alpha} - \boldsymbol{\alpha}^0][\boldsymbol{r} - \boldsymbol{r}^m]^T).\tag{2.5}$$

In general, a response computed using the model can depend nonlinearly and implicitly on the model parameters. Uncertainties due to parameters induce uncertainties in the responses which, in this case, can be computed deterministically using propagation of moments method. The computed response is linearized via a functional Taylor-series expansion around the nominal parameter values $\boldsymbol{\alpha}^0$ as

$$\mathbf{r}(\boldsymbol{\alpha}) = \mathbf{R}(\boldsymbol{\alpha}^0) + \mathbf{S}(\boldsymbol{\alpha} - \boldsymbol{\alpha}^0) + \dots, \quad (2.6)$$

where $\mathbf{R}(\boldsymbol{\alpha}^0)$ represents the vector of computed responses at the nominal parameter values $\boldsymbol{\alpha}^0$ and \mathbf{S} denotes $N_r \times N_\alpha$ dimensional matrix containing the first Gâteaux derivatives of the computed responses with respect to the parameters

$$\mathbf{S} \equiv \begin{pmatrix} \frac{\partial R_1(\boldsymbol{\alpha}^0)}{\partial \alpha_1} & \dots & \frac{\partial R_1(\boldsymbol{\alpha}^0)}{\partial \alpha_{N_\alpha}} \\ \vdots & \frac{\partial R_k(\boldsymbol{\alpha}^0)}{\partial \alpha_i} & \vdots \\ \frac{\partial R_m(\boldsymbol{\alpha}^0)}{\partial \alpha_1} & \dots & \frac{\partial R_m(\boldsymbol{\alpha}^0)}{\partial \alpha_{N_\alpha}} \end{pmatrix}. \quad (2.7)$$

The expectation value, $E(\mathbf{r})$, is computed by integrating the expansion of the responses over the unknown joint probability distribution $p(\boldsymbol{\alpha}, \mathbf{r})$

$$E(\mathbf{r}) = \int_{D_\alpha} \mathbf{r}(\boldsymbol{\alpha}) p(\boldsymbol{\alpha}, \mathbf{r}) d\boldsymbol{\alpha}, \quad (2.8)$$

where D_α is simply the domain of all α values. Substituting in the first-order Taylor expansion yields

$$E(\mathbf{r}) = \int_{D_\alpha} \mathbf{R}(\boldsymbol{\alpha}^0) p(\boldsymbol{\alpha}, \mathbf{r}) d\boldsymbol{\alpha} + \int_{D_\alpha} \sum_{i_1=1}^{N_\alpha} \frac{\partial \mathbf{R}}{\partial \alpha_{i_1}} \Big|_{\boldsymbol{\alpha}^0} \delta \alpha_{i_1} p(\boldsymbol{\alpha}, \mathbf{r}) d\boldsymbol{\alpha}.$$

Pulling terms independent of $\boldsymbol{\alpha}$ out of the integrals gives

$$E(\mathbf{r}) = \mathbf{R}(\boldsymbol{\alpha}^0) \int_{D_\alpha} p(\boldsymbol{\alpha}, \mathbf{r}) d\boldsymbol{\alpha} + \sum_{i_1=1}^{N_\alpha} \frac{\partial \mathbf{R}}{\partial \alpha_{i_1}} \Big|_{\boldsymbol{\alpha}^0} \int_{D_\alpha} \delta \alpha_{i_1} p(\boldsymbol{\alpha}, \mathbf{r}) d\boldsymbol{\alpha}.$$

The integrand in the first term integrates to 1 as $p(\boldsymbol{\alpha}, \mathbf{r})$ is a probability distribution. The integrand in the second term is the first central moment which is identically zero. Thus, the expectation value is

$$E(\mathbf{r}) = \mathbf{R}(\boldsymbol{\alpha}^0). \quad (2.9)$$

The corresponding computed responses covariance matrix may be obtained by computing

$$\begin{aligned} \mathbf{C}_{rc}(\boldsymbol{\alpha}^0) &\equiv E\left([\mathbf{r}(\boldsymbol{\alpha}) - \mathbf{R}(\boldsymbol{\alpha}^0)] [\mathbf{r}(\boldsymbol{\alpha}) - \mathbf{R}(\boldsymbol{\alpha}^0)]^T\right) \\ &= [\mathbf{S}(\boldsymbol{\alpha}^0)] E\left([\boldsymbol{\alpha} - \boldsymbol{\alpha}^0] [\boldsymbol{\alpha} - \boldsymbol{\alpha}^0]^T\right) [\mathbf{S}(\boldsymbol{\alpha}^0)]^T \\ &= [\mathbf{S}(\boldsymbol{\alpha}^0)] \mathbf{C}_\alpha [\mathbf{S}(\boldsymbol{\alpha}^0)]^T. \end{aligned} \quad (2.10)$$

Applying the maximum entropy algorithm described in [10], to the computational and experimental information described previously indicates the most objective probability distribution for this information is a multivariate Gaussian of the form

$$p(\mathbf{z}|\mathbf{C})d\mathbf{z} = \frac{e^{-\frac{1}{2}Q(\mathbf{z})}}{|2\pi\mathbf{C}|^{\frac{1}{2}}}d\mathbf{z}, \quad (2.11)$$

where

$$Q(\mathbf{z}) \equiv \mathbf{z}^T \mathbf{C}^{-1} \mathbf{z}; \quad -\infty < z_j < \infty, \quad (2.12)$$

$$\mathbf{z} = \begin{pmatrix} \boldsymbol{\alpha} - \boldsymbol{\alpha}^0 \\ \mathbf{r} - \mathbf{r}^m \end{pmatrix}, \quad (2.13)$$

$$\mathbf{C} = \begin{pmatrix} \mathbf{C}_\alpha & \mathbf{C}_{\alpha r} \\ \mathbf{C}_{\alpha r}^T & \mathbf{C}_m \end{pmatrix}. \quad (2.14)$$

If no specific loss function is provided, the recommended best-estimate mean vector \mathbf{z}^{BE} and its respective best-estimate posterior covariance matrix are usually evaluated assuming quadratic loss. The bulk of the contribution in Eq. 2.12 is extracted by computing it at the point where the Q attains a minimum subject to Eq. 2.6. When higher-order terms as well as

numerical errors are neglected this relation can be conveniently written in the form

$$\mathbf{Z}(\boldsymbol{\alpha}^0)\mathbf{z} + \mathbf{d} = 0, \quad (2.15)$$

where

$$\mathbf{d} \equiv \mathbf{R}(\boldsymbol{\alpha}^0) - \mathbf{r}^m, \quad (2.16)$$

and \mathbf{Z} denotes the partitioned matrix

$$\mathbf{Z} \equiv (\mathbf{S} \ \mathbf{I}), \quad (2.17)$$

where \mathbf{I} is a $\mathbf{N}_r \times \mathbf{N}_r$ identity matrix. The minimum point of $Q(\mathbf{z})$ subject to Eq. 2.15 is a constrained minimization problem that may be solved by introducing Lagrange multipliers $\boldsymbol{\lambda}$ to construct an augmented functional

$$P(\mathbf{z}, \boldsymbol{\lambda}) \equiv Q(\mathbf{z}) + 2\boldsymbol{\lambda}^T [\mathbf{Z}(\boldsymbol{\alpha}^0)\mathbf{z} + \mathbf{d}] = \min,$$

at

$$\mathbf{z} = \mathbf{z}^{BE} \equiv \begin{pmatrix} \boldsymbol{\alpha}^{BE} - \boldsymbol{\alpha}^0 \\ \mathbf{r}^{BE} - \mathbf{r}^m \end{pmatrix}. \quad (2.18)$$

Where the functional $P(\mathbf{z}, \boldsymbol{\lambda})$ reaches its minimum may be found through the conditions

$$\nabla_{\mathbf{z}}P(\mathbf{z}, \boldsymbol{\lambda}) = 0, \quad \nabla_{\boldsymbol{\lambda}}P(\mathbf{z}, \boldsymbol{\lambda}) = 0, \quad \text{at } \mathbf{z} = \mathbf{z}^{BE}. \quad (2.19)$$

The solution to the constrained minimization problem is detailed in the Appendix of [10]. The resulting best-estimate parameters, responses and reduced uncertainties covariance matrices are detailed below:

1. The best-estimate predicted nominal values for the calibrated parameters:

$$\boldsymbol{\alpha}^{BE} = \boldsymbol{\alpha}^0 + \left(\mathbf{C}_{\alpha r} - \mathbf{C}_{\alpha} [\mathbf{S}(\boldsymbol{\alpha}^0)]^T \right) \mathbf{C}_d^{-1} \mathbf{d}, \quad (2.20)$$

where the deviation-vector uncertainty matrix is defined as

$$\begin{aligned} \mathbf{C}_d &\equiv E(\mathbf{d}\mathbf{d}^T) \\ &= \mathbf{C}_{rc}(\boldsymbol{\alpha}^0) - \mathbf{C}_{\alpha r}^T [\mathbf{S}(\boldsymbol{\alpha}^0)]^T - [\mathbf{S}(\boldsymbol{\alpha}^0)]^T \mathbf{C}_{\alpha r} + \mathbf{C}_m. \end{aligned} \quad (2.21)$$

2. The best-estimate predicted nominal values for the calibrated responses:

$$\mathbf{r}(\boldsymbol{\alpha}^{BE}) = \mathbf{r}^m + \left(\mathbf{C}_m - \mathbf{C}_{\alpha r}^T [\mathbf{S}(\boldsymbol{\alpha}^0)]^T \right) \mathbf{C}_d^{-1} \mathbf{d}. \quad (2.22)$$

3. The best-estimate predicted covariances \mathbf{C}_{α}^{BE} and \mathbf{C}_r^{BE} , corresponding to the best-estimate parameters $\boldsymbol{\alpha}^{BE}$ and responses $\mathbf{r}(\boldsymbol{\alpha}^{BE})$, together with the predicted best-estimate parameter-response covariance matrix $\mathbf{C}_{\alpha r}^{BE}$:

$$\begin{aligned} \mathbf{C}_{\alpha}^{BE} &\equiv E\left([\boldsymbol{\alpha} - \boldsymbol{\alpha}^{BE}] [\boldsymbol{\alpha} - \boldsymbol{\alpha}^{BE}]^T\right) \\ &= \mathbf{C}_{\alpha} - [\mathbf{C}_{\alpha d}(\boldsymbol{\alpha}^0)] [\mathbf{C}_d(\boldsymbol{\alpha}^0)]^{-1} [\mathbf{C}_{\alpha d}(\boldsymbol{\alpha}^0)]^T, \end{aligned} \quad (2.23)$$

$$\begin{aligned} \mathbf{C}_r^{BE} &\equiv E\left([\mathbf{r} - \mathbf{r}(\boldsymbol{\alpha}^{BE})] [\mathbf{r} - \mathbf{r}(\boldsymbol{\alpha}^{BE})]^T\right) \\ &= \mathbf{C}_m - [\mathbf{C}_{rd}(\boldsymbol{\alpha}^0)] [\mathbf{C}_d(\boldsymbol{\alpha}^0)]^{-1} [\mathbf{C}_{rd}(\boldsymbol{\alpha}^0)]^T, \end{aligned} \quad (2.24)$$

$$\begin{aligned} \mathbf{C}_{\alpha r}^{BE} &\equiv E\left([\boldsymbol{\alpha} - \boldsymbol{\alpha}^{BE}] [\mathbf{r} - \mathbf{r}(\boldsymbol{\alpha}^{BE})]^T\right) \\ &= \mathbf{C}_{\alpha r} - [\mathbf{C}_{\alpha d}(\boldsymbol{\alpha}^0)] [\mathbf{C}_d(\boldsymbol{\alpha}^0)]^{-1} [\mathbf{C}_{rd}(\boldsymbol{\alpha}^0)]^T, \end{aligned} \quad (2.25)$$

where

$$\begin{aligned} \mathbf{C}_{\alpha d} &\equiv E([\boldsymbol{\alpha} - \boldsymbol{\alpha}^{BE}] \mathbf{d}^T) \\ &= \mathbf{C}_{\alpha r} - \mathbf{C}_{\alpha} [\mathbf{S}(\boldsymbol{\alpha}^0)], \end{aligned} \quad (2.26)$$

and

$$\begin{aligned} \mathbf{C}_{rd} &\equiv E([\mathbf{r} - \mathbf{r}^m] \mathbf{d}^T) \\ &= \mathbf{C}_m - \mathbf{C}_{\alpha r}^T [\mathbf{S}(\boldsymbol{\alpha}^0)]^T. \end{aligned} \quad (2.27)$$

Note that Eq. 2.24 expresses the best-estimate response covariance matrix \mathbf{C}_r^{BE} in terms of the initial covariance matrix \mathbf{C}_m of the experimental responses. Alternatively, \mathbf{C}_{rc}^{BE} may be derived directly from the model (the extra subscript “c” to distinguish the two). Starting from Eq. 2.6 but generating the expansion about $\boldsymbol{\alpha}^{BE}$ instead of $\boldsymbol{\alpha}^0$ yields

$$\mathbf{r}(\boldsymbol{\alpha}) = \mathbf{R}(\boldsymbol{\alpha}^{BE}) + \mathbf{S}(\boldsymbol{\alpha}^{BE}) (\boldsymbol{\alpha} - \boldsymbol{\alpha}^{BE}) + \dots \quad (2.28)$$

From Eq. 2.28, it follows that

$$\begin{aligned} \mathbf{C}_{rc}^{BE} &= E([\mathbf{r} - \mathbf{R}(\boldsymbol{\alpha}^{BE})] [\mathbf{r} - \mathbf{R}(\boldsymbol{\alpha}^{BE})]^T) \\ &\equiv [\mathbf{S}(\boldsymbol{\alpha}^{BE})] \left([\boldsymbol{\alpha} - \boldsymbol{\alpha}^{BE}] [\boldsymbol{\alpha} - \boldsymbol{\alpha}^{BE}]^T \right) [\mathbf{S}(\boldsymbol{\alpha}^{BE})]^T \\ &= [\mathbf{S}(\boldsymbol{\alpha}^{BE})] \mathbf{C}_{\alpha}^{BE} [\mathbf{S}(\boldsymbol{\alpha}^{BE})]^T. \end{aligned} \quad (2.29)$$

Comparing Eq. 2.29 and Eq. 2.24 shows that in general cases $\mathbf{C}_{rc}^{BE} \neq \mathbf{C}_r^{BE}$ since $\mathbf{S}(\boldsymbol{\alpha}^{BE}) \neq \mathbf{S}(\boldsymbol{\alpha}^0)$. In the case when the model is “perfect” (free of numerical errors) and exactly linear,

then the sensitivities are independent of parameter values

$$\mathbf{S}(\boldsymbol{\alpha}^{BE}) = \mathbf{S}(\boldsymbol{\alpha}^0) = \mathbf{S},$$

for perfect and linear models. (2.30)

And as such, $\mathbf{C}_{\mathbf{rc}}^{BE} = \mathbf{C}_{\mathbf{r}}^{BE}$, for perfect linear models. This concept of inequality between sensitivities evaluated at different state points (in this case: $\boldsymbol{\alpha}^0$ and $\boldsymbol{\alpha}^{BE}$) for nonlinear models will be exploited in Chapter 4 for computation of higher-order moments.

Perhaps, most importantly, is the ability to measure the mutual and joint consistency of the information available for model calibration. The quantity

$$Q_{min} \equiv Q(\mathbf{z}^{BE}) = \mathbf{d}^T [\mathbf{C}_{\mathbf{d}}(\boldsymbol{\alpha}^0)]^{-1} \mathbf{d},$$
(2.31)

measures the deviations between the experimental and nominally computed responses. From [10], Q_{min} obeys a χ^2 distribution with n degrees of freedom. The χ^2 distribution is a measure of the deviation of a true distribution from the hypothetical Gaussian. A practical quantitative criterion for the acceptance or rejection of experimental results in conjunction with a given theoretical model is to accept the value of χ^2/N_r whenever

$$\beta < P_{N_r}(\chi^2) < 1 - \beta,$$
(2.32)

where β , is a user-defined probability $\in [0, 1]$ expressing one's confidence that the experimental results and the computational results are indeed consistent.

To further elucidate, the deviation-vector uncertainty matrix, $\mathbf{C}_{\mathbf{d}}$, contains all uncertainties and sensitivities while deviation-vector, \mathbf{d} , contains the deviation of the computed and experimentally measured responses. This is not a typical " χ^2 " metric that is commonly seen in other works.

2.2 Necessary Conditions for Bona Fide Covariance Matrices

2.2.1 Definitions

For any general variance-covariance matrix, the following tests will determine to what degree the ideal properties for data assimilation best-practices have been met. The notation is carried out specifically for an input parameter covariance matrix but the same may be carried out for experimental covariance matrices as well. In this work, all experimental covariance matrices met the desired properties while all input parameter covariance matrices, to some extent, failed.

Any input parameter variance-covariance matrix $\mathbf{C}_\alpha \in \mathbb{R}^{N_\alpha \times N_\alpha}$, will have a corresponding parameter vector $\alpha \in \mathbb{R}^{N_\alpha \times 1}$ where N_α represents the number of input parameters. This matrix can be classified as either relative or absolute, denoted \mathbf{C}_{rel} and \mathbf{C}_{abs} respectively. Standard deviations of the parameters are represented in general by σ while relative and absolute standard deviations are given by σ_{rel} and σ_{abs} respectively. Correlation matrices will be denoted as \mathbf{C}_{corr} where the correlation $\rho_{i_1 i_2}$ between parameters α_{i_1} and α_{i_2} may be defined as

$$\rho_{i_1 i_2} \equiv \frac{(\mathbf{C})_{i_1 i_2}}{\sigma_{i_1} \sigma_{i_2}} \quad (2.33)$$

and

$$\mathbf{C}_{\text{corr}} \equiv \begin{pmatrix} \rho_{11} & \cdots & \rho_{1N_\alpha} \\ \vdots & \rho_{ii} & \vdots \\ \rho_{N_\alpha 1} & \cdots & \rho_{N_\alpha N_\alpha} \end{pmatrix}. \quad (2.34)$$

2.2.2 Symmetric Positive Definiteness

A matrix must be symmetric positive definite to truly be considered a physically meaningful variance-covariance matrix [8]. In general, this amounts to all eigenvalues of the (assumed real) matrix to be positive (i.e. > 0). The determinant of a positive definite matrix is always positive and hence a positive definite matrix is always nonsingular. Also consequently, each of the matrix's leading principal minors would also be positive [32]. If matrices A and B are

positive definite then so is $A+B$. The matrix inverse of a positive definite matrix is also positive definite.

A matrix which does not exhibit these properties is not a variance-covariance matrix with any meaningful physical system corollary. Matrices that are symmetric positive semi-definite are often used as physical stand-ins for their positive definite counterparts but ultimately represent a lack of sufficient information or poor modeling for the physical system at hand. A positive semi-definite matrix contains eigenvalues that are all non-negative (i.e. ≥ 0).

Testing for positive definiteness may be achieved by attempting a Cholesky Factorization on the matrix in question. A representative algorithm for decomposing a matrix would utilize only the lower triangular (or upper triangular respectively) portion of the matrix plus the diagonal. The Cholesky Factorization is given as follows

$$\mathbf{C} = \mathbf{L}\mathbf{L}^T = \mathbf{U}^T\mathbf{U}, \tag{2.35}$$

where \mathbf{C} , the matrix in question, is decomposed into \mathbf{L} (\mathbf{U}), a lower triangular (upper triangular) matrix with strictly positive diagonal entries, and \mathbf{L}^T (\mathbf{U}^T) denotes the transposition of \mathbf{L} (\mathbf{U}). In the event that one of the leading principal minors of matrix \mathbf{C} is found to be negative, the representative algorithm would exit prematurely because continuing would ultimately lead to attempting to take the square root of a negative number.

2.2.3 Physical Correlations

One of the most familiar measures of dependence between two quantities is the Pearson product-moment correlation coefficient defined in Eq. 2.33. It is a corollary of the Cauchy-Schwarz inequality that the correlation between any two quantities cannot exceed 1 in absolute value.

In the case of a correlation between a quantity x and itself, the correlation necessarily would be equal to 1. On the other end of the spectrum, the correlation between x and $-x$ would be equal to -1 .

The correlation matrix \mathbf{C}_{corr} is a collection of these Pearson correlations between each of the input parameters. \mathbf{C}_{corr} has the property that every correlation along the diagonal should necessarily be equal to 1 since this represents a parameter’s self correlation. Also, every off-diagonal entry must be greater than or equal to -1 or less than or equal to 1 .

2.3 Parameter Covariance Consistency Verification

In the case of a deterministic time-independent Boltzmann neutron transport model, input parameters typically include isotopic densities, fission spectrum data along with microscopic neutron (and potentially gamma) cross section information for a set of particular isotopes and reactions that take place within the problem of interest. This data is tabulated as a function of neutron energy and material temperature in a point-wise form that is considered detailed enough for linear interpolation to form a continuous energy approximation [31]. Oak Ridge National Lab’s (ORNL) SCALE code package releases this data in a binary AMPX format for use within various code modules.

Cross section covariance information in the form of a binary COVERX formatted file is also distributed along with the release of the SCALE code package. This file contains covariance information in a multi-group energy structure from a variety of sources. Main components are broken into high and low fidelity covariances associated with the isotopes included in the SCALE evaluation.

High fidelity covariances are evaluated from nuclear data files that belong to a specific library (e.g. ENDF/B-VII, ENDF/B-VI or JENDL3.3). Differential experimental measurements and their uncertainties are used in a regression algorithm to calibrate parameters in a nuclear physics model [28]. Unfortunately, only a small number of isotopes have yielded such consistent results. Several of the covariances that were included in the ENDF/B-VI release were withheld from the VII.0 release due to incomplete or otherwise inconsistent data and/or practices [13].

In an attempt to provide a complete but approximate release, ORNL’s SCALE group in collaboration with Los Alamos National Lab, Argonne National Lab, the National Nuclear Data

Center and the United States Department of Energy accomplished a low fidelity covariance project which aimed to provide a comprehensive listing of covariances for isotopes included in the ENDF/B-VII release [30]. Low fidelity isotope covariances had to be approximated and decoupled from their original evaluation procedure. To do this, sometimes crude approximations were used to complete the project on schedule.

In the current state, capabilities to construct and evaluate full parameter covariance matrices have been created. These parameter covariance matrices are formed once all input parameters are known and gathered as a result of the desired responses. The proposed tests, detailed in the next section, have been carried out on problem-specific covariance matrices that are generated on the fly at run-time pulling from data stored in quick access Python format known as a pickle.

2.4 Evaluation of SCALE Covariance Matrices

2.4.1 Covariance Data Hierarchy

Nuclear data from the various libraries were processed with Oak Ridge National Lab’s PUFF code and formatted into the binary COVERX file that is released with SCALE [33]. Utilizing the COGNAC module of the AMPX utility suite that ships with SCALE , the binary format was converted to an ASCII version of the COVERX format. Using Python, a reader was created to read in the information given within the file.

It is important to note that the information given in the file is composed of sub-matrices of the eventual complete covariance matrix to be generated on a problem specific basis. For example, a hypothetical experiment which includes water (H_2O) and Uranium-235 contains $m_i = 3$ separate isotopes of interest ($^1H, ^{16}O, ^{235}U$). Then, say that a total of $m_r = 3$, namely fission (f), absorption (a) and neutron scatter (s), reactions occur in the hypothetical experiment. Next, let there be $m_d = 3$ distinct domains α, β and γ which could represent either different temperature or even spatial cells due to self-shielding. Lastly, assume the number of energy groups to be $m_g = 44$. This setup gives an input parameters covariance matrix C_α of

dimension $m = m_d * m_i * m_r * m_g = 1188$.

$$\mathbf{C}_\alpha = \begin{pmatrix} \mathbf{C}_{H1,H1} & \mathbf{C}_{H1,O16} & \mathbf{C}_{H1,U235} \\ \mathbf{C}_{O16,H1} & \mathbf{C}_{O16,O16} & \mathbf{C}_{O16,U235} \\ \mathbf{C}_{U235,H1} & \mathbf{C}_{U235,O16} & \mathbf{C}_{U235,U235} \end{pmatrix},$$

where

$$\mathbf{C}_{i,j} = \begin{pmatrix} \mathbf{C}_{i,j}^{f,f} & \mathbf{C}_{i,j}^{f,a} & \mathbf{C}_{i,j}^{f,s} \\ \mathbf{C}_{i,j}^{a,f} & \mathbf{C}_{i,j}^{a,a} & \mathbf{C}_{i,j}^{a,s} \\ \mathbf{C}_{i,j}^{s,f} & \mathbf{C}_{i,j}^{s,a} & \mathbf{C}_{i,j}^{s,s} \end{pmatrix}; \left(i, j = H1, O16, U235 \right),$$

and

$$\mathbf{C}_{i,j}^{k,l} = \begin{pmatrix} \alpha, \alpha \mathbf{C}_{i,j}^{k,l} & \alpha, \beta \mathbf{C}_{i,j}^{k,l} & \alpha, \gamma \mathbf{C}_{i,j}^{k,l} \\ \beta, \alpha \mathbf{C}_{i,j}^{k,l} & \beta, \beta \mathbf{C}_{i,j}^{k,l} & \beta, \gamma \mathbf{C}_{i,j}^{k,l} \\ \gamma, \alpha \mathbf{C}_{i,j}^{k,l} & \gamma, \beta \mathbf{C}_{i,j}^{k,l} & \gamma, \gamma \mathbf{C}_{i,j}^{k,l} \end{pmatrix}; \left(\begin{array}{l} i, j = H1, O16, U235 \\ k, l = f, a, s \end{array} \right),$$

where

$${}^{o,p}\mathbf{C}_{i,j}^{k,l} = \begin{pmatrix} {}^{o,p}\mathbf{C}_{i,j}^{k,l}(1,1) & {}^{o,p}\mathbf{C}_{i,j}^{k,l}(1,2) & \dots & {}^{o,p}\mathbf{C}_{i,j}^{k,l}(1,44) \\ {}^{o,p}\mathbf{C}_{i,j}^{k,l}(2,1) & {}^{o,p}\mathbf{C}_{i,j}^{k,l}(2,2) & \dots & {}^{o,p}\mathbf{C}_{i,j}^{k,l}(2,44) \\ \vdots & \vdots & \ddots & \vdots \\ {}^{o,p}\mathbf{C}_{i,j}^{k,l}(44,1) & {}^{o,p}\mathbf{C}_{i,j}^{k,l}(44,2) & \dots & {}^{o,p}\mathbf{C}_{i,j}^{k,l}(44,44) \end{pmatrix}; \dots$$

$$\left(\begin{array}{l} i, j = H1, O16, U235 \\ k, l = f, a, s \\ o, p = \alpha, \beta, \gamma \end{array} \right).$$

The sub-matrices found in the COVERX formatted file are represented by ${}^{o,p}\mathbf{C}_{i,j}^{k,l}$ and are given as relative covariances. All of the diagonal sub-matrix data ($i = j$, $k = l$ and $o = p$) are provided while off-diagonal sub-matrices are more likely to be found within a specific isotope ($i = j$, $k \neq l$) versus within a specific reaction type ($i \neq j$, $k = l$). Cross domain data ($o \neq p$) are not given. The correlations of sub-matrices that are not given may be set to zero by arguments

of the maximum entropy principle described in [10].

2.4.2 Specific Tests Conducted on Covariance Matrices

2.4.2.1 Symmetry

For every covariance matrix, the symmetry was checked via

$$\|\mathbf{C}_\alpha - \mathbf{C}_\alpha^T\|_\infty < \epsilon_s.$$

A tolerance, ϵ_s was specified and as long as the infinity norm was less than ϵ_s , the matrix passed.

2.4.2.2 Non-physical Correlations

Since the correlations are not explicitly provided in the COVERX file, round-off and truncation error will cause diagonals to potentially be slightly greater than 1. If, however, correlations exist that are either noticeably greater (or smaller) than 1 (or -1) there is an obvious non-physical discrepancy between the given relative covariance and the given relative standard deviations.

The diagonal elements of \mathbf{C}_α were checked to make sure that the value was between $1 + \epsilon_c$ and $1 - \epsilon_c$. For all other elements, the value was checked to make sure it was between $-1 - \epsilon_c$ and $1 + \epsilon_c$.

2.4.2.3 Relative Standard Deviation Consistency

Since both relative standard deviations and relative covariances were given for each SCALE sub-matrix, it is possible to check that the square of the relative standard deviations (variances) match the diagonal elements of the relative covariance matrix, i.e.

$${}^{o,o}\mathbf{C}_{i,i}^{k,k}(g, g) - \epsilon_r \leq \sigma_{rel}^2(g) \leq {}^{o,o}\mathbf{C}_{i,i}^{k,k}(g, g) + \epsilon_r; \quad g = 1, \dots, m_g.$$

A check was also performed to make sure that the magnitudes of the relative standard

deviations were sufficiently large enough not to cause unwanted division issues when computing the correlation sub-matrices. As long as the relative standard deviation was greater than ϵ_d , the division was deemed acceptable.

2.4.2.4 Positive Definiteness

As mentioned, the positive definiteness of a matrix may be confirmed if it admits the Cholesky Factorization. Specifically, for each covariance matrix, an attempt to factorize was made via LAPACK's computational routine DPOTRF (version 3.3.1) [1]. As part of the routine, all leading minors are confirmed to be positive. If one of the leading minors is not positive, the routine returns prematurely and supplies an error code to warn the user that the matrix is not positive definite.

2.4.2.5 Singular Value Decomposition

In the event that a covariance matrix fails to admit the Cholesky Factorization, a singular value decomposition of the form

$$\mathbf{C}_\alpha = \mathbf{U}_\alpha \mathbf{\Sigma}_\alpha \mathbf{V}_\alpha^T,$$

where \mathbf{U}_α and \mathbf{V}_α are orthonormal matrices, i.e. $\mathbf{U}_\alpha^T \mathbf{U}_\alpha = \mathbf{I}$; $\mathbf{V}_\alpha^T \mathbf{V}_\alpha = \mathbf{I}$ and $\mathbf{\Sigma}_\alpha$ is a diagonal matrix whose elements are the singular values of the original matrix. This decomposition allows the user to ascertain some measure of rank deficiency within the covariance matrix.

2.4.3 Summary of Results

The tests were conducted for each experimental setup once the parameter covariance matrix \mathbf{C}_α was constructed. Results for the Godiva, Jezebel and LCT benchmarks (described in Chapter 3) are outlined below.

Each system was broken down into isotopes, reaction types, energy groups and domains. The choice of the number of energy groups included either 44 or 27 energy groups. According to the SCALE manual, both choices are acceptable for either fast or thermal neutron systems

[33]. Godiva’s system included 9 relevant isotopes, 7 reaction types, 9 domains and 27 energy groups. Jezebel’s system included 12 relevant isotopes, 10 reaction types, 9 domains and 27 energy groups. LCT’s system included 30 relevant isotopes, 12 reaction types, 15 domains and 44 energy groups. In this case, choices for either 44 or 27 group energy structure were made merely for convenience. Nevertheless, information regarding covariance matrix structure is reported for both energy group structures.

Note that covariances are not domain-dependent and not every combination of isotope / reaction type / domain are physically meaningful. For instance, a particular domain may only have 3 out of 30 isotopes present and only 4 of the 12 reaction types occur for those particular isotopes. Nevertheless, sensitivities *are* given as a function of domain and, as such, either block multiplication can be implemented or problem sizes could reflect this extra dimension when propagating uncertainties if not prohibitively large.

Table 2.1 contains a concise summary of dimensions (N_α) with regard to each system. The first column contains the Full problem dimension, including distinction between SCALE material domains, isotopes, reaction types and energy groups. Column 2 contains the dimension of the Fundamental parameter covariance matrix when domain-dependence is eliminated. Column 3 further reduces on column 2 by removing all of the row / column pairs which contain only zeros and is denoted as the Non-Zero Fundamental covariance dimension. Finally, column 4 reveals the numerical rank via SVD of the non-zero fundamental covariance matrix given a cutoff for the singular values of $\epsilon = 1e - 14$.

As is evident from the SVD column of Table 2.1, none of the parameter covariance matrices are positive definite. While the covariance data must be positive definite on the original energy grid used by the evaluator to pass ENDF standards, [35], this does not hold once the cross section information has been processed numerically to a different energy grid.

With regard to the other tests, including symmetry, physical correlations and relative standard deviation consistency, all covariance matrices passed with tolerances set no greater than $1.0e - 4$ (the significant figures of the covariances were at best 4).

Table 2.1: Input parameter covariance matrix (C_α) dimension summary.

27-Group Covariance Evaluation				
Benchmark			Non-Zero	SVD
System	Full	Fundamental	Fundamental	$\epsilon = 1e - 14$
LCT	15930	2862	935	884
Godiva	756	729	545	411
Jezebel	1188	1160	670	477
44-Group Covariance Evaluation				
Benchmark			Non-Zero	SVD
System	Full	Fundamental	Fundamental	$\epsilon = 1e - 14$
LCT	25960	4664	1501	591
Godiva	1232	1188	883	640
Jezebel	1936	1892	1082	774

Chapter 3

Optimized Responses & Parameters Following Data Assimilation

3.1 Computational Framework

3.1.1 Denovo

3.1.1.1 Overview

Denovo is a recent code development from ORNL that solves the three dimensional time-independent Boltzmann transport equation given as

$$\boldsymbol{\Omega} \cdot \vec{\nabla} \psi(\vec{r}, \boldsymbol{\Omega}, E) + \Sigma_t(\vec{r}, E) \psi(\vec{r}, \boldsymbol{\Omega}, E) = \int_{4\pi} d\boldsymbol{\Omega}' \int_0^\infty dE' \Sigma_s(\vec{r}, \boldsymbol{\Omega}' \rightarrow \boldsymbol{\Omega}, E' \rightarrow E) \psi(\vec{r}, \boldsymbol{\Omega}', E') + Q(\vec{r}, \boldsymbol{\Omega}, E). \quad (3.1)$$

This parallel code has demonstrated excellent scaling up to tens of thousands of cores [16]. Written predominantly in C++ with a Python front-end and utilizing Sandia National Lab's Trilinos solvers, this discrete ordinates code is capable of handling extremely large problem sizes up to and including full reactor core calculations.

What highlights Denovo as the workhorse for this research is the recent implementation of adjoint solution capabilities. With the adjoint, first-order sensitivities are obtained for responses such as the k-eigenvalue, nuclide density and reaction rate ratios of the form

$$r_k \equiv \frac{\langle \sigma_1, \phi \rangle_w}{\langle \sigma_2, \phi \rangle_w}, \quad (3.2)$$

where σ_i , $i = 1, 2$ represent (usually but not necessarily) cross sections (microscopic or macroscopic), ϕ the scalar flux and $\langle \cdot, \cdot \rangle_w$ may denote a user-defined inner-product space. For convenience, the inner-product can be taken over the state space. To solve the k-eigenvalue problem, recast Eq. 3.1 into an equation of the form

$$\begin{aligned} \mathbf{\Omega} \cdot \vec{\nabla} \psi(\vec{r}, \mathbf{\Omega}, E) + \Sigma_t(\vec{r}, E) \psi(\vec{r}, \mathbf{\Omega}, E) = \\ \int_{4\pi} d\mathbf{\Omega}' \int_0^\infty dE' \Sigma_s(\vec{r}, \mathbf{\Omega}' \rightarrow \mathbf{\Omega}, E' \rightarrow E) \psi(\vec{r}, \mathbf{\Omega}', E') + \\ \frac{\chi(\vec{r}, E)}{4\pi k} \int_{4\pi} d\mathbf{\Omega}' \int_0^\infty dE' \nu_f(\vec{r}, E') \Sigma_f(\vec{r}, E') \psi(\vec{r}, \mathbf{\Omega}', E'), \end{aligned} \quad (3.3)$$

where the angular flux ψ and k-eigenvalue k are both implicitly functions of the cross sections Σ_t , Σ_s and Σ_f , the fission spectrum χ and neutron multiplicity ν_f which are all considered input parameters α and, in general, functions of space \vec{r} and energy E and neutron angle $\mathbf{\Omega}$.

For convenience, Eq. 3.3 may be written in operator form as

$$\mathbf{A}\psi = \lambda \mathbf{F}\psi, \quad (3.4)$$

where

$$\begin{aligned} \mathbf{A} &\equiv \mathbf{\Omega} \cdot \vec{\nabla} + \Sigma_t(\vec{r}, E) - \int_{4\pi} d\mathbf{\Omega}' \int_0^\infty dE' \Sigma_s(\vec{r}, \mathbf{\Omega}' \rightarrow \mathbf{\Omega}, E' \rightarrow E), \\ \mathbf{F} &\equiv \frac{\chi(\vec{r}, E)}{4\pi} \int_{4\pi} d\mathbf{\Omega}' \int_0^\infty dE' \nu_f(\vec{r}, E') \Sigma_f(\vec{r}, E'), \end{aligned}$$

and $\lambda \equiv \frac{1}{k}$. This forward eigenvalue system may be solved to obtain ψ and k . From these, the

response r_k may then be computed.

3.1.1.2 Adjoint Sensitivity Analysis

Given the forward, nominal eigenvalue system in Eq. 3.4

$$(\mathbf{A}(\boldsymbol{\alpha}^0) - \lambda^0 \mathbf{F}(\boldsymbol{\alpha}^0)) \psi^0 = 0, \quad (3.5)$$

with superscript “0” denoting the nominal state and with a slightly more general (but no less enlightening) response than in Eq. 3.2

$$R(\mathbf{e}^0) = R(\psi^0, \boldsymbol{\alpha}^0) = R^0 = \frac{\langle \sigma_1^0, \psi^0 \rangle_w}{\langle \sigma_2^0, \psi^0 \rangle_w}, \quad (3.6)$$

the sensitivity of the response with respect to a variation in parameters $\boldsymbol{\alpha}$ is represented as $\delta R(\mathbf{e}^0; \mathbf{h})$; where $\mathbf{e}^0 \equiv (\mathbf{u}^0, \boldsymbol{\alpha}^0)$ denotes the nominal values of the state vector \mathbf{u} and parameter vector $\boldsymbol{\alpha}$ while $\mathbf{h} \equiv (\mathbf{h}_u, \mathbf{h}_\alpha)$ represent arbitrary increment vectors in state (\mathbf{h}_u) and parameter (\mathbf{h}_α) spaces. In this particular case, the state vector contains the angular flux while the parameter vector contains the cross sections mentioned in the previous section.

As will be shown shortly, because $\delta R(\mathbf{e}^0; \mathbf{h})$ is linear in the state variable, the sensitivity is denoted $DR(\mathbf{e}^0; \mathbf{h})$ in accordance with general practices [8]. The sensitivity can consequently be written as

$$\delta R(\mathbf{e}^0; \mathbf{h}) \xrightarrow{\text{linear}} DR(\mathbf{e}^0; \mathbf{h}) = R'_u(\mathbf{e}^0) \mathbf{h}_u + R'_\alpha(\mathbf{e}^0) \mathbf{h}_\alpha \quad (3.7)$$

where $R'_u(\mathbf{e}^0)$ and $R'_\alpha(\mathbf{e}^0)$ denote, respectively, the partial Gâteaux derivatives at \mathbf{e}^0 of $R(\mathbf{e})$ with respect to \mathbf{u} and $\boldsymbol{\alpha}$. For convenience in determining DR , take the natural log of the response

$$\ln R^0 = \ln \langle \sigma_1^0, \psi^0 \rangle_w - \ln \langle \sigma_2^0, \psi^0 \rangle_w. \quad (3.8)$$

Taking the Gâteaux derivative

$$\frac{d}{d\epsilon} \left\{ \ln(R^0 + \epsilon\delta R) = \ln \langle (\sigma_1^0 + \epsilon\delta\sigma_1), (\psi^0 + \epsilon h_\psi) \rangle_w - \ln \langle (\sigma_2^0 + \epsilon\delta\sigma_2), (\psi^0 + \epsilon h_\psi) \rangle_w \right\} \Big|_{\epsilon=0}. \quad (3.9)$$

Expanding and noting that only the terms that are first-order in ϵ will survive, the sensitivity is

$$\frac{DR(\mathbf{e}^0; \mathbf{h})}{R^0} = \frac{\langle \delta\sigma_1, \psi^0 \rangle_w + \langle \sigma_1^0, h_\psi \rangle_w}{\langle \sigma_1^0, \psi^0 \rangle_w} - \frac{\langle \delta\sigma_2, \psi^0 \rangle_w + \langle \sigma_2^0, h_\psi \rangle_w}{\langle \sigma_2^0, \psi^0 \rangle_w}. \quad (3.10)$$

Regrouping the terms yields

$$\frac{DR(\mathbf{e}^0; \mathbf{h})}{R^0} = \left\langle \left[\frac{\sigma_1^0}{\langle \sigma_1^0, \psi^0 \rangle_w} - \frac{\sigma_2^0}{\langle \sigma_2^0, \psi^0 \rangle_w} \right], h_\psi \right\rangle_w + \left(\frac{\langle \delta\sigma_1, \psi^0 \rangle_w}{\langle \sigma_1^0, \psi^0 \rangle_w} - \frac{\langle \delta\sigma_2, \psi^0 \rangle_w}{\langle \sigma_2^0, \psi^0 \rangle_w} \right). \quad (3.11)$$

The first term only contains variations (h_ψ) in the angular flux while the second term only contains variations ($\delta\sigma_1, \delta\sigma_2$) contained within the parameter vector. It is the variations in the state which, at this point, are unknown. To obtain h_ψ either the forward sensitivity analysis procedure (FSAP) or the adjoint sensitivity analysis procedure (ASAP) from [8] may be performed. In lieu of the fact that the typical number of input parameters far exceed the typical number of output parameters in a transport model calculation, the ASAP will prove computationally more efficient.

To utilize the ASAP and, thus, remove the dependence on h_ψ in the sensitivity of the response, first, the Gâteaux derivative of the system (Eq. 3.5) is taken:

$$\frac{d}{d\epsilon} \left\{ [(\mathbf{A}^0 + \epsilon\delta\mathbf{A}) - (\lambda^0 + \epsilon\delta\lambda)(\mathbf{F}^0 + \epsilon\delta\mathbf{F})] (\psi^0 + \epsilon h_\psi) \right\} \Big|_{\epsilon=0} = 0 \quad (3.12)$$

Again, expanding, only terms first-order in ϵ will survive, yielding

$$(\delta\mathbf{A} - \lambda^0\delta\mathbf{F} - \mathbf{F}^0\delta\lambda)\psi^0 + (\mathbf{A}^0 - \lambda^0\mathbf{F}^0)h_\psi = 0. \quad (3.13)$$

Eq. 3.13 is termed the forward sensitivity analysis equation. The unknowns are the variation in the flux, h_ψ , and the variation in the eigenvalue, $\delta\lambda$. Given a variation(s) in an input parameter cross section(s), subsequent variations in \mathbf{A} and \mathbf{F} are readily available and the eigenvalue system may be solved for h_ψ and $\delta\lambda$. To continue towards elimination of the h_ψ dependency in both Eq. 3.11 and Eq. 3.13, multiply Eq. 3.13 with an (as of yet) arbitrary function Γ_p^\dagger and integrate over the same space utilized in the response

$$\left\langle \Gamma_p^\dagger, (\delta\mathbf{A} - \lambda^0 \delta\mathbf{F} - \mathbf{F}^0 \delta\lambda) \psi^0 \right\rangle_w + \left\langle \Gamma_p^\dagger, (\mathbf{A}^0 - \lambda^0 \mathbf{F}^0) h_\psi \right\rangle_w = 0. \quad (3.14)$$

The terms multiplying h_ψ may be transferred to Γ_p^\dagger by taking the adjoint of the operators (denoted here as a “dagger” †)

$$\left\langle \Gamma_p^\dagger, (\delta\mathbf{A} - \lambda^0 \delta\mathbf{F} - \mathbf{F}^0 \delta\lambda) \psi^0 \right\rangle_w + \left\langle (\mathbf{A}^\dagger - \lambda^\dagger \mathbf{F}^\dagger) \Gamma_p^\dagger, h_\psi \right\rangle_w = 0, \quad (3.15)$$

where, by mathematical uniqueness $\lambda^\dagger = \lambda^0$. Γ_p^\dagger may be chosen specifically such that

$$\left(\mathbf{A}^\dagger - \lambda^\dagger \mathbf{F}^\dagger \right) \Gamma_p^\dagger = S^\dagger = \frac{\sigma_1^0}{\langle \sigma_1^0, \psi^0 \rangle_w} - \frac{\sigma_2^0}{\langle \sigma_2^0, \psi^0 \rangle_w}. \quad (3.16)$$

This apropos choice is exercised by multiplying Eq. 3.16 by h_ψ and integrating over the appropriate space

$$\left\langle (\mathbf{A}^\dagger - \lambda^\dagger \mathbf{F}^\dagger) \Gamma_p^\dagger, h_\psi \right\rangle_w = \left\langle \left[\frac{\sigma_1^0}{\langle \sigma_1^0, \psi^0 \rangle_w} - \frac{\sigma_2^0}{\langle \sigma_2^0, \psi^0 \rangle_w} \right], h_\psi \right\rangle_w \quad (3.17)$$

recalling Eq. 3.11 and Eq. 3.16, this leads to the following expression for the sensitivity

$$\frac{DR(\mathbf{e}^0; \mathbf{h})}{R^0} = \frac{\langle \delta\sigma_1, \psi^0 \rangle_w}{\langle \sigma_1^0, \psi^0 \rangle_w} - \frac{\langle \delta\sigma_2, \psi^0 \rangle_w}{\langle \sigma_2^0, \psi^0 \rangle_w} - \left\langle \Gamma_p^\dagger, (\delta\mathbf{A} - \lambda^0 \delta\mathbf{F} - \mathbf{F}^0 \delta\lambda) \psi^0 \right\rangle_w. \quad (3.18)$$

The operator on the left-hand side of Eq. 3.16 is singular and \mathbf{A}^\dagger is a linear compact operator. According to the Fredholm Alternative Theorem, if the homogeneous adjoint equation,

$(\mathbf{A}^\dagger - \lambda \mathbf{F}^\dagger) \psi^\dagger = 0$, has a non-zero solution and if and only if the adjoint source, S^\dagger on the right-hand side of Eq. 3.16, satisfies $\langle S^\dagger, \psi \rangle_w = 0$, then the inhomogeneous adjoint equation has a necessarily non-unique solution. This condition is indeed met, as shown below:

$$\langle S^\dagger, \psi \rangle_w = \frac{\langle \sigma_1^0, \psi^0 \rangle_w}{\langle \sigma_1^0, \psi^0 \rangle_w} - \frac{\langle \sigma_2^0, \psi^0 \rangle_w}{\langle \sigma_2^0, \psi^0 \rangle_w} = 1 - 1 = 0. \quad (3.19)$$

Moreover, because the solution to the inhomogeneous equation is non-unique, a unique solution may be chosen as long as the orthogonality condition with the homogeneous forward angular flux holds. Since the homogeneous adjoint flux is contained in the left nullspace of the adjoint transport operator, i.e. $(\mathbf{A}^\dagger - \lambda^\dagger \mathbf{F}^\dagger) \psi^\dagger = 0$, any additional terms involving the homogeneous adjoint angular flux may be added to the general solution without affecting the answer. Note that in Eq. 3.18, in the indirect term, there exists a dependence on the variation of the eigenvalue, $\delta\lambda$. To eliminate this dependence, an additional term may be subtracted from Γ_p^\dagger to give a unique solution, Γ^\dagger :

$$\Gamma^\dagger \equiv \Gamma_p^\dagger - \gamma \psi^\dagger. \quad (3.20)$$

γ is chosen as

$$\gamma \equiv \frac{\langle \Gamma_p^\dagger, \mathbf{F}^0 \psi^0 \rangle_w}{\langle \psi^\dagger, \mathbf{F}^0 \psi^0 \rangle_w}. \quad (3.21)$$

To illustrate the elimination:

$$\begin{aligned} \langle \Gamma^\dagger, \mathbf{F}^0 \psi^0 \delta\lambda \rangle_w &= \delta\lambda \langle (\Gamma_p^\dagger - \gamma \psi^\dagger), \mathbf{F}^0 \psi^0 \rangle_w \\ &= \delta\lambda \langle \Gamma_p^\dagger, \mathbf{F}^0 \psi^0 \rangle_w - \delta\lambda \frac{\langle \Gamma_p^\dagger, \mathbf{F}^0 \psi^0 \rangle_w}{\langle \psi^\dagger, \mathbf{F}^0 \psi^0 \rangle_w} \langle \psi^\dagger, \mathbf{F}^0 \psi^0 \rangle_w \\ &= 0. \end{aligned}$$

Thus, the sensitivity of response $R(\mathbf{e}^0)$ with respect to the input parameters $\boldsymbol{\alpha}$ can be computed as

$$\frac{DR(\mathbf{e}^0; \mathbf{h})}{R^0} = \frac{\langle \delta\sigma_1, \psi^0 \rangle_w}{\langle \sigma_1^0, \psi^0 \rangle_w} - \frac{\langle \delta\sigma_2, \psi^0 \rangle_w}{\langle \sigma_2^0, \psi^0 \rangle_w} - \langle \Gamma^\dagger, (\delta\mathbf{A} - \lambda^0 \delta\mathbf{F}) \psi^0 \rangle_w, \quad (3.22)$$

which only depends on the homogeneous forward angular flux (ψ^0), the homogeneous adjoint angular flux (ψ^\dagger), the inhomogeneous adjoint angular flux (Γ^\dagger) and variations in the operators due to variations in the parameters. Given other responses, $\mathbf{r} = (r_k; k = 1, \dots, \mathbf{N}_r)$, of the same form as Eq. 3.6, only \mathbf{N}_r inhomogeneous adjoint runs need be completed to acquire sensitivities to every parameter in $\boldsymbol{\alpha} = (\alpha_i; i = 1, \dots, \mathbf{N}_\alpha)$. This is opposed to \mathbf{N}_α homogeneous forward runs if one were to utilize just the forward sensitivity analysis equation.

As outlined in [15], a standard method of solving the inhomogeneous adjoint system would be via a fixed-point iteration algorithm similar to

$$\mathbf{A}^\dagger \Gamma^{\dagger, n+1} = \lambda \mathbf{F}^\dagger \Gamma^{\dagger, n} + \mathbf{S}^\dagger. \quad (3.23)$$

where Γ^\dagger is orthogonalized with respect to $\mathbf{F}^0 \psi^0$ after each outer-iteration. While reliable, this method proves slow to converge. Instead, R. T. Evans and Cacuci showed that a fixed-source Generalized Minimum Residual (GMRES) algorithm yields mathematically the same answer without outer-iterations using methods from [24]. With this new solution technique, the inhomogeneous adjoint solve was demonstrated at over 37 times faster than a standard fixed-point iteration with Gauss-Seidel for the Godiva Benchmark problem outlined in section 3.2.1.1.

3.1.2 best_pred

3.1.2.1 Overview

best_pred, or “best predictions”, is an in-house parallel FORTRAN2003 code written to perform the task of first order data assimilation as described in Chapter 2. This code was specifically written and has been demonstrated to be scalable from a desktop PC all the way up to ORNL’s 2.3 peta-FLOP machine, Jaguar.

This highly modularized stand alone code encapsulates data in user-defined structures that borrow principles based on current object-oriented programming standards. best_pred utilizes

the robust and highly optimized libraries of ScaLAPACK to complete the matrix algebra necessary to compute best-estimate updates for parameters and covariances [3].

Typically in a reactor physics model, the input parameter space is larger than the response space; in most cases, more than an order of magnitude larger. In general, and most certainly after best-estimate values have been calculated, all matrices involved will be dense. This fact is what drove the decision to use ScaLAPACK as a solution library versus other open source libraries such as SNL's Trilinos which supports (mostly only) sparse matrix forms [22].

3.1.2.2 Code Inputs

Define Inputs to best_pred :

N_α	:	Input Parameter Dimension
N_r	:	Output Response Dimension
$\alpha \in \mathbb{R}^{N_\alpha \times 1}$:	Input Parameters
$C_\alpha \in \mathbb{R}^{N_\alpha \times N_\alpha}$:	Input Parameters Covariance Matrix
$r^m \in \mathbb{R}^{N_r \times 1}$:	Experimentally Measured Output Responses
$C_m \in \mathbb{R}^{N_r \times N_r}$:	Experimentally Measured Output Responses Covariance Matrix
$r \in \mathbb{R}^{N_r \times 1}$:	Computed Output Responses
$S \in \mathbb{R}^{N_r \times N_\alpha}$:	Computed Sensitivities
$C_{\alpha r} \in \mathbb{R}^{N_\alpha \times N_r}$:	Input Parameter Output Response Correlation Matrix

In the current state, best_pred reads in these seven matrices/vectors from separate files. Consistency checks are performed to make sure the dimensions match and the user has an option to check the input parameters and measured responses covariance matrices using some of the tests discussed in Chapter 2.3.

3.1.2.3 Computed Matrices/Vectors

Define Computed Matrices/Vectors in best_pred :

$$\begin{aligned}
\mathbf{d} &\in \mathbb{R}^{N_r \times 1} &= \mathbf{r} - \mathbf{r}^m \\
\mathbf{C}_{rc} &\in \mathbb{R}^{N_r \times N_r} &= \mathbf{S} \mathbf{C}_\alpha \mathbf{S}^T \\
\mathbf{C}_d &\in \mathbb{R}^{N_r \times N_r} &= \mathbf{C}_{rc} - \mathbf{C}_{\alpha r}^T \mathbf{S}^T - \mathbf{C}_{\alpha r} \mathbf{S} + \mathbf{C}_m \\
\chi^2 &\in \mathbb{R}^{1 \times 1} &= \mathbf{d}^T \mathbf{C}_d^{-1} \mathbf{d} \\
\mathbf{C}_{\alpha d} &\in \mathbb{R}^{N_\alpha \times N_r} &= \mathbf{C}_{\alpha r} - \mathbf{C}_\alpha \mathbf{S}^T \\
\mathbf{C}_{rd} &\in \mathbb{R}^{N_r \times N_r} &= \mathbf{C}_m - \mathbf{C}_{\alpha r}^T \mathbf{S}^T \\
\boldsymbol{\alpha}^{BE} &\in \mathbb{R}^{N_\alpha \times 1} &= \boldsymbol{\alpha} + \mathbf{C}_{\alpha d} \mathbf{C}_d^{-1} \mathbf{d} \\
\mathbf{r}^{BE} &\in \mathbb{R}^{N_r \times 1} &= \mathbf{r}^m + \mathbf{C}_{rd} \mathbf{C}_d^{-1} \mathbf{d} \\
\mathbf{C}_\alpha^{BE} &\in \mathbb{R}^{N_\alpha \times N_\alpha} &= \mathbf{C}_\alpha - \mathbf{C}_{\alpha d} \mathbf{C}_d^{-1} \mathbf{C}_{\alpha d}^T \\
\mathbf{C}_r^{BE} &\in \mathbb{R}^{N_r \times N_r} &= \mathbf{C}_m - \mathbf{C}_{rd} \mathbf{C}_d^{-1} \mathbf{C}_{rd}^T \\
\mathbf{C}_{\alpha r}^{BE} &\in \mathbb{R}^{N_\alpha \times N_r} &= \mathbf{C}_{\alpha r} - \mathbf{C}_{\alpha d} \mathbf{C}_d^{-1} \mathbf{C}_{rd}^T
\end{aligned}$$

More specifically, each of these data objects is represented on the computer as a set of independent distributed memory blocks set up in a two dimensional block cyclic distribution [3]. Typically, the symmetry (and positive definiteness) of the covariance matrices can be taken advantage of and a Cholesky Factorization, similar to that shown in Eq. 2.35 can be used most efficiently to compute solutions. Extensions have been made via linkages to LU Factorization and also to singular value decomposition routines in case more detailed analyses are sought.

3.1.3 Lemon

3.1.3.1 Overview

Lemon serves as the automated coupling mechanism between Denovo and best_pred . The input parameters, $\boldsymbol{\alpha}$, the computed output responses, \mathbf{r} , and the computed first order sensitivities, \mathbf{S} , are delivered by Denovo to best_pred . Input parameter covariances are read in from a COVERX file described in section 2.3. Experimentally measured responses and covariances,

\mathbf{r}^m and \mathbf{C}_m , are constructed manually based on information given in sections 3.2.1.1, 3.2.2.1 and 3.2.3.1. For the experiments described below, $\mathbf{C}_{\alpha r}$ is initially set to zero.

The problems in this work generate large volumes of data that need to be stored and organized efficiently. Lemon , a set of Python scripts currently still under development, will be able to complete not only the data transfer and run sequences necessary for everything described in this Chapter but also for items described in Chapter 4.

3.2 Applications

A reaction rate ratio (fission or activation) is defined here as the ratio of a particular isotope’s neutron reaction rate divided by a different isotope’s neutron reaction rate at a particular volume ΔV in the reactor core

$$r_k \equiv \frac{\langle \sigma_1, \phi \rangle_{foil}}{\langle \sigma_2, \phi \rangle_{foil}}, \quad (3.24)$$

where

$$\langle a, b \rangle_{foil} \equiv \int_{\Delta V} \int_0^\infty ab \, dE dV$$

and $\sigma_i \equiv \sigma_i(\vec{r}, E)$, $i = 1, 2$ denote microscopic cross sections as a function of space (\vec{r}) and energy (E). This type of response as well as the critical eigenvalue will be the focus of the following experiments described below.

3.2.1 Godiva

3.2.1.1 Benchmark Description

From Los Alamos Scientific Laboratory in the 1950’s, an experiment to determine the critical mass of a bare, 94 wt% ^{235}U sphere of highly enriched uranium was termed “Lady Godiva”. The sphere consisted of two identical sets of nested “Oak Ridge” alloy (oralloy) hemispheres shown in Figure 3.1. The top hemisphere rested on a 0.015 inch thick plate of stainless steel while the lower hemisphere rested on a thin-wall aluminum cylinder. Remotely, the lower half

was raised in contact with the underside of the stainless steel plate and neutron multiplication measurements were taken.

Two configurations were utilized: a bare, unreflected sphere and a series of concentric shells deemed Godiva “bare” and “shell” experiments respectively. In this work, only the bare configuration will be used. For the purposes of this demonstration, the pertinent information compiled by the International Criticality Safety Benchmark Evaluation Project (ICSBEP) on Godiva bare is repeated in this document for completeness [4].

The radius of the bare sphere was 8.7407 *cm* with a density of 18.74 *g/cm*³. The weight percent of ²³⁴U is given as 1.02 *wt%* while ²³⁵U is 93.71 *wt%*. The remaining fraction contains ²³⁸U . Table 3.1 contains the atom densities for the bare sphere.

Table 3.1: Composition of the uranium in Godiva bare.

Isotope	Atom Density (atoms/barn – cm)
²³⁴ U	4.9184e-4
²³⁵ U	4.4994e-2
²³⁸ U	2.4984e-3

There were several experimental measurements using Godiva bare but of interest for this work were the spectral indices at the core center. More specifically, central fission ratios and central activation ratios of several isotopes are compatible with Denovo ’s inhomogeneous adjoint capabilities described in section 3.1.1.

Table 3.2 contains the experimentally measured spectral indices of the responses used in this work along with their relative standard deviations. It also contains the measured k-eigenvalue with its relative standard deviation. A typical input listing for cross section processing preparation via SCALE 6.1 is given in Appendix A.1.

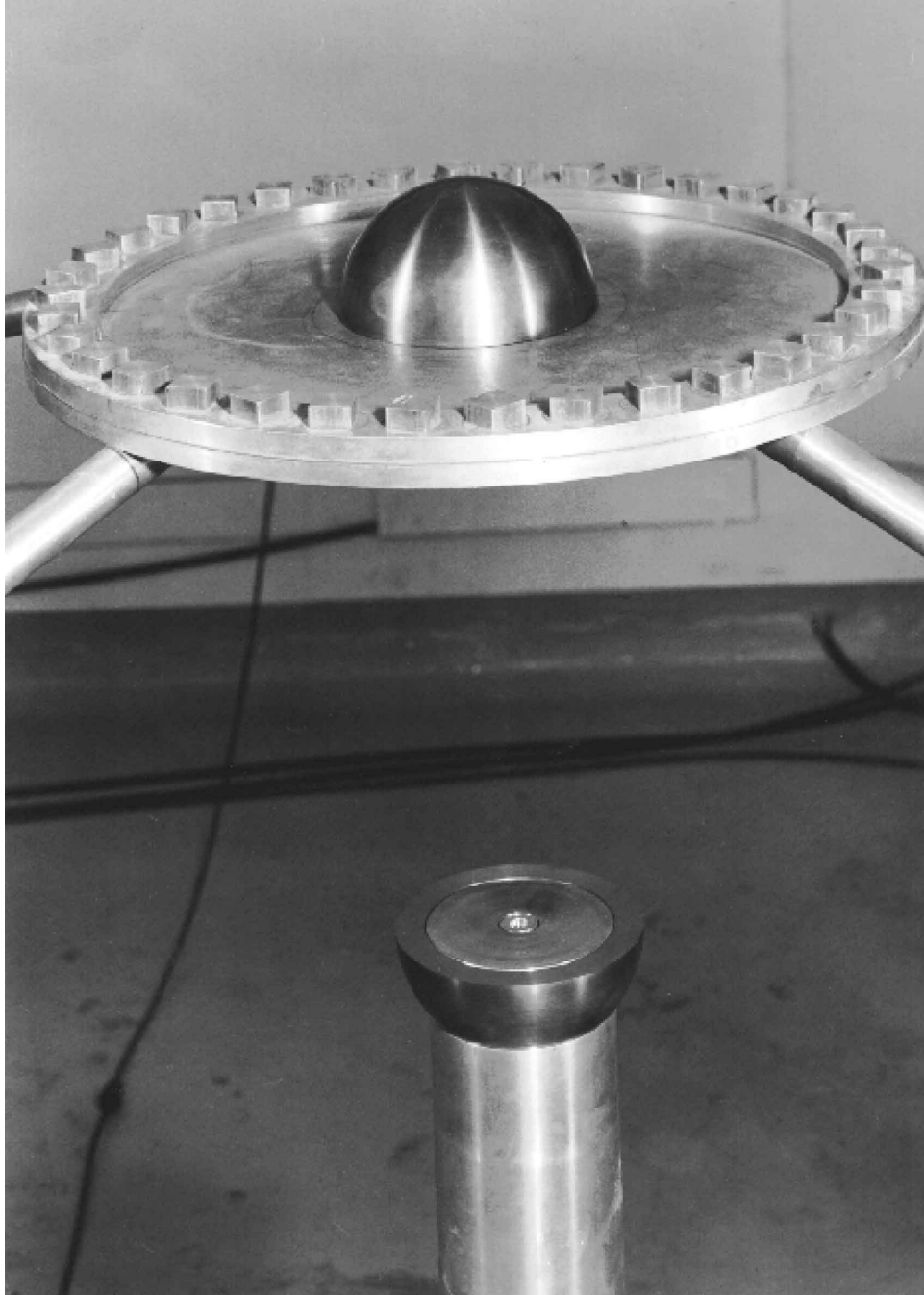


Figure 3.1: View of Godiva shell in disassembled mode with one hemisphere resting above on the stainless steel plate and one below on an aluminum thin-wall cylinder.

Table 3.2: Experimentally measured response values for Godiva bare. Values were taken from ICSBEP HEU-MET-FAST-001 Appendix B, Table F unless otherwise noted.

Response	Measured \pm Rel. Std. Dev.
k_{eff}	1.000 ^a \pm 0.001
$\sigma_f(^{238}\text{U})/\sigma_f(^{235}\text{U})$	0.1647 \pm 0.011
$\sigma_f(^{233}\text{U})/\sigma_f(^{235}\text{U})$	1.59 \pm 0.019
$\sigma_f(^{237}\text{Np})/\sigma_f(^{235}\text{U})$	0.837 \pm 0.016
$\sigma_f(^{239}\text{Pu})/\sigma_f(^{235}\text{U})$	1.402 \pm 0.018
$\sigma_\gamma(^{55}\text{Mn})/\sigma_f(^{235}\text{U})$	0.0027 ^a \pm 0.07
$\sigma_\gamma(^{63}\text{Cu})/\sigma_f(^{235}\text{U})$	0.0117 ^b \pm 0.05
$\sigma_\gamma(^{93}\text{Nb})/\sigma_f(^{235}\text{U})$	0.030 ^a \pm 0.1

^a ICSBEP HEU-MET-FAST-001 Appendix D, Table D; see [4].

^b CSEWG Table 7; see [17].

3.2.1.2 Computation of the Space-Dependent Neutron Flux Sensitivities

All theory in this section is based on the information from Cacuci’s Sensitivity and Uncertainty Analysis book, volume I [8] and original article [7] that introduced the “ASAP for operator-type responses.”

Given the energy integrated scalar flux and macroscopic fission operators

$$\phi(x, y, z) = \int_0^E dE \int_{4\pi} d\Omega \psi(x, y, z, E, \Omega), \quad (3.25)$$

$$\Sigma_f(x, y, z) = \frac{\int_0^E dE \Sigma_f(x, y, z, E) \phi(x, y, z, E)}{\int_0^E dE \phi(x, y, z, E)}, \quad (3.26)$$

consider a response

$$R(\phi, \alpha) \equiv \frac{\phi(x, y, z)}{\langle \Sigma_f, \phi \rangle_w}, \quad (3.27)$$

where the inner-product space is defined as

$$\langle f, g \rangle_w = \frac{1}{V} \int_0^a dx \int_0^b dy \int_0^c dz f(x, y, z) g(x, y, z). \quad (3.28)$$

The inner-product is defined over a symmetric octant of a reactor core with the volume $V \equiv abc$.

As in Eq. 3.8, take the natural log of the response for convenience

$$\ln R^0 = \ln \phi^0(x, y, z) - \ln \langle \Sigma_f^0, \phi^0 \rangle_w. \quad (3.29)$$

Next, take the Gâteaux derivative

$$\frac{d}{d\epsilon} \left\{ \ln (R^0 + \epsilon \delta R) = \ln (\phi^0 + \epsilon h_\phi) - \ln \langle (\Sigma_f^0 + \epsilon \delta \Sigma_f), (\phi^0 + \epsilon h_\phi) \rangle_w \right\} \Big|_{\epsilon=0}, \quad (3.30)$$

which gives the sensitivity

$$\frac{DR(\mathbf{e}^0; \mathbf{h})}{R^0} = \frac{h_\phi(x, y, z)}{\phi(x, y, z)} - \frac{\langle \Sigma_f^0, h_\phi \rangle_w}{\langle \Sigma_f^0, \phi^0 \rangle_w} - \frac{\langle \phi^0, \delta \Sigma_f \rangle_w}{\langle \Sigma_f^0, \phi^0 \rangle_w}. \quad (3.31)$$

The first two terms both belong to the partial Gâteaux derivative of R with respect to the scalar flux

$$R'_\phi(\mathbf{e}^0) h_\phi = \frac{h_\phi(x, y, z)}{\phi(x, y, z)} - \frac{\langle \Sigma_f^0, h_\phi \rangle_w}{\langle \Sigma_f^0, \phi^0 \rangle_w} = \left[\frac{1}{\phi(x, y, z)} - \frac{\langle \Sigma_f^0, \cdot \rangle_w}{\langle \Sigma_f^0, \phi^0 \rangle_w} \right] h_\phi(x, y, z). \quad (3.32)$$

What distinguishes this indirect term from the one shown in section 3.1.1.2 is the fact that it is an operator as opposed to a functional. The previous adjoint sensitivity analysis procedure relied on the fact that the response was indeed a functional.

To proceed with the evaluation of the indirect effect term, consider an orthonormal set of basis functions (as proposed by Cacuci in [8]): in this case, a three dimensional Fourier series expansion. If the global origin of the system is chosen at the center of the reactor core, the flux,

for the Godiva, Jezebel and LCT systems, is even in each independent spatial variable, i.e.

$$\phi(x, y, z) = \phi(-x, y, z); \phi(x, y, z) = \phi(x, -y, z); \phi(x, y, z) = \phi(x, y, -z).$$

In this case, the sine term is identically zero and subsequently dropped in the Fourier expansion:

$$\begin{aligned} R'_\phi(\mathbf{e}^0) h_\phi = & \\ & - \frac{a_{000}}{\langle \Sigma_f^0, \phi^0 \rangle_w} \int_0^a dx \int_0^b dy \int_0^c dz \Sigma_f^0(x, y, z) h_\phi(x, y, z) + \\ & \sum_{\ell=0}^{\infty} \sum_{m=0}^{\infty} \sum_{n=0}^{\infty} \left\{ a_{\ell mn} \int_0^a dx \int_0^b dy \int_0^c dz \frac{h_\phi(x, y, z)}{\phi(x, y, z)} \cos\left(\ell \frac{\pi x}{a}\right) \cos\left(m \frac{\pi y}{b}\right) \cos\left(n \frac{\pi z}{c}\right) \right\} \times \\ & \cos\left(\ell \frac{\pi x}{a}\right) \cos\left(m \frac{\pi y}{b}\right) \cos\left(n \frac{\pi z}{c}\right). \end{aligned} \quad (3.33)$$

The first term and the terms in between the curly braces $\{\cdot\}$ represent the Fourier coefficients with $a_{\ell mn}$ the normalization coefficients for each term. Because the indirect effect term is part of an inner-product for the Fourier coefficients, the terms multiplying h_ϕ may now be represented as

$$\begin{aligned} R'_\phi(\mathbf{e}^0) h_\phi = & \\ & - \frac{a_{000}}{\langle \Sigma_f^0, \phi^0 \rangle_w} \langle \Sigma_f^0, h_\phi \rangle_w + \\ & \sum_{\ell=0}^{\infty} \sum_{m=0}^{\infty} \sum_{n=0}^{\infty} \left\{ a_{\ell mn} \left\langle \frac{1}{\phi(x, y, z)} \cos\left(\ell \frac{\pi x}{a}\right) \cos\left(m \frac{\pi y}{b}\right) \cos\left(n \frac{\pi z}{c}\right), h_\phi \right\rangle_w \right\} \times \\ & \cos\left(\ell \frac{\pi x}{a}\right) \cos\left(m \frac{\pi y}{b}\right) \cos\left(n \frac{\pi z}{c}\right). \end{aligned} \quad (3.34)$$

In the case of a response functional, only one term of the Fourier series (the constant term) would survive. Although the summations here are infinite, in practice, only a finite number of terms are evaluated, depending on the complexity of the system and the nature of the variation.

Recalling Eq. 3.17, the same procedure for choosing adjoint sources may be utilized for each

term of the Fourier expansion, leading to the following inhomogeneous adjoint equations

$$\left(\mathbf{A}^\dagger - \lambda^\dagger \mathbf{F}^\dagger\right) \Gamma_{\ell mn}^\dagger = S_{\ell mn}^\dagger = a_{\ell mn} \left(\frac{1}{\phi(x, y, z)} - \frac{\Sigma_f^0(x, y, z)}{\langle \Sigma_f^0, \phi^0 \rangle_w} \right); (\ell, m, n) = (0, 0, 0), \quad (3.35)$$

$$\left(\mathbf{A}^\dagger - \lambda^\dagger \mathbf{F}^\dagger\right) \Gamma_{\ell mn}^\dagger = \frac{a_{\ell mn}}{\phi(x, y, z)} \cos\left(\ell \frac{\pi x}{a}\right) \cos\left(m \frac{\pi y}{b}\right) \cos\left(n \frac{\pi z}{c}\right); (\ell, m, n) \neq (0, 0, 0). \quad (3.36)$$

Note that all adjoint sources are orthogonal to the forward flux as is required for a non-trivial solution to exist. Lastly, the summation of all adjoint fluxes yields the final inhomogeneous adjoint flux that is used in computing (x, y, z) -dependent sensitivities

$$\Gamma^\dagger(x, y, z) = \sum_{\ell=0}^{\infty} \sum_{m=0}^{\infty} \sum_{n=0}^{\infty} \Gamma_{\ell mn}^\dagger \cos\left(\ell \frac{\pi x}{a}\right) \cos\left(m \frac{\pi y}{b}\right) \cos\left(n \frac{\pi z}{c}\right). \quad (3.37)$$

Finally, normalization coefficients may be generated via:

$$a_{\ell mn} = \frac{1}{\int_0^a dx \int_0^b dy \int_0^c dz \cos\left(\ell \frac{\pi x}{a}\right)^2 \cos\left(m \frac{\pi y}{b}\right)^2 \cos\left(n \frac{\pi z}{c}\right)^2}. \quad (3.38)$$

Thus, instead of computing a response for many spatial locations (points) within a reactor, it is possible to compute a few inhomogeneous adjoint fluxes up to a particular wave number $(\ell + m + n)$ of the Fourier expansion and obtain a very good approximation granted that the user chooses the appropriate basis functions for the given application. For instance, Chebyshev polynomials would likely make for an excellent choice given that they can be, by definition, exactly equal to the underlying response value at a given set of user-chosen points.

One more worthy note, since the systems are in three dimensions and the flux is symmetric, there is the convenient fact that

$$\int_\alpha^\beta \frac{\cos\left(\ell \frac{\pi x}{L}\right)}{\phi(x, r_0, r_0)} dx = \int_\alpha^\beta \frac{\cos\left(\ell \frac{\pi y}{L}\right)}{\phi(r_0, y, r_0)} dy = \int_\alpha^\beta \frac{\cos\left(\ell \frac{\pi z}{L}\right)}{\phi(r_0, r_0, z)} dz, \quad (3.39)$$

where α and β in this case are arbitrary bounds, L is some arbitrary distance and r_0 is some

arbitrary fixed point in space. So, if the x , y and z boundaries defined within the inner-product are equal to one another, i.e. $a = b = c$, then the number of Fourier coefficients that need be computed can be reduced. Put in other words, given the Fourier coefficients:

$$A_{lmn} \equiv a_{lmn} \left\langle \frac{1}{\phi(x, y, z)} \cos\left(\ell \frac{\pi x}{a}\right) \cos\left(m \frac{\pi y}{b}\right) \cos\left(n \frac{\pi z}{c}\right), h_\phi \right\rangle_w \quad (3.40)$$

then, when $a = b = c \implies A_{lmn} = A_{lnm} = A_{n\ell m} = A_{nm\ell} = A_{mnl} = A_{m\ell n}$. In the context of, say, including wave number combinations up to $(\ell, m, n) = (20, 20, 20)$, this would reduce the number of adjoint sources from 9261 to 1771.

3.2.1.3 Sensitivities of the Normalized Space-Dependent Flux

For the purposes of demonstration and rapid development, the Godiva sphere as described in Chapter 3 is used. This $10 \times 10 \times 10$ mesh restricts the number of Fourier wave number combinations that may be resolved to a total of 10^3 . Given that the problem domain boundaries are all equal this reduces the number of Fourier coefficients needed to 220. This means that with a total of 220 inhomogeneous adjoint runs the entire space may be characterized and there will be no difference (to machine-precision) of the evaluated sensitivity using the operator-type response or a functional-type response similar to Eq. 3.2 evaluated at a single point. Now, if machine-precision accuracy is not required, many fewer runs may be carried out to achieve the desired accuracy at select points within the system.

For the actual demonstration, without loss of generality, the response of interest is given as

$$R(x, y, z, \phi) \equiv \frac{\phi(x, y, z)}{\phi_{\text{avg}}}, \quad (3.41)$$

where ϕ_{avg} is the average flux throughout the problem domain. All 220 inhomogeneous runs were completed for the operator-type response to demonstrate the full convergence throughout the three-dimensional problem domain (despite the fact that Godiva and the operator-type response can be treated in one-dimension). In addition, 10 inhomogeneous adjoint runs with

responses of the form

$$R(x_i, y_j, z_k, \phi) \equiv \frac{\phi(x_i, y_j, z_k)}{\phi_{\text{avg}}}, \quad (3.42)$$

where (x_i, y_j, z_k) represents a particular cell within the problem domain. Specifically, the delta responses chosen for this demonstration include the 10 points that belong to the (x_i, y_i, z_i) ; $i = 0, \dots, 9$. Similar cases have been demonstrated with a combination of all x , y and z data that produce identical results but the data is taken for convenience in plotting techniques.

Wave number bounds are defined as a single number to keep notation concise. A wave number bound of 0 would only include contributions from the inhomogeneous adjoint solve with $(\ell, m, n) = (0, 0, 0)$. A wave number bound of 1 would include the inhomogeneous adjoint solves $(\ell, m, n) = (0, 0, 0), (1, 0, 0), (0, 1, 0)$ and $(0, 0, 1)$ (keeping in mind that in actuality only $(0, 0, 0)$ and $(1, 0, 0)$ would need to be solved because $a = b = c$ and the flux is symmetric). To obtain the (ℓ, m, n) combinations that belong to a particular wave number bound, any combination of $\ell + m + n$ that is less than or equal to the wave number bound would be counted provided that each individual ℓ , m or n value remains below the resolution of the mesh. For example, a wave number bound of 27 on this $10 \times 10 \times 10$ problem would include every wave number combination $(9, 9, 9)$ and lower but not, for instance, $(27, 0, 0)$. The following python code snippet will generate the (ℓ, m, n) combinations used for this Godiva example.


```

#!/usr/bin/env python
from numpy import *
# combinationList contains all 1000 combinations
combinationList = list()
waveNumberBounds = 27
maxMeshResolution = 10
for l in xrange(waveNumberBounds+1):
    for m in xrange(waveNumberBounds+1):
        for n in xrange(waveNumberBounds+1):
            if l + m + n > waveNumberBounds: continue
            if l >= maxMeshResolution: continue
            if m >= maxMeshResolution: continue
            if n >= maxMeshResolution: continue
            combinationList.append(tuple((l,m,n)))

sortedCombinationList = list()
for combination in combinationList:
    sortedCombinationList.append(tuple((sorted(combination, reverse = True))))

# sortedCombinationSet contains the reduced 220 combinations
sortedCombinationSet = sorted(list(set(sortedCombinationList)))

```

Figure 3.2 illustrates a typical output for the sensitivity of the response due to a change in the cross section for Uranium-235 fission. Several wave number bounds have been chosen to illustrate the convergence of the sensitivity. Figure 3.3 compliments the previous figure, demonstrating that by wave number bound 7 the percent difference between the operator-type response and the delta response is less than 10% for a majority of spatial locations. Continuing, by the point at which wave number bound 15 is reached, the percent difference is less than 2% for all locations. This behavior is system, response and basis choice dependent. The smoother the variation in the response, the easier to capture the effect with fewer terms in an expansion.

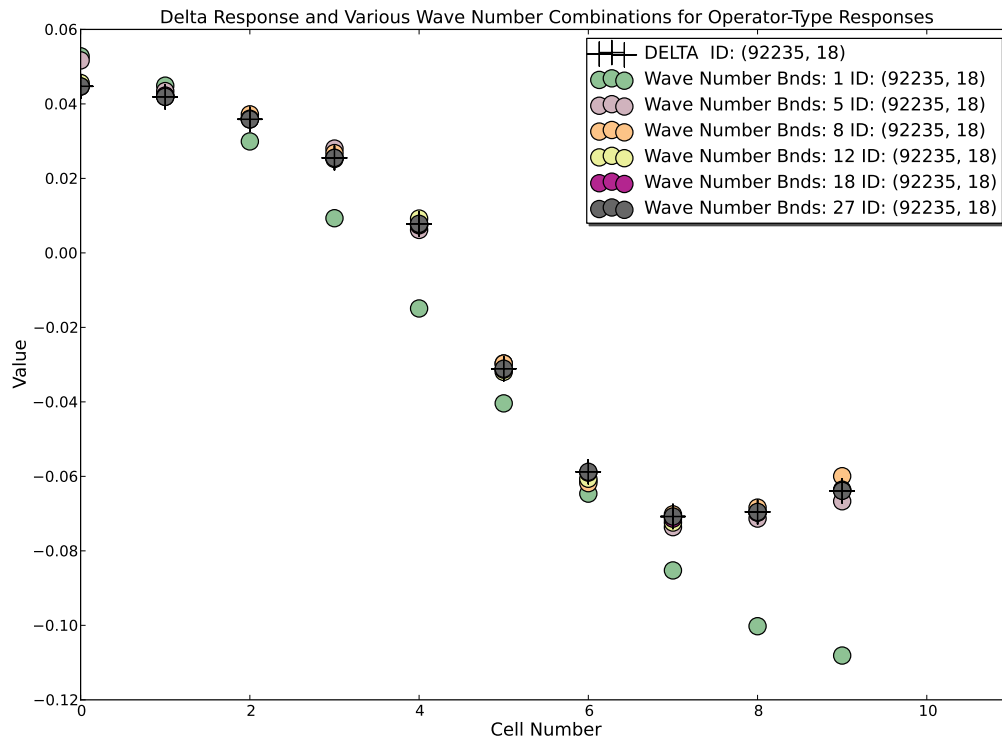


Figure 3.2: Godiva representative operator-type response sensitivity to parameter Uranium-235 fission plotted throughout the problem domain for various wave number bounds.

Operator-Type Response Sensitivity Percent Difference from Delta Response Sensitivity as a Function of Wave Number Bounds (Zoom)

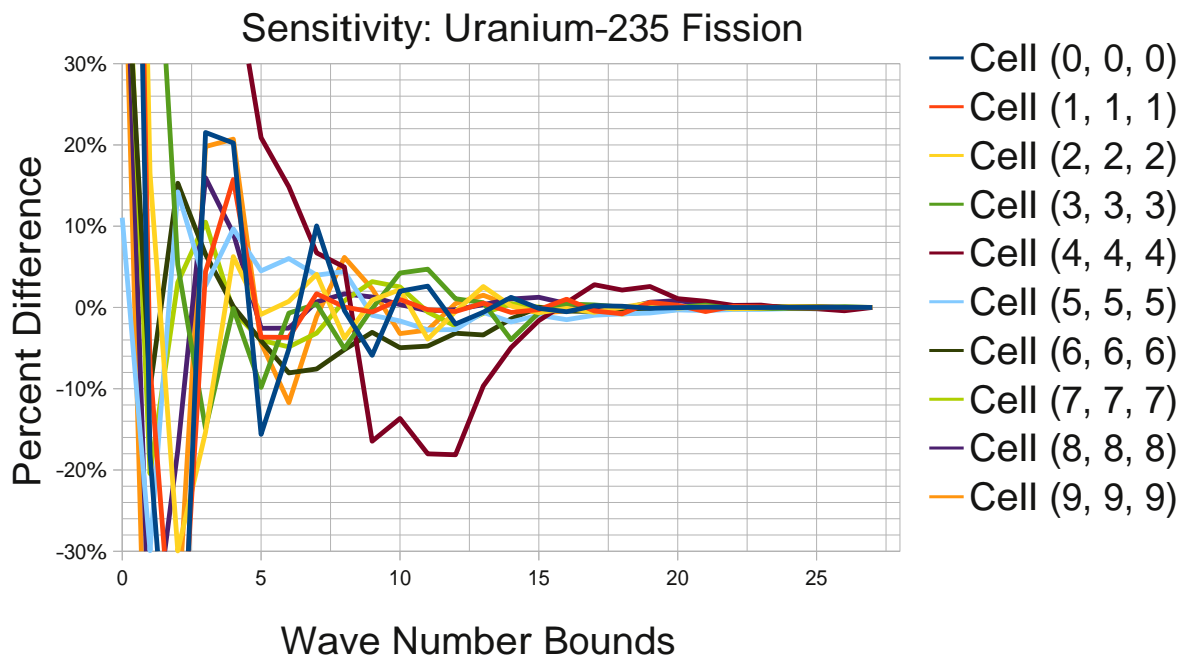


Figure 3.3: Godiva representative operator-type response percent difference compared with delta-type response plotted throughout the problem domain ($\text{Cell}(x_i, y_j, z_k)$) for all wave number bounds (0 through 27).

3.2.1.4 Calibration Results

Godiva bare was run using SCALE 's ENDF/BVII.0 27 group neutron library on an (x,y,z) mesh of (10,10,10) for a symmetric octant of the sphere. With $N_r = 8$ output responses and $m = 756$ input parameters the normalized chi-square metric was $\chi^2/N_r = 0.558304$ (see Eq. 2.32). Assuming a significance level of the central 90% range of a chi-square test yields (0.34158, 1.9384138). This amounts to giving a degree of confidence that the experimental and computed responses are indeed mutually and jointly consistent since the Godiva value falls well within this range.

Table 3.3 contains the measured, computed and best-estimate response values along with their respective percent standard deviations. Notice how the standard deviations, at worst (to the precision of the table), do not change and at best improve the least well known responses by several percent. Figure 3.4 represents a graphical version of the same data, only all the values have been normalized by the mean value of the measured response.

Figure 3.5 illustrates, for each response, the top eight relative sensitivities. For each response r_k , relative sensitivities were ranked such that $|S_{r_1}^k| < |S_{r_2}^k| < \dots < |S_{r_{N_\alpha}}^k|$. In other words, the eight parameters corresponding to the largest relative sensitivities are displayed in Figure 3.5. Recall that each response (except k_{eff}) includes the $^{235}\text{U}_{\text{fission}}$ reaction rate in the denominator and, as expected, due to this direct contribution the parameter appears in each response's top eight ranked relative sensitivities. These sensitivities were generated with R. T. Evans's sensitivity module implementation described in section 3.1.1.2.

Table 3.3: Godiva (M)asured responses values along with Denovo (C)omputed nominal values and (B)est-estimate predicted values with respective percent standard deviations.

Response		Value	± % Std. Dev.
k_{eff}	M	1.000	±0.1
	C	1.000770	±1.036
	B	0.999965	±0.099
$\frac{\sigma_f(^{238}\text{U})}{\sigma_f(^{235}\text{U})}$	M	0.1647	±1.1
	C	0.158845	±2.986
	B	0.164003	±1.022
$\frac{\sigma_f(^{233}\text{U})}{\sigma_f(^{235}\text{U})}$	M	1.590	±1.9
	C	1.566124	±1.062
	B	1.571240	±0.917
$\frac{\sigma_f(^{237}\text{Np})}{\sigma_f(^{235}\text{U})}$	M	0.837	±1.6
	C	0.852371	±6.802
	B	0.838473	±1.554
$\frac{\sigma_f(^{239}\text{Pu})}{\sigma_f(^{235}\text{U})}$	M	1.402	±1.8
	C	1.385034	±0.718
	B	1.390735	±0.547
$\frac{\sigma_\gamma(^{55}\text{Mn})}{\sigma_f(^{235}\text{U})}$	M	0.0027	±7.
	C	0.002931	±9.481
	B	0.002763	±5.642
$\frac{\sigma_\gamma(^{63}\text{Cu})}{\sigma_f(^{235}\text{U})}$	M	0.0117	±5.
	C	0.010735	±11.665
	B	0.011506	±4.603
$\frac{\sigma_\gamma(^{93}\text{Nb})}{\sigma_f(^{235}\text{U})}$	M	0.03	±10
	C	0.035269	±8.628
	B	0.032354	±6.517

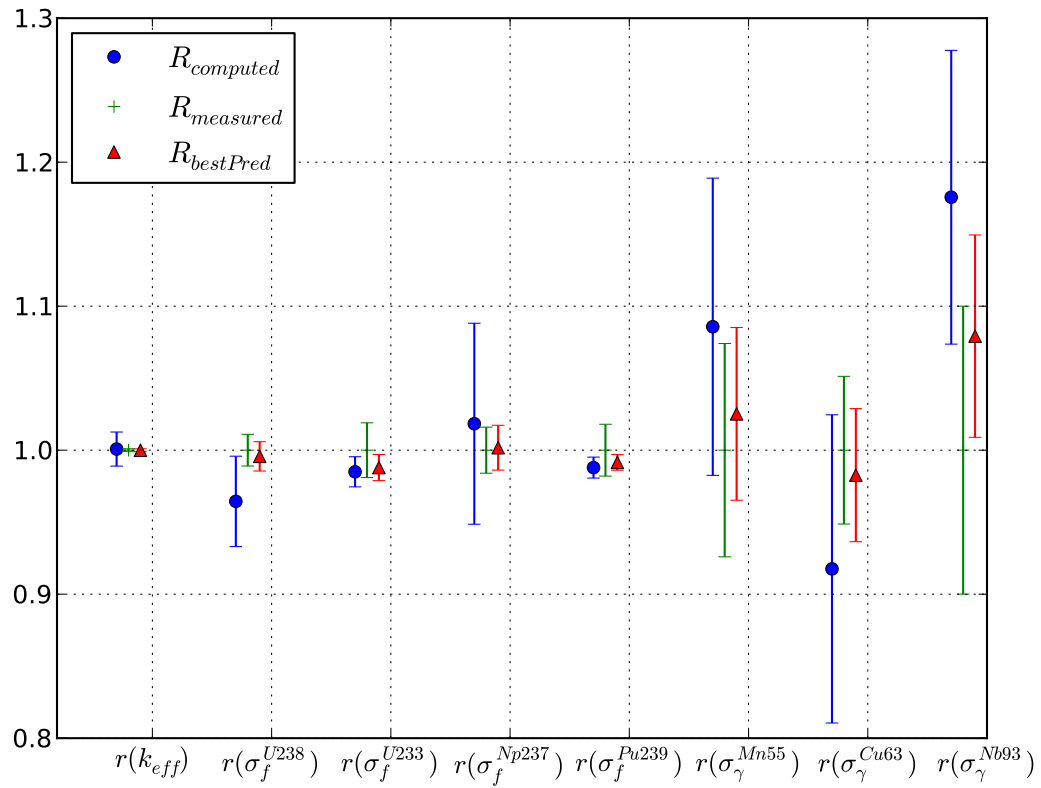


Figure 3.4: Godiva bare comparison of measured, computed and best-estimate response values. The figure is normalized to the mean of measured response on the y-axis while each response considered spans the x-axis.

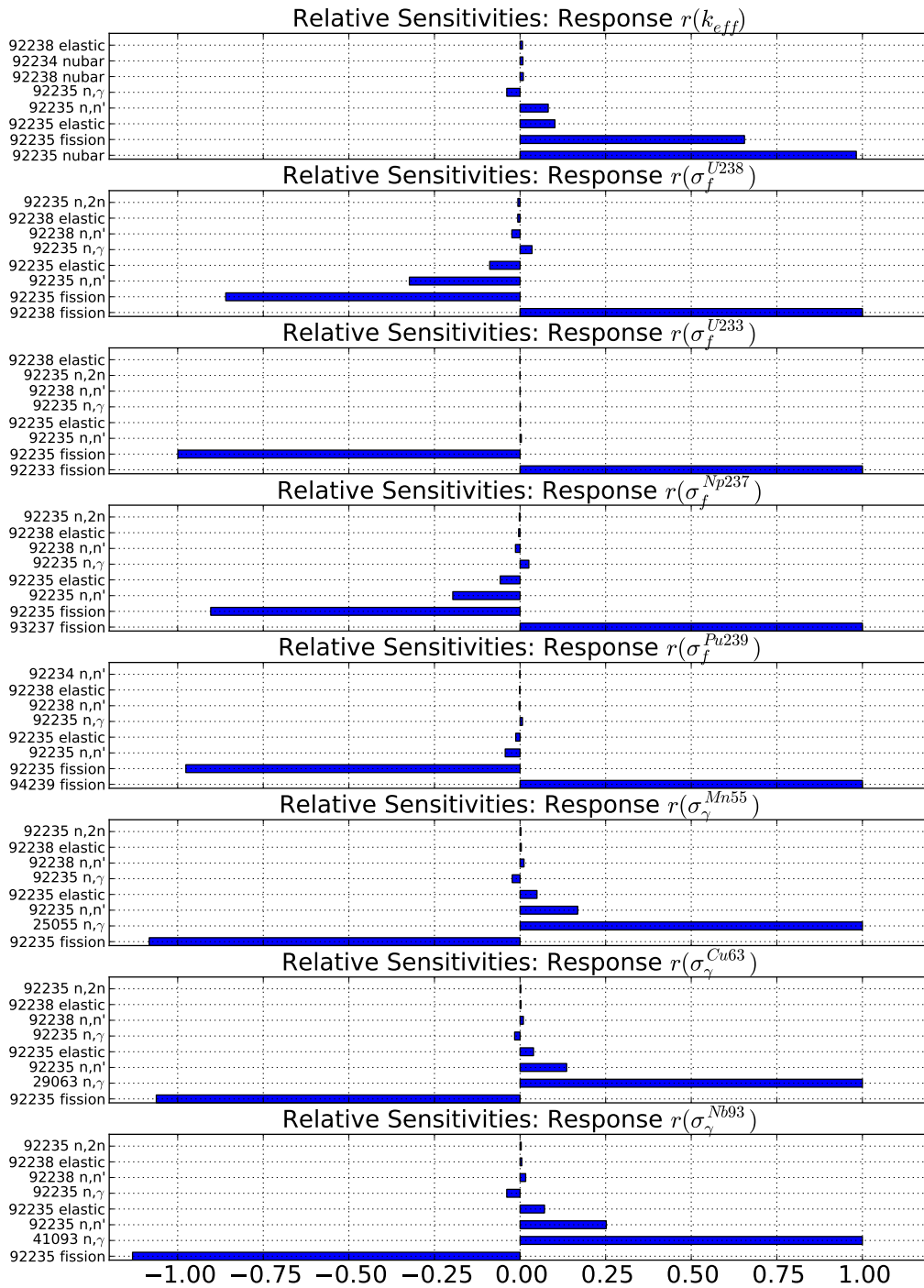


Figure 3.5: Godiva bare energy integrated relative sensitivities for each response for the top 8 contributing parameters. Y-axis label denotes particular parameter while x-axis denotes the (unit-less) relative sensitivity. X-axes for each sub-plot are common.

3.2.2 Jezebel

3.2.2.1 Benchmark Description

During the 1950's, the ^{239}Pu Jezebel critical assembly was built and operated at the Los Alamos Scientific Laboratory [25]. Actually, there were three separate Jezebel assemblies referred to as ^{239}Pu , ^{240}Pu and ^{233}U Jezebel. For the purposes of this demonstration, the pertinent information compiled by the ICSBEP on ^{239}Pu Jezebel is repeated in this document for completeness [4].

The exact specifications of all the parts and pieces that comprised the original ^{239}Pu Jezebel shown in Figure 3.6 are not available but the Los Alamos staff determined an equivalent uniform, homogeneous spherical computational model that is well defined and has been accepted as a critical benchmark experiment [21].

The average composition of the delta-phase plutonium alloy was 98.98 *wt.%* plutonium and 1.02 *wt.%* gallium. The isotopic composition of the plutonium is given in Table 3.4. The sphere of plutonium alloy had a mass of 17,020 grams with a density of 15.61 g/cm^3 and radius 6.3849 *cm*.

Table 3.4: Composition of the plutonium in ^{239}Pu Jezebel

Isotope	Abundance (at.%)
^{239}Pu	95.2
^{240}Pu	4.5
^{241}Pu	0.3

There were several experimental measurements using ^{239}Pu Jezebel but of interest for this work were the spectral indices at the core center. More specifically, central fission ratios and central activation ratios of several isotopes are compatible with Denovo's inhomogeneous adjoint capabilities described in section 3.1.1.

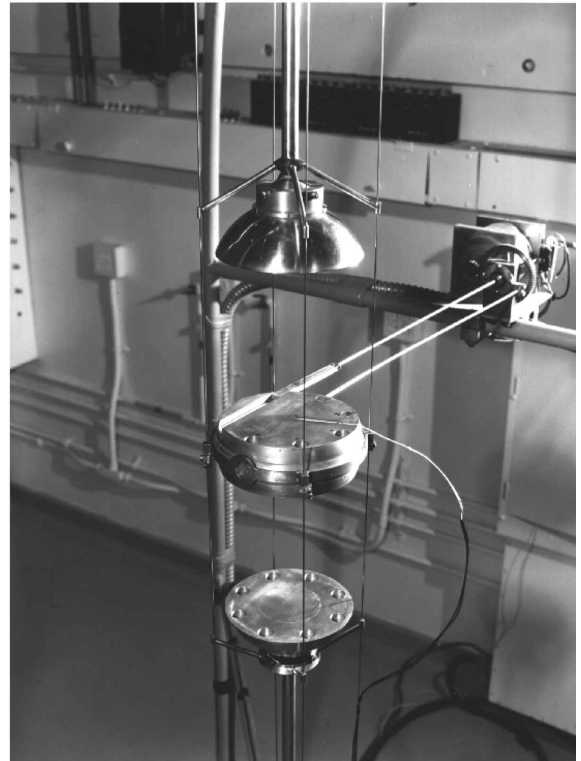
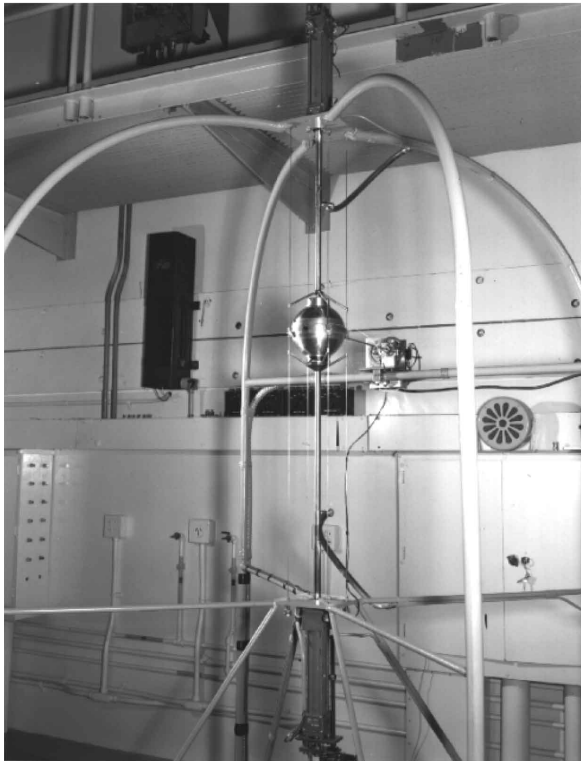
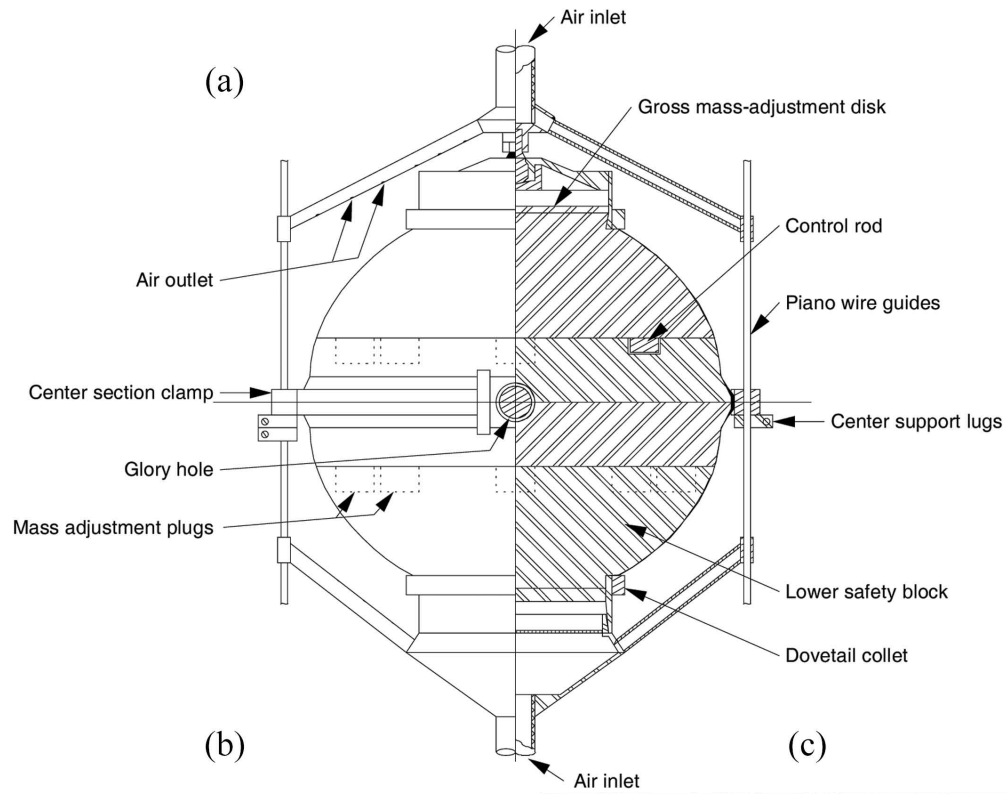


Figure 3.6: (a) The active portion of the original Jezebel assembly. (b) Jezebel in its assembled configuration. (c) Jezebel in its disassembled, or safe, configuration.

Eq. 3.24 is what is reported in [4] although originally only individual microscopic cross section reaction rates were reported in [5]. Ratios were given to compare the ^{239}Pu Jezebel experiment to other experiments including Flattop-25, Big Ten, Topsy and Van de Graaff. Table 3.6 contains the experimentally measured spectral indices of the responses used in this work along with their relative standard deviations. It also contains the measured k-eigenvalue with its relative standard deviation. A typical input listing for cross section processing preparation via SCALE 6.1 is given in Appendix A.2.

Table 3.5: Atom densities for ^{239}Pu Jezebel

Nuclide	Atom Density (atoms/barn-cm)
Ga	1.3752e-03
^{239}Pu	3.7047e-02
^{240}Pu	1.7512e-03
^{241}Pu	1.1674e-04

Table 3.6: Experimentally measured response values for ^{239}Pu Jezebel. Values were taken from ICSBEP PU-MET-FAST-001 Appendix C, Table D

Response	Measured \pm Rel. Std. Dev.
k_{eff}	1.000 \pm 0.002
$\sigma_f(^{238}\text{U})/\sigma_f(^{235}\text{U})$	0.2133 \pm 0.011
$\sigma_f(^{233}\text{U})/\sigma_f(^{235}\text{U})$	1.578 \pm 0.017
$\sigma_f(^{237}\text{Np})/\sigma_f(^{235}\text{U})$	0.9835 \pm 0.014
$\sigma_f(^{239}\text{Pu})/\sigma_f(^{235}\text{U})$	1.4609 \pm 0.0089
$\sigma_\gamma(^{55}\text{Mn})/\sigma_f(^{235}\text{U})$	0.0024 \pm 0.1
$\sigma_\gamma(^{63}\text{Cu})/\sigma_f(^{235}\text{U})$	0.0100 \pm 0.06
$\sigma_\gamma(^{93}\text{Nb})/\sigma_f(^{235}\text{U})$	0.023 \pm 0.09

3.2.2.2 Calibration Results

^{239}Pu Jezebel was run using SCALE 's ENDF/BVII.0 27 group neutron library on an (x,y,z) mesh of (10,10,10) for a symmetric octant of the sphere. With $N_r = 8$ output responses and $m = 1188$ input parameters the normalized chi-square metric was $\chi^2/N_r = 1.1030540$ (see Eq. 2.32). Assuming a significance level of the central 90% range of a chi-square test yields (0.34158, 1.9384138). This amounts to giving a degree of confidence that the experimental and computed responses are indeed mutually and jointly consistent since the Jezebel value falls well within this range.

Table 3.7 contains the measured, computed and best-estimate response values along with their respective percent standard deviations. Notice how the standard deviations, at worst (to the precision of the table), do not change and at best improve the least well known responses by several percent. Figure 3.7 represents a graphical version of the same data, only all the values have been normalized by the mean value of the measured response.

Figure 3.8 illustrates, for each response, the top eight relative sensitivities. For each response r_k , relative sensitivities were ranked such that $|S_{r_1}^k| < |S_{r_2}^k| < \dots < |S_{r_{N_\alpha}}^k|$. In other words, the eight parameters corresponding to the largest relative sensitivities are displayed in Figure 3.8. Recall that each response (except k_{eff}) includes the $^{235}\text{U}_{\text{fission}}$ reaction rate in the denominator and, as expected, due to this direct contribution the parameter appears in each response's top eight.

Table 3.7: Jezebel (M)easured responses values along with Denovo (C)omputed nominal values and (B)est-estimate predicted values with respective percent standard deviations.

Response		Value	± % Std. Dev.
k_{eff}	M	1.000	±0.2
	C	1.004021	±1.597
	B	0.999947	±0.198
$\frac{\sigma_f(^{238}\text{U})}{\sigma_f(^{235}\text{U})}$	M	0.2133	±1.1
	C	0.206333	±3.186
	B	0.213382	±0.971
$\frac{\sigma_f(^{233}\text{U})}{\sigma_f(^{235}\text{U})}$	M	1.578	±1.7
	C	1.553344	±1.036
	B	1.562144	±0.879
$\frac{\sigma_f(^{237}\text{Np})}{\sigma_f(^{235}\text{U})}$	M	0.9835	±1.4
	C	0.977273	±7.039
	B	0.984262	±1.392
$\frac{\sigma_f(^{239}\text{Pu})}{\sigma_f(^{235}\text{U})}$	M	1.4609	±0.89
	C	1.421973	±0.794
	B	1.439883	±0.509
$\frac{\sigma_\gamma(^{55}\text{Mn})}{\sigma_f(^{235}\text{U})}$	M	0.0024	±10
	C	0.002557	±9.1485
	B	0.002465	±7.3579
$\frac{\sigma_\gamma(^{63}\text{Cu})}{\sigma_f(^{235}\text{U})}$	M	0.0100	±6.
	C	0.009512	±10.570
	B	0.009828	±5.225
$\frac{\sigma_\gamma(^{93}\text{Nb})}{\sigma_f(^{235}\text{U})}$	M	0.023	±7.
	C	0.029013	±8.626
	B	0.025186	±6.026

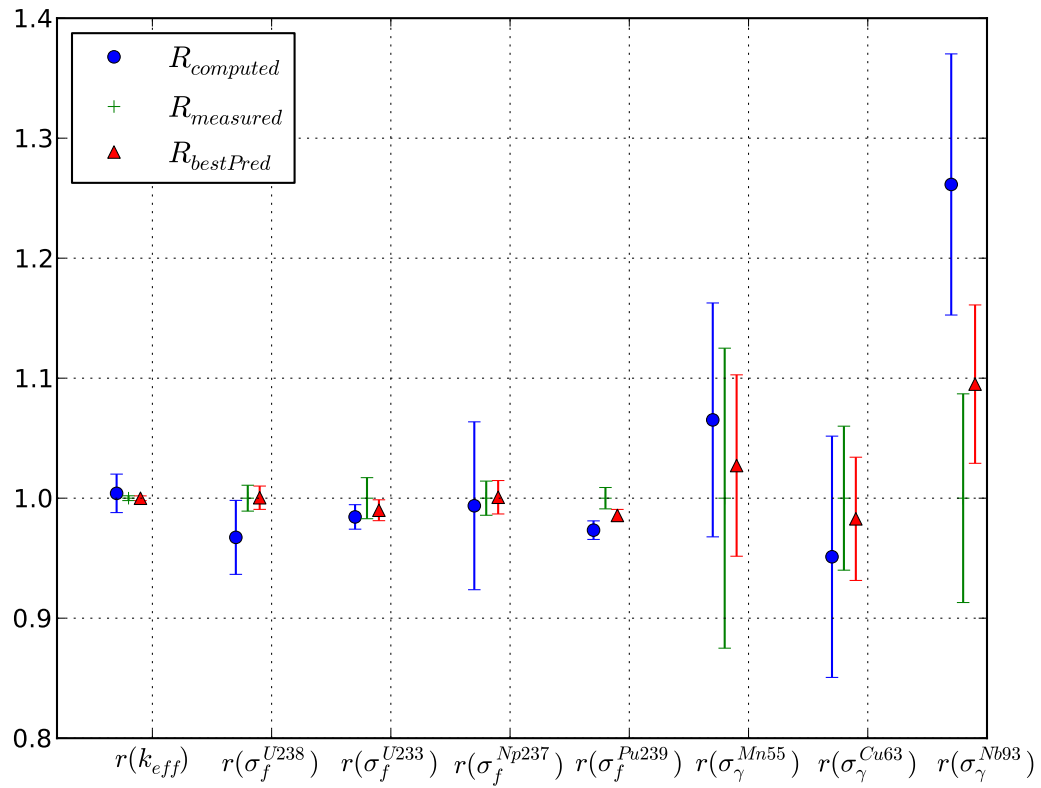


Figure 3.7: Jezebel comparison of measured, computed and best-estimate response values. The figure is normalized to the mean of measured response on the y-axis while each response considered spans the x-axis.

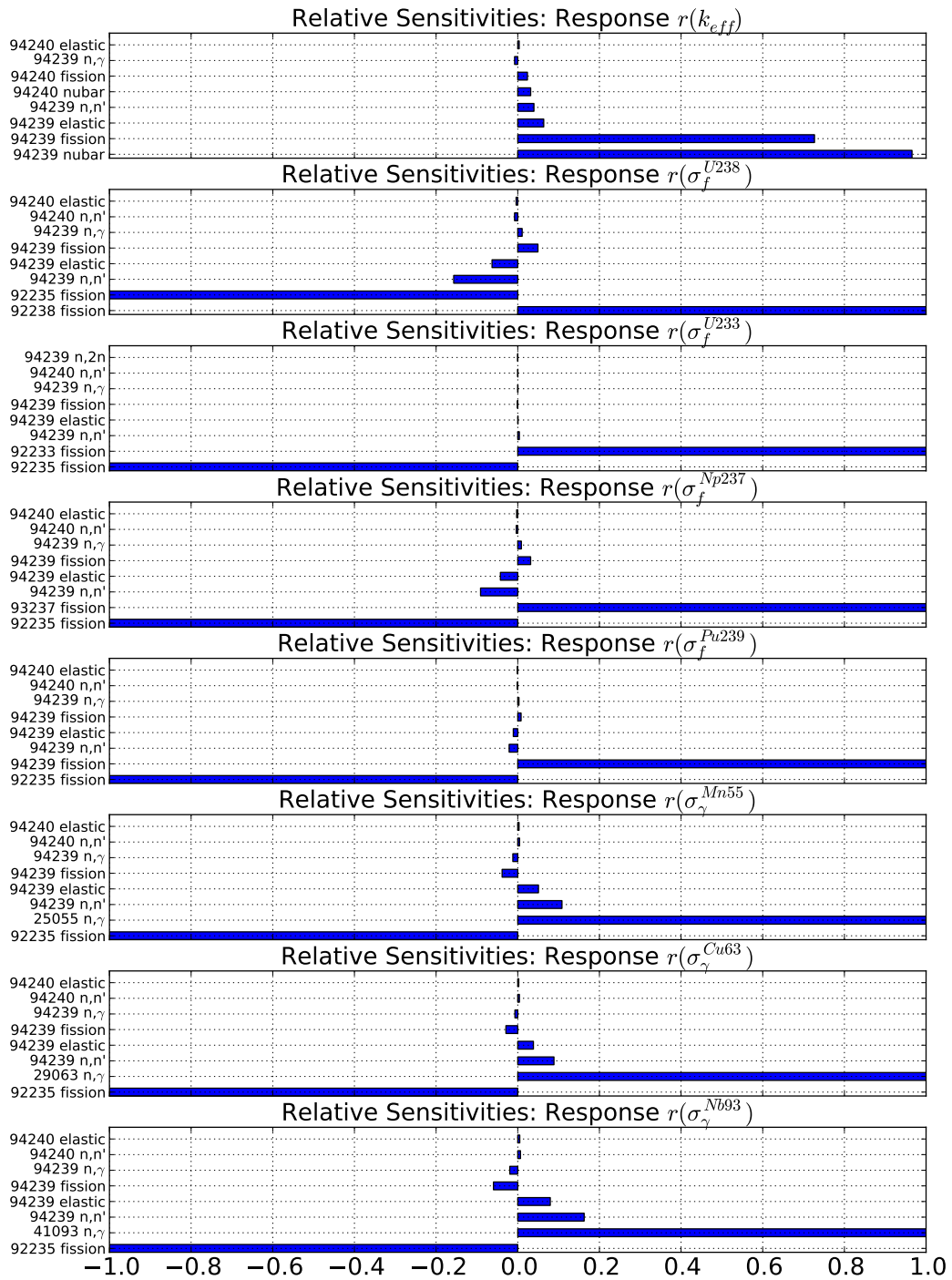


Figure 3.8: Jezebel energy integrated relative sensitivities for each response for the top 8 contributing parameters. Y-axis label denotes particular parameter while x-axis denotes the (unit-less) relative sensitivity. X-axes for each sub-plot are common.

3.2.3 LEU-COMP-THERM-008

3.2.3.1 Benchmark Description

Babcock and Wilcox's Lynchberg Research Center performed a series of lattice experiments with low-enriched UO_2 fuel in the early 1970's. In total, there were a series of 17 experiments conducted. All have been documented as part of the ICSBEP under the designation "LEU-COMP-THERM-008" (shorthand LCT) [4]. For this work, only "loading 2" will be considered.

Experiments were conducted inside of a large aluminum tank containing borated water and UO_2 fuel rods. Water height was kept at exactly 145 *cm* and soluble boron concentration was adjusted until the particular fuel configuration was slightly supercritical at 1.0007 for k_{eff} . The boron concentration was determined by titration with a standard deviation of ± 3 *PPM* boron.

LCT, shown in Figure 3.9, closely resembled a 3×3 array of pressurized water reactor (PWR) fuel assemblies with lattices configuration of 15×15 fuel pins per assembly. The 9 assemblies were surrounded by an irregularly shaped driver region that contained identical fuel.

For loading 2, a total of 4808 fuel rods and 153 water holes are configured in a uniform square pitch of 1.63576 *cm*. Dimensions are given in Figure 3.10. The outer radii of fuel rods and their aluminum 6061 cladding were 0.514858 *cm* and 0.602996 *cm* respectively. The density of UO_2 was taken as 10.24 *gm/cm*³ while the density of the Al was taken as 2.5052 *g/cm*³ to correct for fuel/clad gap. The density of the water was taken at 20°C; 0.99823 *g/cm*³. Isotopic number densities are given in Table 3.8. The effect of impurities in the fuel is modeled as an addition of ¹⁰B .

In addition to criticality measurements, relative rod-by-rod power densities were tabulated for the central assembly along a symmetric octant of the assembly in the $z = 0$ plane shown in Figure 3.11. The numbers are used as labels for the experimental data shown in Figure 3.12. Note that the data in Figure 3.12 is modified from its original ICSBEP source. The report claimed that the pin powers had been normalized by the average pin power across the entire central assembly. Upon calculation of the average, it was equal to 1.0338. The figure was

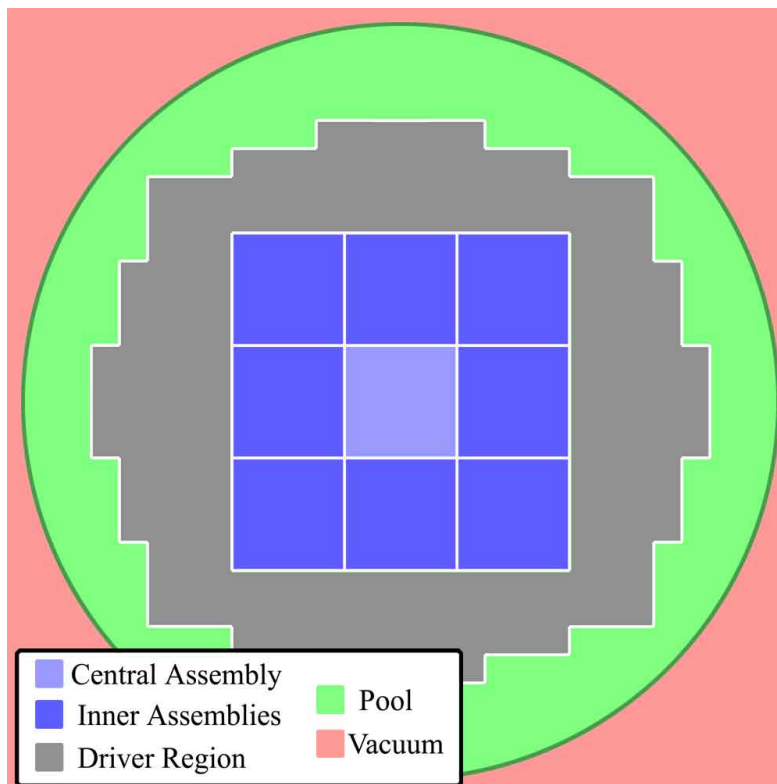


Figure 3.9: LCT Core Configuration.

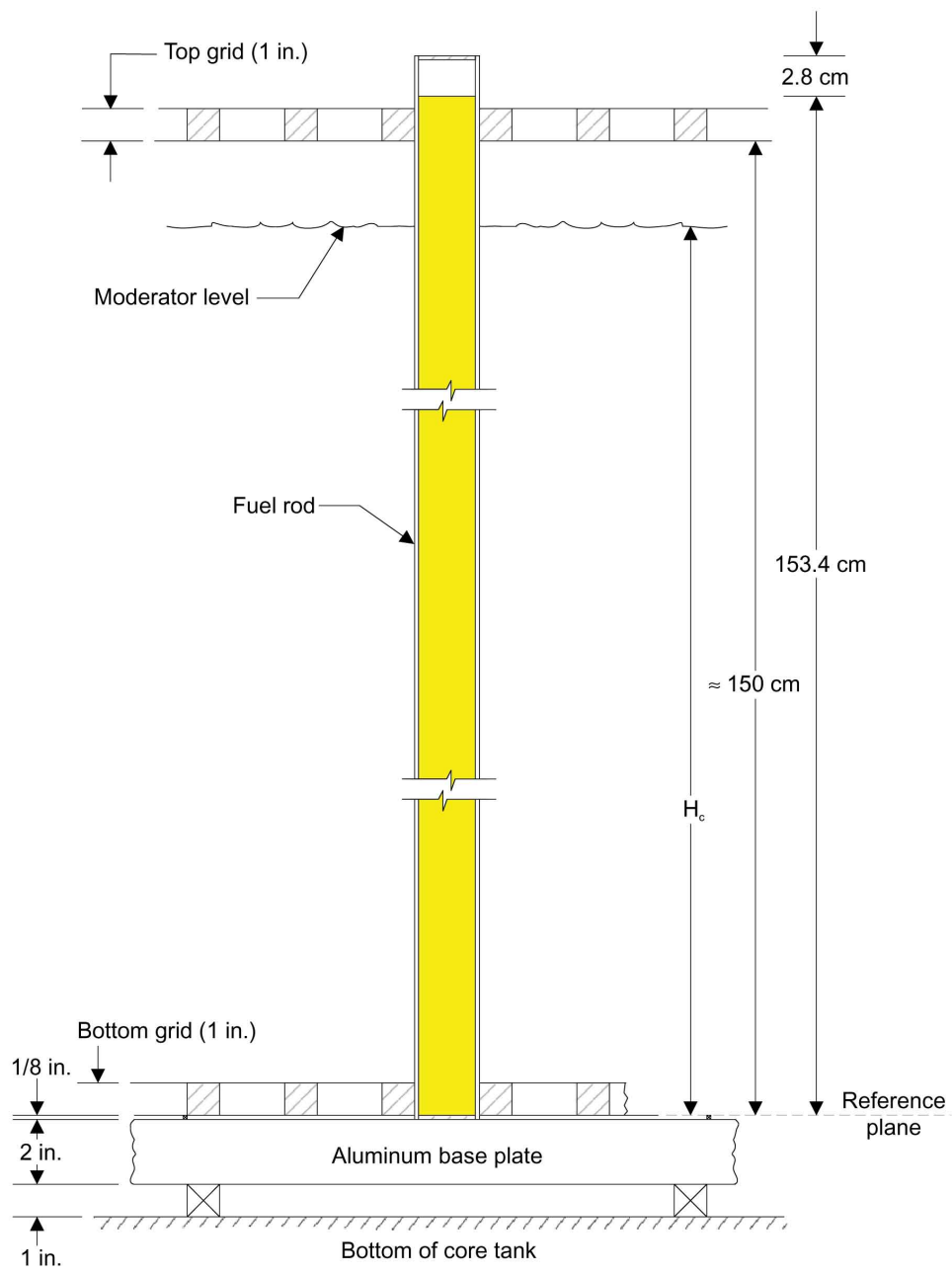


Figure 3.10: Vertical Dimensions of LCT.

Table 3.8: Atom densities for LCT Loading
 2. (Imp)urities modeled as boron;(Nat)ural
 isotope ratios; (Wat)er; (Sol)uable in water.

Nuclide	Atom Density (<i>atoms/barn - cm</i>)
²³⁴ U	4.5689e-6
²³⁵ U	5.6868e-4
²³⁸ U	2.2268e-2
¹⁶ O (Fuel)	4.5683e-2
¹⁰ B (Imp.)	2.6055e-7
Mg (Nat.)	6.2072e-4
²⁷ Al	5.3985e-2
Si (Nat.)	3.2230e-4
Ti (Nat.)	4.7263e-5
Cr (Nat.)	5.8029e-5
⁵⁵ Mn	4.1191e-5
Fe (Nat.)	1.8910e-4
Cu (Nat.)	5.9353e-5
Zn (Nat.)	5.7679e-5
¹ H	6.6737e-2
¹⁶ O (Wat.)	3.3369e-2
¹⁰ B (Sol.)	1.4821e-5
¹¹ B (Sol.)	5.9657e-5

renormalized to a value of one and this is what is shown here.

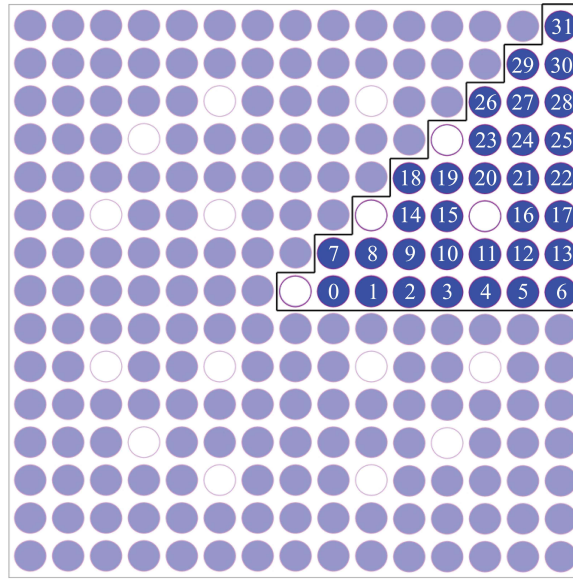


Figure 3.11: LCT central assembly pin numbering for a symmetric octant. White cylinders are water holes while the rest is fuel.

After having attempted parameter and response optimization via first-order data assimilation, some of the computed responses were discrepant with their measured counterparts. It was not clear exactly how the pin powers were measured other than for a specific excerpt in the ICSBEP write up. Unfortunately, the original text was not able to be located.

The only words given to the experimental setup with regards to the pin powers were “[t]he mid-plane relative power density over one-eighth of the central element was obtained for selected loadings. . . by using a sodium iodide (thallium activated) scintillation counter to count collimated fission product gammas from activated fuel rods”.

To be able to model what was experimentally collected would require more detailed information about the dimensions and setup of the detector(s), what conditions were the measurements taken at, etc. Another important piece that Denovo is capable of but is not being used currently is the coupled neutron gamma libraries. Based on these grounds, drawing conclusions

							31 0.89 (1.4%)
						29 0.938 (0.6%)	30 0.919 (0.5%)
					26 0.98 (0.2%)	27 0.941 (2.4%)	28 0.939 (1.2%)
			Water Hole	23 1.07 (0.6%)	24 0.97 (1.4%)	25 0.942 (2.7%)	
		18 1.06 (0.8%)	19 1.11 (0.7%)	20 1.1 (0.9%)	21 1 (2.5%)	22 0.894 (0.6%)	
	Water Hole	14 1.08 (1.1%)	15 1.08 (1.0%)	Water Hole	16 1.03 (0.9%)	17 0.935 (1.0%)	
	7 1.03 (0.2%)	8 1.04 (0.0%)	9 1 (0.7%)	10 1.01 (0.4%)	11 1.06 (0.6%)	12 0.99 (2.2%)	13 0.97 (3.1%)
Water Hole	0 1.07 (0.2%)	1 0.99 (0.6%)	2 0.97 (0.1%)	3 0.99 (0.7%)	4 0.99 (0.3%)	5 0.948 (2.1%)	6 0.951 (0.8%)

Figure 3.12: LCT central assembly experimental relative pin-by-pin power densities for a symmetric octant at the $z = 0$ plane. Top numbers are labels shown in Figure 3.11; Middle numbers are the power densities for that rod relative to the average for all rods in the central assembly; Bottom numbers are relative standard deviations.

from data adjustment procedures was deemed inappropriate. Nevertheless, this problem still can serve as a vehicle for the demonstration purposes of data optimization and higher-order validation techniques.

A typical input listing for cross section processing preparation via SCALE 6.1 is given in Appendix A.3.

3.2.3.2 Calibration Results

The responses to be computed, with the intention of comparing directly to the reported measurements, consist of k_{eff} and relative pin powers in the central assembly. The relative pin power for pin i can be defined by

$$r_i \equiv \frac{\langle \sigma_f, \phi \rangle_{\text{pin}_i}}{\langle \sigma_f, \phi \rangle_{\text{central assembly}}}, \quad (3.43)$$

where

$$\langle \sigma_f, \phi \rangle_{\text{pin}_i} = \int_{\Delta A_i} dx dy dE \sigma_f(x, y, z_0, E) \phi(x, y, z_0, E), \quad (3.44)$$

$$\langle \sigma_f, \phi \rangle_{\text{central assembly}} = \int_{\Delta A} dx dy dE \sigma_f(x, y, z_0, E) \phi(x, y, z_0, E), \quad (3.45)$$

and ϕ is the scalar flux, z_0 is the axial midpoint of the assembly, ΔA_i is the area to be integrated for pin i , and ΔA is the area to be integrated for the entire 15×15 central assembly. There is an implicit integration over z : the integrals are computed as sums over the cells contributing to the integration range, where each cell has a finite length in the z direction.

LCT was run on Jaguar as a single octant configuration with up to 7000 processors. The normalized fission reaction rates are shown in Figure 3.13. Relative rod-by-rod pin powers are shown for the central assembly in Figure 3.14. The quarter assembly is mirrored to produce the full result.

Cases were run with varying levels of detail, including spatial resolutions of 6×6 , 8×8 and 10×10 cells per fuel pin; 27, 44 and 238 neutron energy groups as well as different discretizations and angular quadratures. The computed versus measured response data shown in Figure 3.15 suggests that there may be differences greater than two standard deviations between measured and computed values (even without the error bars calculated for the computed responses).

Denovo computed responses were compared directly with the given MCNP computed responses as a check on the validity of the answers. Results of the comparison are given in Figure 3.16.

The decision was made to compute only a few of the responses with an associated adjoint calculation to produce first-order sensitivity values. These responses were specifically chosen by looking at Figure 3.15 and trying to find some of the “least discrepant” data. As discussed previously, not enough information was given in the ICSBEP writeup to draw conclusions on best-estimate predictions because the differences in computed and measured pin power procedures serve as too large of a discrepancy to warrant meaningful information. Nevertheless, the data assimilation framework may still be carried out at such a scale as long as the computational

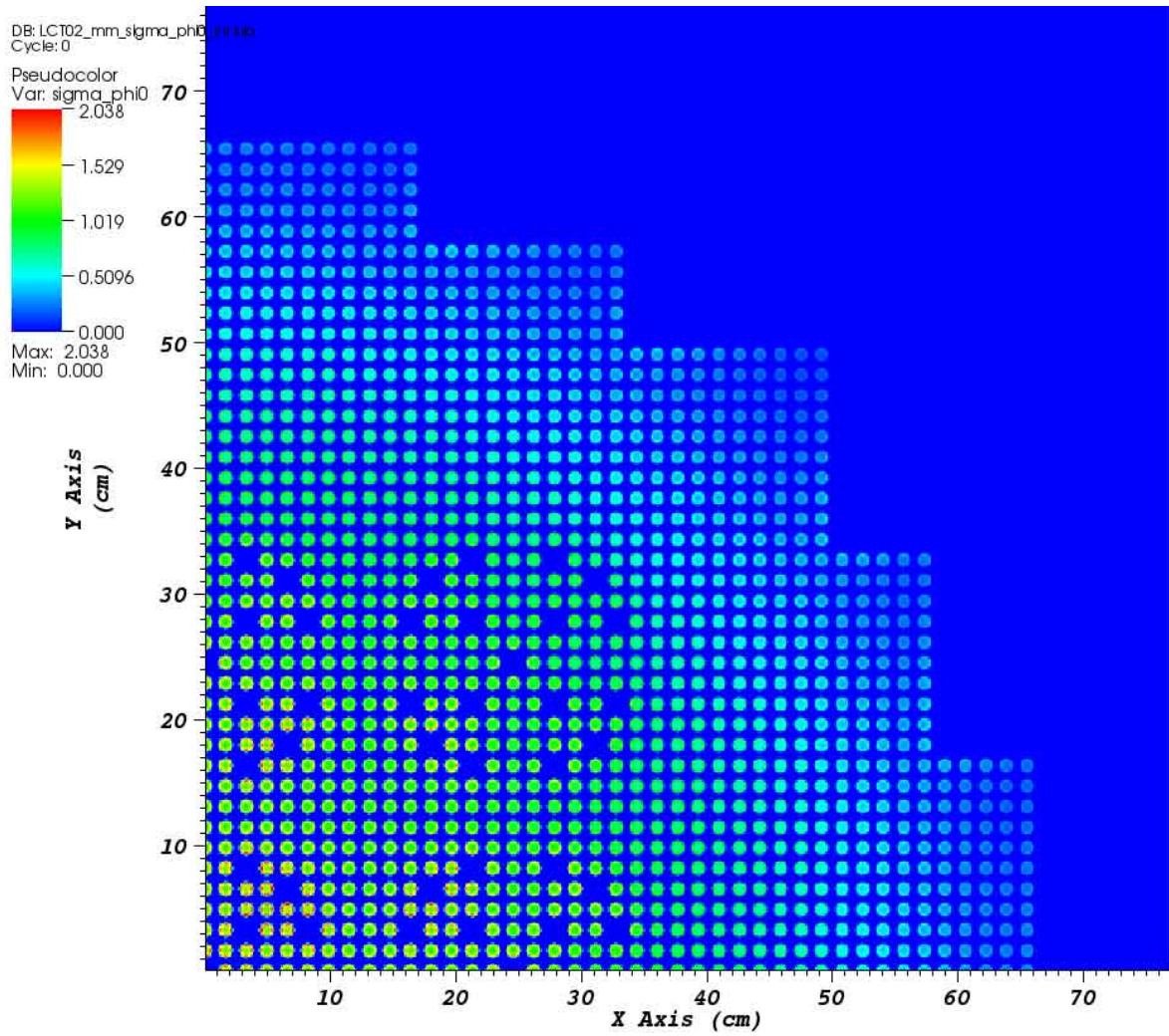


Figure 3.13: LCT axial $z = 0$ normalized fission reaction rate for quarter core symmetry.

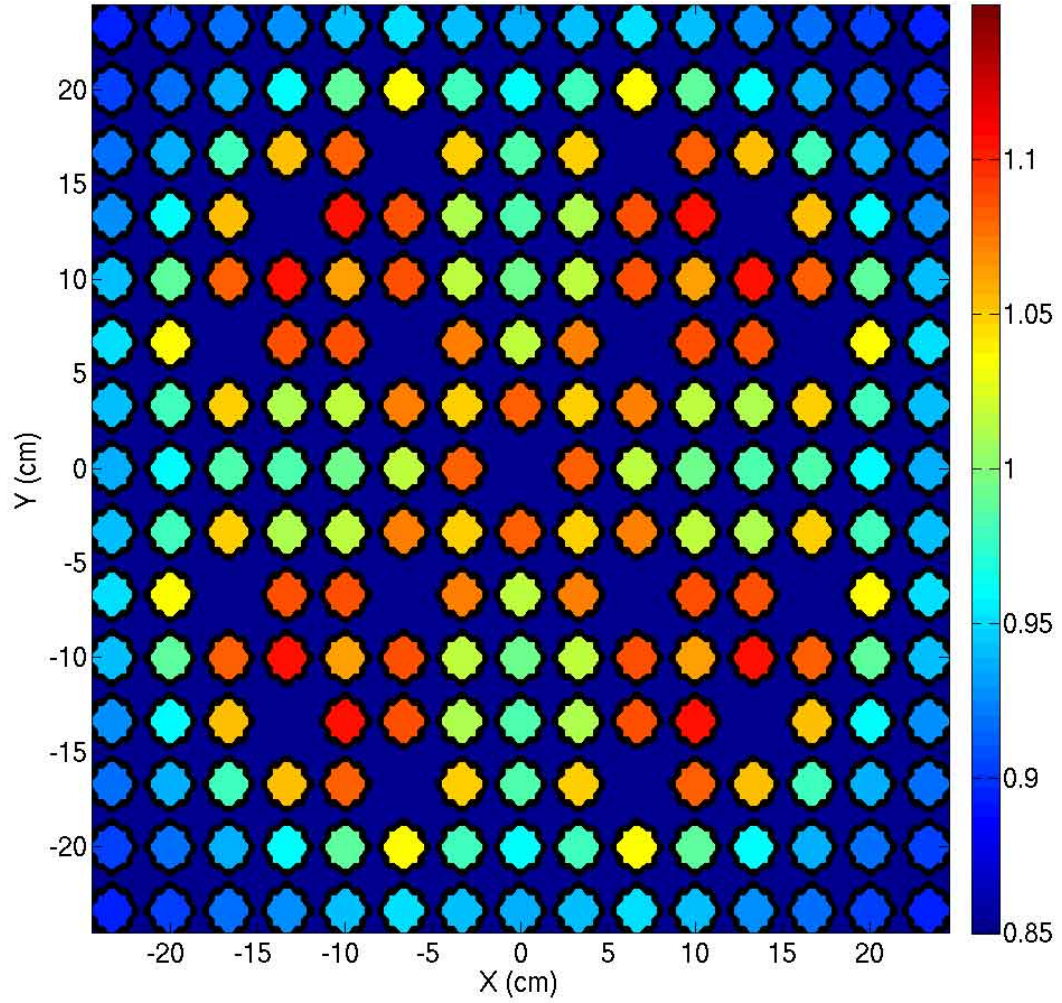


Figure 3.14: LCT axial $z = 0$ relative rod-by-rod power densities for the central assembly (mirrored for full assembly depiction).

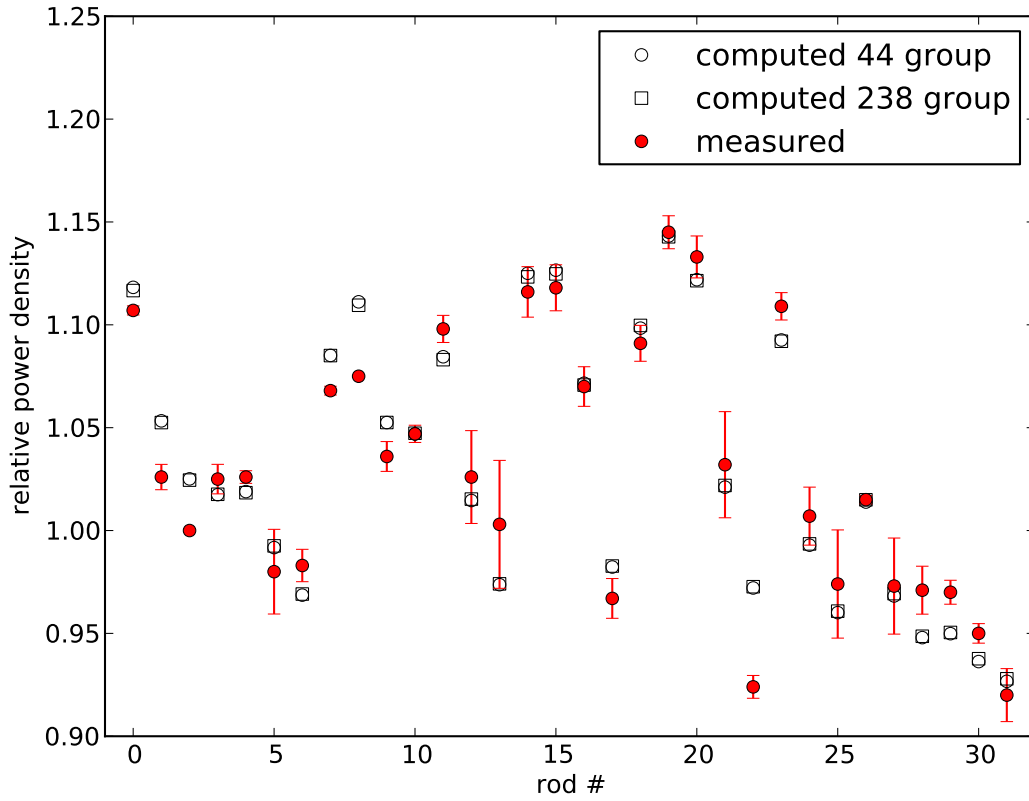


Figure 3.15: LCT 44 and 238 energy group computed vs. measured responses. Rod numbers are given in Figure 3.11.

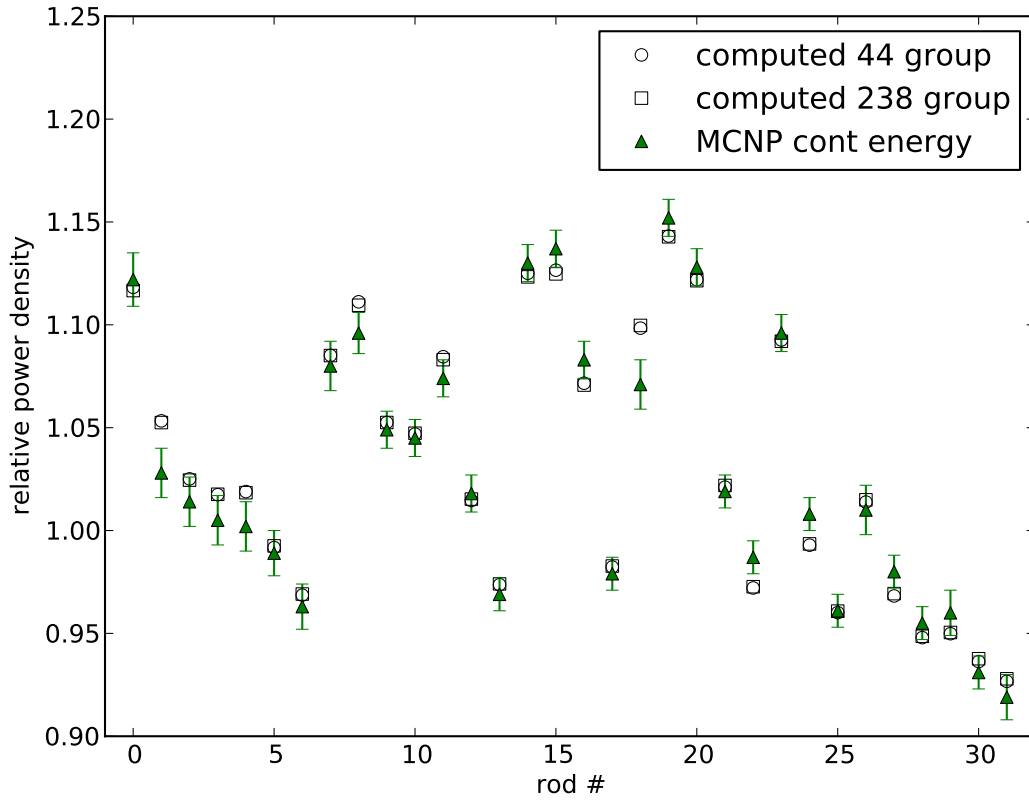


Figure 3.16: LCT 44 and 238 energy group computed vs. MCNP computed responses. Rod numbers are given in Figure 3.11.

resources are available.

For a particular instance, LCT was run using SCALE 's ENDF/BVII.0 44 group neutron library on a mesh of 8×8 cells per fuel pin for a symmetric octant of the core. With $N_r = 6$ output responses and $N_\alpha = 25960$ input parameters the normalized chi-square metric was $\chi^2/N_r = 0.38868053$ (see Eq. 2.32). Assuming a significance level of the central 90% range of a chi-square test yields (0.272563, 2.09860). The χ^2 metric is nearer to the boundary of the 90% confidence interval than either Godiva or Jezebel but still well within the given range.

In this case, where the experimentally measured uncertainties are much larger than the computational uncertainties, the data assimilation framework still reduces the overall uncertainties (albeit only slightly). The uncertainties will necessarily always be reduced no matter the quality of the experimental or computational data, even in scenarios with discrepant data.

Table 3.9 contains the measured, computed and best-estimate response values along with their respective percent standard deviations. Figure 3.17 represents a graphical version of the same data, only all the values have been normalized by the mean value of the measured response.

Figure 3.18 illustrates, for each response, the top ten relative sensitivities. For each response r_k , relative sensitivities were ranked such that $|S_{r_1}^k| < |S_{r_2}^k| < \dots < |S_{r_{N_\alpha}}^k|$. In other words, the ten parameters corresponding to the largest relative sensitivities are displayed in Figure 3.18.

Table 3.9: LCT (M)easured responses values along with Denovo (C)omputed nominal values and (B)est-estimate predicted values with respective percent standard deviations.

Response		Value	\pm % Std. Dev.
k_{eff}	M	1.0007	± 0.060
	C	0.999523	± 0.483
	B	1.000682	± 0.0595
Pin 10	M	1.047	± 0.4
	C	1.012703	± 0.00545
	B	1.012701	± 0.00541
Pin 12	M	1.026	± 2.2
	C	0.981426	± 0.00189
	B	0.981427	± 0.00187
Pin 13	M	1.003	± 3.1
	C	0.941852	± 0.00560
	B	0.941855	± 0.00551
Pin 14	M	1.116	± 1.1
	C	1.088263	± 0.00802
	B	1.088258	± 0.00785
Pin 15	M	1.118	± 1.0
	C	1.089721	± 0.00741
	B	1.089716	± 0.00728

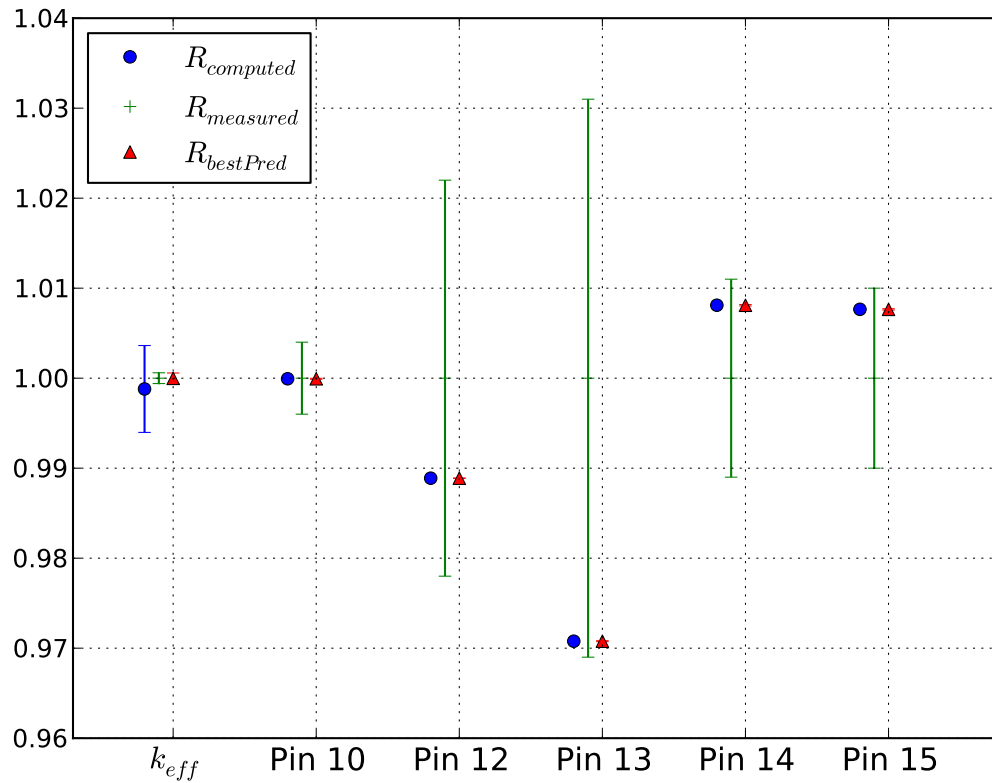


Figure 3.17: LCT comparison of measured, computed and best-estimate response values. Figure is normalized to the mean of measured response on the y-axis while each response considered spans the x-axis.

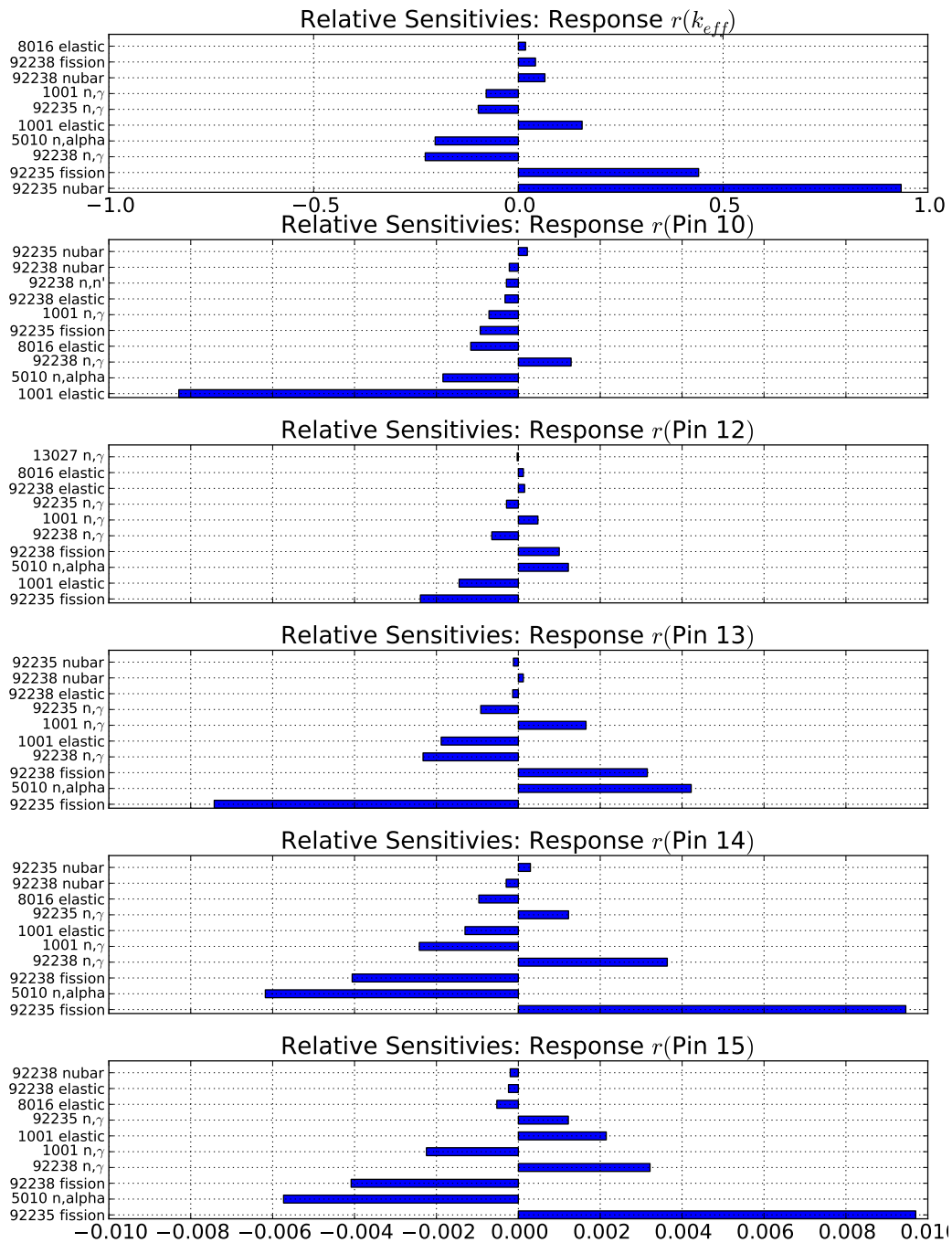


Figure 3.18: LCT energy integrated relative sensitivities for each response for the top 10 contributing parameters. Y-axis label denotes particular parameter while x-axis denotes the (unit-less) relative sensitivity. X-axes for each sub-plot are common except for k_{eff} .

Chapter 4

Higher-Order Moments for Quantifying Non-Gaussian Response Features

4.1 Mathematical Expressions

In the case that numerical and/or modeling errors may be treated via input parameters uncertainties within the input parameter vector $\boldsymbol{\alpha} = (\alpha_1, \dots, \alpha_{N_\alpha})^T$, a typical representation of the vector of responses, \boldsymbol{r} , as a function of the parameters is

$$\boldsymbol{r} = \boldsymbol{r}^c(\boldsymbol{\alpha}) = (r_1^c(\boldsymbol{\alpha}), \dots, r_{N_r}^c(\boldsymbol{\alpha}))^T, \quad (4.1)$$

where $\boldsymbol{r}^c(\boldsymbol{\alpha})$ indicates the computed response vector for a given set of parameters $\boldsymbol{\alpha}$.

Typically, to propagate parameter uncertainties through a computational model, a Taylor series expansion of the responses about a set of nominal parameter values, $\boldsymbol{\alpha}^0$ is carried out to the desired order of accuracy. In contradistinction to Chapter 2, second-order derivatives will

explicitly be taken into account, implying an expansion of the form

$$\mathbf{r}(\boldsymbol{\alpha}) = \mathbf{r}^c(\boldsymbol{\alpha}^0) + \nabla \mathbf{r}^c(\boldsymbol{\alpha}^0) + \frac{1}{2}(\boldsymbol{\alpha} - \boldsymbol{\alpha}^0)^T \nabla^2 \mathbf{r}^c(\boldsymbol{\alpha}^0)(\boldsymbol{\alpha} - \boldsymbol{\alpha}^0) + \dots \quad (4.2)$$

Rewritten in component form

$$\mathbf{r}(\boldsymbol{\alpha}) \approx \mathbf{r}^c(\boldsymbol{\alpha}^0) + \sum_{i_1=1}^{N_\alpha} \left. \frac{\partial \mathbf{r}^c}{\partial \alpha_{i_1}} \right|_{\boldsymbol{\alpha}^0} \delta \alpha_{i_1} + \frac{1}{2} \sum_{i_1=1}^{N_\alpha} \sum_{i_2=1}^{N_\alpha} \left. \frac{\partial^2 \mathbf{r}^c}{\partial \alpha_{i_1} \partial \alpha_{i_2}} \right|_{\boldsymbol{\alpha}^0} \delta \alpha_{i_1} \delta \alpha_{i_2}, \quad (4.3)$$

where $\delta \alpha_i = (\alpha_i - \alpha_i^0)$. For readability, the superscript “c” on \mathbf{r}^c will be suppressed in subsequent equations. Note that the following expressions are given in [9]. This work is a restatement of the proposed framework given by Cacuci.

4.1.1 Expectation Value

The expectation value, $E(\mathbf{r})$, is computed by integrating the expansion of the responses over the unknown joint probability distribution $p(\boldsymbol{\alpha}, \mathbf{r})$

$$E(\mathbf{r}) \equiv E(\mathbf{r}(\boldsymbol{\alpha})) = \int_{D_\alpha} \mathbf{r}(\boldsymbol{\alpha}) p(\boldsymbol{\alpha}, \mathbf{r}) d\boldsymbol{\alpha}, \quad (4.4)$$

where D_α is simply the domain of all α values. Substituting in the second-order Taylor expansion yields

$$\begin{aligned} E(\mathbf{r}) &= \int_{D_\alpha} \mathbf{r}(\boldsymbol{\alpha}^0) p(\boldsymbol{\alpha}, \mathbf{r}) d\boldsymbol{\alpha} + \int_{D_\alpha} \sum_{i_1=1}^{N_\alpha} \left. \frac{\partial \mathbf{r}}{\partial \alpha_{i_1}} \right|_{\boldsymbol{\alpha}^0} \delta \alpha_{i_1} p(\boldsymbol{\alpha}, \mathbf{r}) d\boldsymbol{\alpha} \\ &\quad + \frac{1}{2} \int_{D_\alpha} \sum_{i_1=1}^{N_\alpha} \sum_{i_2=1}^{N_\alpha} \left. \frac{\partial^2 \mathbf{r}}{\partial \alpha_{i_1} \partial \alpha_{i_2}} \right|_{\boldsymbol{\alpha}^0} \delta \alpha_{i_1} \delta \alpha_{i_2} p(\boldsymbol{\alpha}, \mathbf{r}) d\boldsymbol{\alpha}. \end{aligned}$$

Pulling terms independent of $\boldsymbol{\alpha}$ out of the integrals gives

$$\begin{aligned}
E(\mathbf{r}) &= \mathbf{r}(\boldsymbol{\alpha}^0) \int_{D_{\boldsymbol{\alpha}}} p(\boldsymbol{\alpha}, \mathbf{r}) d\boldsymbol{\alpha} + \sum_{i_1=1}^{N_{\boldsymbol{\alpha}}} \left. \frac{\partial \mathbf{r}}{\partial \alpha_{i_1}} \right|_{\boldsymbol{\alpha}^0} \int_{D_{\boldsymbol{\alpha}}} \delta \alpha_{i_1} p(\boldsymbol{\alpha}, \mathbf{r}) d\boldsymbol{\alpha} \\
&\quad + \frac{1}{2} \sum_{i_1=1}^{N_{\boldsymbol{\alpha}}} \sum_{i_2=1}^{N_{\boldsymbol{\alpha}}} \left. \frac{\partial^2 \mathbf{r}}{\partial \alpha_{i_1} \partial \alpha_{i_2}} \right|_{\boldsymbol{\alpha}^0} \int_{D_{\boldsymbol{\alpha}}} \delta \alpha_{i_1} \delta \alpha_{i_2} p(\boldsymbol{\alpha}, \mathbf{r}) d\boldsymbol{\alpha}.
\end{aligned}$$

The integrand in the first term integrates to 1 as $p(\boldsymbol{\alpha}, \mathbf{r})$ is a probability distribution. The integrand in the second term is the first central moment which is identically zero. The integrand in the third term is defined as the covariance between parameter α_{i_1} and parameter α_{i_2} . Thus, the second-order expectation value is

$$E(\mathbf{r}) = \mathbf{r}(\boldsymbol{\alpha}^0) + \frac{1}{2} \sum_{i_1=1}^{N_{\boldsymbol{\alpha}}} \sum_{i_2=1}^{N_{\boldsymbol{\alpha}}} \left. \frac{\partial^2 \mathbf{r}}{\partial \alpha_{i_1} \partial \alpha_{i_2}} \right|_{\boldsymbol{\alpha}^0} cov(\alpha_{i_1}, \alpha_{i_2}). \quad (4.5)$$

4.1.2 Variance-Covariance

The variance-covariance matrix of computed responses is defined as

$$\mathbf{C}_{\mathbf{r}\mathbf{c}} \equiv E([\mathbf{r} - E(\mathbf{r})][\mathbf{r} - E(\mathbf{r})]^T). \quad (4.6)$$

Focusing on a single general element we obtain

$$(\mathbf{C}_{\mathbf{r}\mathbf{c}})_{kl} = E([r_k - E(r_k)][r_l - E(r_l)]); \quad k, l = 1, \dots, \mathbf{N}_r.$$

Looking first at $[r_k - E(r_k)]$ gives

$$\begin{aligned}
r_k - E(r_k) &= \sum_{i_1=1}^{N_{\boldsymbol{\alpha}}} \left. \frac{\partial r_k}{\partial \alpha_{i_1}} \right|_{\boldsymbol{\alpha}^0} \delta \alpha_{i_1} + \\
&\quad \frac{1}{2} \sum_{i_1=1}^{N_{\boldsymbol{\alpha}}} \sum_{i_2=1}^{N_{\boldsymbol{\alpha}}} \left. \frac{\partial^2 r_k}{\partial \alpha_{i_1} \partial \alpha_{i_2}} \right|_{\boldsymbol{\alpha}^0} \delta \alpha_{i_1} \delta \alpha_{i_2} - \frac{1}{2} \sum_{i_1=1}^{N_{\boldsymbol{\alpha}}} \sum_{i_2=1}^{N_{\boldsymbol{\alpha}}} \left. \frac{\partial^2 r_k}{\partial \alpha_{i_1} \partial \alpha_{i_2}} \right|_{\boldsymbol{\alpha}^0} cov(\alpha_{i_1}, \alpha_{i_2}).
\end{aligned}$$

Multiply with $[r_l - E(r_l)]$:

$$\begin{aligned}
& [r_k - E(r_k)][r_l - E(r_l)] = \\
& \left[\sum_{i_1=1}^{N_\alpha} \frac{\partial r_k}{\partial \alpha_{i_1}} \Big|_{\alpha^0} \delta \alpha_{i_1} \right] \left[\sum_{i_2=1}^{N_\alpha} \frac{\partial r_l}{\partial \alpha_{i_2}} \Big|_{\alpha^0} \delta \alpha_{i_2} \right] + \\
& \frac{1}{2} \left[\sum_{i_1=1}^{N_\alpha} \frac{\partial r_k}{\partial \alpha_{i_1}} \Big|_{\alpha^0} \delta \alpha_{i_1} \right] \left[\sum_{i_2=1}^{N_\alpha} \sum_{i_3=1}^{N_\alpha} \frac{\partial^2 r_l}{\partial \alpha_{i_2} \partial \alpha_{i_3}} \Big|_{\alpha^0} \delta \alpha_{i_2} \delta \alpha_{i_3} - \sum_{i_2=1}^{N_\alpha} \sum_{i_3=1}^{N_\alpha} \frac{\partial^2 r_l}{\partial \alpha_{i_2} \partial \alpha_{i_3}} \Big|_{\alpha^0} cov(\alpha_{i_2}, \alpha_{i_3}) \right] + \\
& \frac{1}{2} \left[\sum_{i_1=1}^{N_\alpha} \sum_{i_2=1}^{N_\alpha} \frac{\partial^2 r_k}{\partial \alpha_{i_1} \partial \alpha_{i_2}} \Big|_{\alpha^0} \delta \alpha_{i_1} \delta \alpha_{i_2} - \sum_{i_1=1}^{N_\alpha} \sum_{i_2=1}^{N_\alpha} \frac{\partial^2 r_k}{\partial \alpha_{i_1} \partial \alpha_{i_2}} \Big|_{\alpha^0} cov(\alpha_{i_1}, \alpha_{i_2}) \right] \left[\sum_{i_3=1}^{N_\alpha} \frac{\partial r_l}{\partial \alpha_{i_3}} \Big|_{\alpha^0} \delta \alpha_{i_3} \right] + \\
& \frac{1}{2} \left[\sum_{i_1=1}^{N_\alpha} \sum_{i_2=1}^{N_\alpha} \frac{\partial^2 r_k}{\partial \alpha_{i_1} \partial \alpha_{i_2}} \Big|_{\alpha^0} \delta \alpha_{i_1} \delta \alpha_{i_2} - \sum_{i_1=1}^{N_\alpha} \sum_{i_2=1}^{N_\alpha} \frac{\partial^2 r_k}{\partial \alpha_{i_1} \partial \alpha_{i_2}} \Big|_{\alpha^0} cov(\alpha_{i_1}, \alpha_{i_2}) \right] \times \\
& \frac{1}{2} \left[\sum_{i_3=1}^{N_\alpha} \sum_{i_4=1}^{N_\alpha} \frac{\partial^2 r_l}{\partial \alpha_{i_3} \partial \alpha_{i_4}} \Big|_{\alpha^0} \delta \alpha_{i_3} \delta \alpha_{i_4} - \sum_{i_3=1}^{N_\alpha} \sum_{i_4=1}^{N_\alpha} \frac{\partial^2 r_l}{\partial \alpha_{i_3} \partial \alpha_{i_4}} \Big|_{\alpha^0} cov(\alpha_{i_3}, \alpha_{i_4}) \right].
\end{aligned}$$

Rearranging:

$$\begin{aligned}
& [r_k - E(r_k)][r_l - E(r_l)] = \\
& \sum_{i_1=1}^{N_\alpha} \sum_{i_2=1}^{N_\alpha} \frac{\partial r_k}{\partial \alpha_{i_1}} \frac{\partial r_l}{\partial \alpha_{i_2}} \Big|_{\alpha^0} \delta \alpha_{i_1} \delta \alpha_{i_2} + \\
& \frac{1}{2} \sum_{i_1=1}^{N_\alpha} \sum_{i_2=1}^{N_\alpha} \sum_{i_3=1}^{N_\alpha} \left(\frac{\partial r_k}{\partial \alpha_{i_1}} \frac{\partial^2 r_l}{\partial \alpha_{i_2} \partial \alpha_{i_3}} + \frac{\partial r_l}{\partial \alpha_{i_1}} \frac{\partial^2 r_k}{\partial \alpha_{i_2} \partial \alpha_{i_3}} \right) \Big|_{\alpha^0} [\delta \alpha_{i_1} \delta \alpha_{i_2} \delta \alpha_{i_3} - \delta \alpha_{i_1} cov(\alpha_{i_2}, \alpha_{i_3})] + \\
& \frac{1}{4} \sum_{i_1=1}^{N_\alpha} \sum_{i_2=1}^{N_\alpha} \sum_{i_3=1}^{N_\alpha} \sum_{i_4=1}^{N_\alpha} \frac{\partial^2 r_k}{\partial \alpha_{i_1} \partial \alpha_{i_2}} \frac{\partial^2 r_l}{\partial \alpha_{i_3} \partial \alpha_{i_4}} \Big|_{\alpha^0} \times \\
& [\delta \alpha_{i_1} \delta \alpha_{i_2} \delta \alpha_{i_3} \delta \alpha_{i_4} - \delta \alpha_{i_1} \delta \alpha_{i_2} cov(\alpha_{i_3}, \alpha_{i_4}) \\
& - cov(\alpha_{i_1}, \alpha_{i_2}) \delta \alpha_{i_3} \delta \alpha_{i_4} + cov(\alpha_{i_1}, \alpha_{i_2}) cov(\alpha_{i_3}, \alpha_{i_4})]. \tag{4.7}
\end{aligned}$$

Multiply by probability $p(\boldsymbol{\alpha}, \mathbf{r})$, integrate over the parameter domain and factor out constants evaluated at $\boldsymbol{\alpha}^0$:

$$\begin{aligned}
& E([r_k - E(r_k)][r_l - E(r_l)]) = \\
& \sum_{i_1=1}^{N_\alpha} \sum_{i_2=1}^{N_\alpha} \frac{\partial r_k}{\partial \alpha_{i_1}} \frac{\partial r_l}{\partial \alpha_{i_2}} \Big|_{\boldsymbol{\alpha}^0} \int_{D_\alpha} \delta \alpha_{i_1} \delta \alpha_{i_2} p(\boldsymbol{\alpha}, \mathbf{r}) d\boldsymbol{\alpha} + \\
& \frac{1}{2} \sum_{i_1=1}^{N_\alpha} \sum_{i_2=1}^{N_\alpha} \sum_{i_3=1}^{N_\alpha} \left(\frac{\partial r_k}{\partial \alpha_{i_1}} \frac{\partial^2 r_l}{\partial \alpha_{i_2} \partial \alpha_{i_3}} + \frac{\partial r_l}{\partial \alpha_{i_1}} \frac{\partial^2 r_k}{\partial \alpha_{i_2} \partial \alpha_{i_3}} \right) \Big|_{\boldsymbol{\alpha}^0} \times \\
& \left(\int_{D_\alpha} [\delta \alpha_{i_1} \delta \alpha_{i_2} \delta \alpha_{i_3}] p(\boldsymbol{\alpha}, \mathbf{r}) d\boldsymbol{\alpha} - \right. \\
& \left. cov(\alpha_{i_2}, \alpha_{i_3}) \int_{D_\alpha} [\delta \alpha_{i_1}] p(\boldsymbol{\alpha}, \mathbf{r}) d\boldsymbol{\alpha} \right) + \\
& \frac{1}{4} \sum_{i_1=1}^{N_\alpha} \sum_{i_2=1}^{N_\alpha} \sum_{i_3=1}^{N_\alpha} \sum_{i_4=1}^{N_\alpha} \left(\frac{\partial^2 r_k}{\partial \alpha_{i_1} \partial \alpha_{i_2}} \frac{\partial^2 r_l}{\partial \alpha_{i_3} \partial \alpha_{i_4}} \Big|_{\boldsymbol{\alpha}^0} \right) \times \\
& \left(\int_{D_\alpha} [\delta \alpha_{i_1} \delta \alpha_{i_2} \delta \alpha_{i_3} \delta \alpha_{i_4}] p(\boldsymbol{\alpha}, \mathbf{r}) d\boldsymbol{\alpha} - \right. \\
& cov(\alpha_{i_3}, \alpha_{i_4}) \int_{D_\alpha} [\delta \alpha_{i_1} \delta \alpha_{i_2}] p(\boldsymbol{\alpha}, \mathbf{r}) d\boldsymbol{\alpha} - \\
& cov(\alpha_{i_1}, \alpha_{i_2}) \int_{D_\alpha} [\delta \alpha_{i_3} \delta \alpha_{i_4}] p(\boldsymbol{\alpha}, \mathbf{r}) d\boldsymbol{\alpha} + \\
& \left. cov(\alpha_{i_1}, \alpha_{i_2}) cov(\alpha_{i_3}, \alpha_{i_4}) \int_{D_\alpha} p(\boldsymbol{\alpha}, \mathbf{r}) d\boldsymbol{\alpha} \right).
\end{aligned}$$

Evaluating the integrals and collapsing the summation symbols for readability:

$$\begin{aligned}
& E([r_k - E(r_k)][r_l - E(r_l)]) = \\
& \sum_{i_1, i_2=1}^{N_\alpha} \frac{\partial r_k}{\partial \alpha_{i_1}} \frac{\partial r_l}{\partial \alpha_{i_2}} \Big|_{\boldsymbol{\alpha}^0} cov(\alpha_{i_1}, \alpha_{i_2}) + \\
& \frac{1}{2} \sum_{i_1, i_2, i_3=1}^{N_\alpha} \left(\frac{\partial r_k}{\partial \alpha_{i_1}} \frac{\partial^2 r_l}{\partial \alpha_{i_2} \partial \alpha_{i_3}} + \frac{\partial r_l}{\partial \alpha_{i_1}} \frac{\partial^2 r_k}{\partial \alpha_{i_2} \partial \alpha_{i_3}} \right) \Big|_{\boldsymbol{\alpha}^0} \mu_{1,1,1}(\alpha_{i_1}, \alpha_{i_2}, \alpha_{i_3}) + \\
& \frac{1}{4} \sum_{i_1, i_2, i_3, i_4=1}^{N_\alpha} \frac{\partial^2 r_k}{\partial \alpha_{i_1} \partial \alpha_{i_2}} \frac{\partial^2 r_l}{\partial \alpha_{i_3} \partial \alpha_{i_4}} \Big|_{\boldsymbol{\alpha}^0} \times \\
& (\mu_{1,1,1,1}(\alpha_{i_1}, \alpha_{i_2}, \alpha_{i_3}, \alpha_{i_4}) - cov(\alpha_{i_1}, \alpha_{i_2}) cov(\alpha_{i_3}, \alpha_{i_4})),
\end{aligned}$$

where $\mu_{1,1,1}(\alpha_{i_1}, \alpha_{i_2}, \alpha_{i_3})$ and $\mu_{1,1,1,1}(\alpha_{i_1}, \alpha_{i_2}, \alpha_{i_3}, \alpha_{i_4})$ represent the third and fourth order mixed central moments respectively. Neglecting parameter cross-correlations that are higher than second-order and are multiplied by second-order derivatives reduces $\mu_{1,1,1}(\alpha_{i_1}, \alpha_{i_2}, \alpha_{i_3})$ and $\mu_{1,1,1,1}(\alpha_{i_1}, \alpha_{i_2}, \alpha_{i_3}, \alpha_{i_4})$ to simply third (unnormalized skewness) and fourth (unnormalized kurtosis) order central moments $\mu_3(\alpha_{i_1})$ and $\mu_4(\alpha_{i_1})$. The computed response variance-covariance matrix \mathbf{C}_{rc} of element (k, l) is finally given by

$$\begin{aligned}
(\mathbf{C}_{rc})_{kl} = & \sum_{i_1, i_2=1}^{N_\alpha} \frac{\partial r_k}{\partial \alpha_{i_1}} \frac{\partial r_l}{\partial \alpha_{i_2}} \Big|_{\boldsymbol{\alpha}^0} cov(\alpha_{i_1}, \alpha_{i_2}) \\
& + \frac{1}{2} \sum_{i_1=1}^{N_\alpha} \left(\frac{\partial r_k}{\partial \alpha_{i_1}} \frac{\partial^2 r_l}{\partial \alpha_{i_1}^2} + \frac{\partial r_l}{\partial \alpha_{i_1}} \frac{\partial^2 r_k}{\partial \alpha_{i_1}^2} \right) \Big|_{\boldsymbol{\alpha}^0} \mu_3(\alpha_{i_1}) \\
& + \frac{1}{4} \sum_{i_1=1}^{N_\alpha} \frac{\partial^2 r_k}{\partial \alpha_{i_1}^2} \frac{\partial^2 r_l}{\partial \alpha_{i_1}^2} \Big|_{\boldsymbol{\alpha}^0} \mu_4(\alpha_{i_1}) \\
& - \frac{1}{4} \sum_{i_1, i_2, i_3, i_4=1}^{N_\alpha} \frac{\partial^2 r_k}{\partial \alpha_{i_1} \partial \alpha_{i_2}} \frac{\partial^2 r_l}{\partial \alpha_{i_3} \partial \alpha_{i_4}} \Big|_{\boldsymbol{\alpha}^0} cov(\alpha_{i_1}, \alpha_{i_2}) cov(\alpha_{i_3}, \alpha_{i_4}). \quad (4.8)
\end{aligned}$$

For convenience, computed response variance-covariance matrix \mathbf{C}_{rc} of diagonal element (k, k) is given by

$$\begin{aligned}
(\mathbf{C}_{rc})_{kk} \equiv E([r_k - E(r_k)]^2) = & \sum_{i_1, i_2=1}^{N_\alpha} \frac{\partial r_k}{\partial \alpha_{i_1}} \frac{\partial r_k}{\partial \alpha_{i_2}} \Big|_{\boldsymbol{\alpha}^0} cov(\alpha_{i_1}, \alpha_{i_2}) \\
& + \sum_{i_1=1}^{N_\alpha} \frac{\partial r_k}{\partial \alpha_{i_1}} \frac{\partial^2 r_k}{\partial \alpha_{i_1}^2} \Big|_{\boldsymbol{\alpha}^0} \mu_3(\alpha_{i_1}) \\
& + \frac{1}{4} \sum_{i_1=1}^{N_\alpha} \frac{\partial^2 r_k}{\partial \alpha_{i_1}^2} \frac{\partial^2 r_k}{\partial \alpha_{i_1}^2} \Big|_{\boldsymbol{\alpha}^0} \mu_4(\alpha_{i_1}) \\
& - \frac{1}{4} \left(\sum_{i_1, i_2=1}^{N_\alpha} \frac{\partial^2 r_k}{\partial \alpha_{i_1} \partial \alpha_{i_2}} \Big|_{\boldsymbol{\alpha}^0} cov(\alpha_{i_1}, \alpha_{i_2}) \right)^2. \quad (4.9)
\end{aligned}$$

4.1.3 Skewness

Skewness is a measure of the asymmetry of a probability distribution. Referring to Figure 4.1, a distribution with a long right tail would have a positive skewness while a distribution with a long left tail would have a negative skewness. The skewness of a response r_k is

$$\gamma_1(r_k) \equiv \sqrt{\beta_1(r_k)} \equiv \frac{E([r_k - E(r_k)]^3)}{[E([r_k - E(r_k)]^2)]^{3/2}} = \frac{\mu_3(r_k)}{\mu_2(r_k)^{3/2}}. \quad (4.10)$$

Only the central moment of order 3 need be computed since the denominator was obtained

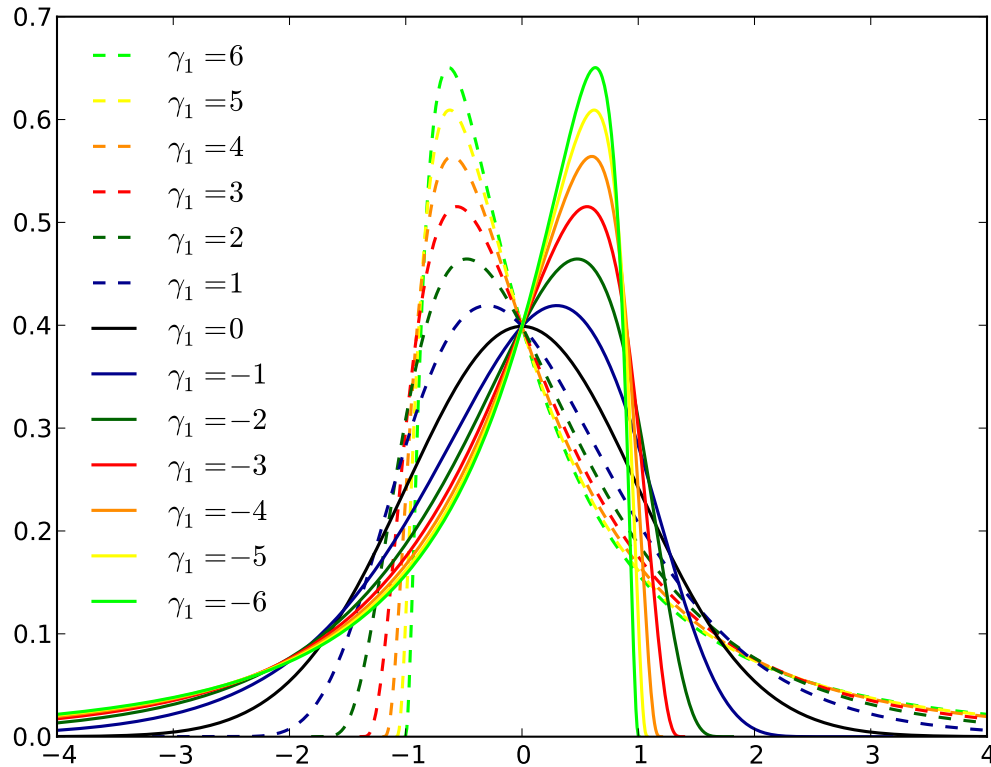


Figure 4.1: Examples of distributions whose tails are skewed to the left (negative skewness) and to the right (positive skewness) for a generalized Normal distribution.

as the response covariance. The result of the full derivation of the third order central moment may be found in Appendix B.1. The final result is reproduced here as

$$\begin{aligned}
\mu_3(r_k) &\equiv E([r_k - E(r_k)]^3) = \\
&\frac{1}{2} \sum_{i_1=1}^{N_\alpha} \left(\frac{\partial^2 r_k}{\partial \alpha_{i_1}^2} \right) \mu_4(\alpha_{i_1}) \left[3 \left(\frac{\partial r_k}{\partial \alpha_{i_1}} \right)^2 - \frac{3}{4} \left(\frac{\partial^2 r_k}{\partial \alpha_{i_1}^2} \right) \sum_{i_2, i_3=1}^{N_\alpha} \left(\frac{\partial^2 r_k}{\partial \alpha_{i_2} \partial \alpha_{i_3}} \right) cov(\alpha_{i_2}, \alpha_{i_3}) \right] \\
&+ \sum_{i_1=1}^{N_\alpha} \left(\frac{\partial r_k}{\partial \alpha_{i_1}} \right) \mu_3(\alpha_{i_1}) \left[\left(\frac{\partial r_k}{\partial \alpha_{i_1}} \right)^2 - \frac{3}{2} \left(\frac{\partial^2 r_k}{\partial \alpha_{i_1}^2} \right) \sum_{i_2, i_3=1}^{N_\alpha} \left(\frac{\partial^2 r_k}{\partial \alpha_{i_2} \partial \alpha_{i_3}} \right) cov(\alpha_{i_2}, \alpha_{i_3}) \right] \\
&+ \sum_{\substack{i_1, i_2, i_3=1 \\ i_1 \neq i_2 \neq i_3}}^{N_\alpha} \left(\frac{\partial r_k}{\partial \alpha_{i_1}} \right) \left(\frac{\partial r_k}{\partial \alpha_{i_2}} \right) \left(\frac{\partial r_k}{\partial \alpha_{i_3}} \right) \mu_{1,1,1}(\alpha_{i_1}, \alpha_{i_2}, \alpha_{i_3}) \\
&- \frac{3}{2} \left[\sum_{i_1, i_2=1}^{N_\alpha} \left(\frac{\partial r_k}{\partial \alpha_{i_1}} \right) \left(\frac{\partial r_k}{\partial \alpha_{i_2}} \right) cov(\alpha_{i_1}, \alpha_{i_2}) \right] \left[\sum_{i_3, i_4=1}^{N_\alpha} \left(\frac{\partial^2 r_k}{\partial \alpha_{i_3} \partial \alpha_{i_4}} \right) cov(\alpha_{i_3}, \alpha_{i_4}) \right] \\
&+ \frac{1}{4} \left(\sum_{i_1, i_2=1}^{N_\alpha} \left(\frac{\partial^2 r_k}{\partial \alpha_{i_1} \partial \alpha_{i_2}} \right) cov(\alpha_{i_1}, \alpha_{i_2}) \right)^3. \tag{4.11}
\end{aligned}$$

4.1.4 Kurtosis

Kurtosis is any measure of "peakedness" of a probability distribution when compared with a normal distribution. As illustrated in Figure 4.2, more acute peaks are called leptokurtic and have a kurtosis value greater than 3 while flatter peaks are deemed platykurtic and have a kurtosis value less than 3. Kurtosis is defined as the fourth central moment divided by the square of the variance:

$$\beta_2(r_k) \equiv \frac{E([r_k - E(r_k)]^4)}{[E([r_k - E(r_k)]^2)]^2} = \frac{\mu_4(r_k)}{\mu_2(r_k)^2}. \tag{4.12}$$

A similar measure, the excess kurtosis, is defined as the kurtosis minus three:

$$\gamma_2(r_k) \equiv \beta_2(r_k) - 3. \tag{4.13}$$

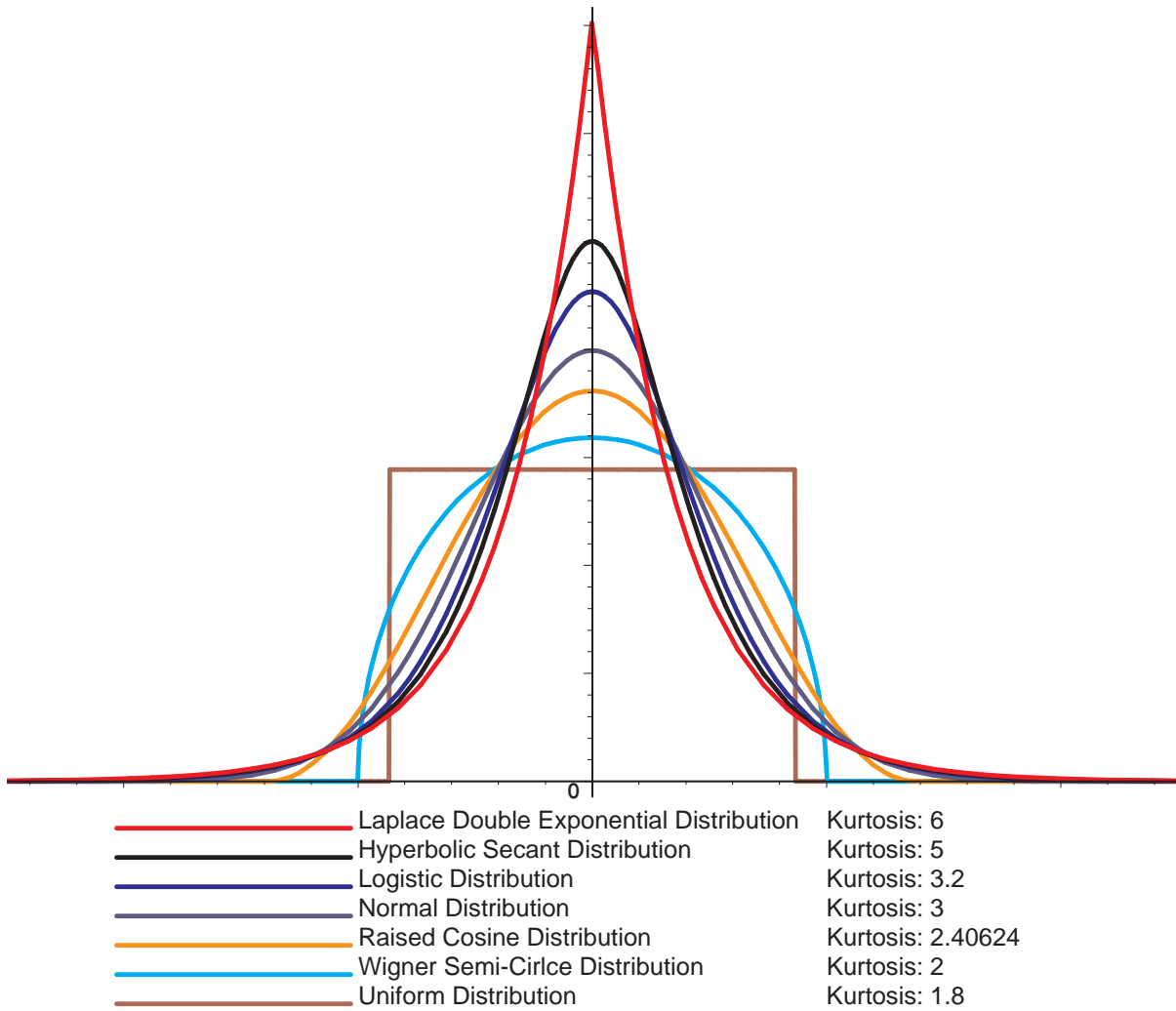


Figure 4.2: Examples of distributions whose peaks are higher (leptokurtic), equal to (mesokurtic) and less than (platykurtic) a standard Gaussian.

The derivation of the fourth central moment can be found in Appendix B.2. The final result is reproduced here as

$$\begin{aligned}
\mu_4(r_k) &\equiv E([r_k - E(r_k)]^4) = \\
&\sum_{i_1=1}^{N_\alpha} \mu_4(\alpha_{i_1}) \left\{ \left(\frac{\partial r_k}{\partial \alpha_{i_1}} \right)^4 + \frac{3}{8} \left(\frac{\partial^2 r_k}{\partial \alpha_{i_1}^2} \right)^2 \left[\sum_{i_2, i_3=1}^{N_\alpha} \left(\frac{\partial^2 r_k}{\partial \alpha_{i_2} \partial \alpha_{i_3}} \right) \text{cov}(i_2, i_3) \right]^2 \right. \\
&\quad \left. - 3 \left(\frac{\partial r_k}{\partial \alpha_{i_1}} \right)^2 \left(\frac{\partial^2 r_k}{\partial \alpha_{i_1}^2} \right) \left[\sum_{i_2, i_3=1}^{N_\alpha} \left(\frac{\partial^2 r_k}{\partial \alpha_{i_2} \partial \alpha_{i_3}} \right) \text{cov}(\alpha_{i_2}, \alpha_{i_3}) \right] \right\} \\
&\quad + \sum_{\substack{i_1, i_2, i_3, i_4=1 \\ i_1 \neq i_2 \neq i_3 \neq i_4}}^{N_\alpha} \left(\frac{\partial r_k}{\partial \alpha_{i_1}} \right) \left(\frac{\partial r_k}{\partial \alpha_{i_2}} \right) \left(\frac{\partial r_k}{\partial \alpha_{i_3}} \right) \left(\frac{\partial r_k}{\partial \alpha_{i_4}} \right) \mu_{1,1,1,1}(\alpha_{i_1}, \alpha_{i_2}, \alpha_{i_3}, \alpha_{i_4}) \\
&\quad + \sum_{i_1=1}^{N_\alpha} \mu_3(\alpha_{i_1}) \left(\frac{\partial r_k}{\partial \alpha_{i_1}} \right) \left\{ \frac{3}{2} \left(\frac{\partial^2 r_k}{\partial \alpha_{i_1}^2} \right) \left[\sum_{i_2, i_3=1}^{N_\alpha} \left(\frac{\partial^2 r_k}{\partial \alpha_{i_2} \partial \alpha_{i_3}} \right) \text{cov}(i_2, i_3) \right]^2 \right. \\
&\quad \left. - 2 \left(\frac{\partial r_k}{\partial \alpha_{i_1}} \right)^2 \left[\sum_{i_2, i_3=1}^{N_\alpha} \left(\frac{\partial^2 r_k}{\partial \alpha_{i_2} \partial \alpha_{i_3}} \right) \text{cov}(i_2, i_3) \right] \right\} \\
&\quad + \frac{3}{2} \left[\sum_{i_1, i_2=1}^{N_\alpha} \left(\frac{\partial r_k}{\partial \alpha_{i_1}} \right) \left(\frac{\partial r_k}{\partial \alpha_{i_2}} \right) \text{cov}(\alpha_{i_1}, \alpha_{i_2}) \right] \left[\sum_{i_3, i_4=1}^{N_\alpha} \left(\frac{\partial^2 r_k}{\partial \alpha_{i_3} \partial \alpha_{i_4}} \right) \text{cov}(\alpha_{i_3}, \alpha_{i_4}) \right]^2 \\
&\quad - \frac{3}{16} \left[\sum_{i_1, i_2=1}^{N_\alpha} \left(\frac{\partial^2 r_k}{\partial \alpha_{i_1} \partial \alpha_{i_2}} \right) \text{cov}(i_1, i_2) \right]^4. \tag{4.14}
\end{aligned}$$

4.2 Higher-Order Computed Response Moments: Applications

4.2.1 Computational Framework

All of the derivatives given in section 4.1 are evaluated at nominal parameter values $\boldsymbol{\alpha}^0$. One quantity in particular, the mixed second-order response derivatives, denoted here as

$$q_k(\rho_{i_1 i_2}) \equiv \sum_{i_1, i_2=1}^{N_\alpha} \frac{\partial^2 r_k(\boldsymbol{\alpha}^0)}{\partial \alpha_{i_1} \partial \alpha_{i_2}} \text{cov}(\alpha_{i_1}, \alpha_{i_2}) = \sum_{i_1, i_2=1}^{N_\alpha} \frac{\partial^2 r_k(\boldsymbol{\alpha}^0)}{\partial \alpha_{i_1} \partial \alpha_{i_2}} \rho_{i_1 i_2} \sigma_{i_1} \sigma_{i_2}, \tag{4.15}$$

appears multiple times in expressions for $E(r_k)$, $cov(r_k, r_l)$, $var(r_k)$, $\mu_3(r_k)$ and $\mu_4(r_k)$. For reference $\rho_{i_1 i_2}$ is the correlation between parameters α_{i_1} and α_{i_2} while σ_{i_1} and σ_{i_2} , denote the standard deviations of the respective parameters. To fully evaluate these derivatives would require $O(\mathbf{N}_\alpha^2)$ forward model computations for each response $r_k(\boldsymbol{\alpha}^0)$ [18].

In the limiting case where all input parameters are completely correlated, $\rho_{i_1 i_2} = 1$, the quantity $q_k(\rho_{i_1 i_2} = 1)$ may be computed very efficiently by considering the column vector of standard deviations

$$\boldsymbol{\sigma} \equiv (\sigma_1, \sigma_2, \dots, \sigma_{\mathbf{N}_\alpha})^T,$$

and by acknowledging that the Hessian-vector product $\nabla^2 \mathbf{r}_k(\boldsymbol{\alpha}^0) \boldsymbol{\sigma}$ can be quantified most efficiently by using two computations of the gradients $\nabla_\alpha(\mathbf{r}_k)$, as follows:

$$\mathbf{y}_k(\boldsymbol{\alpha}^0) \equiv \nabla^2 \mathbf{r}_k(\boldsymbol{\alpha}^0) \boldsymbol{\sigma} \cong \frac{\nabla_\alpha [\mathbf{r}_k(\boldsymbol{\alpha}^0 + b\boldsymbol{\sigma})] - \nabla_\alpha [\mathbf{r}_k(\boldsymbol{\alpha}^0)]}{b}; \quad k = 1, \dots, \mathbf{N}_r, \quad (4.16)$$

where b is some small scalar quantity. The vector, $\mathbf{y}_k(\boldsymbol{\alpha}^0)$, may be approximated utilizing only two adjoint model computations per response instead of the $O(\mathbf{N}_\alpha^2)$ runs using only forward model computations. With one more inner product, the quantity $q_k(\rho_{i_1 i_2} = 1)$ is obtained as

$$q_k(\rho_{i_1 i_2} = 1) = \boldsymbol{\sigma}^T \mathbf{y}_k(\boldsymbol{\alpha}^0). \quad (4.17)$$

For a realistic case where the model parameters $\boldsymbol{\alpha}$ are only partially correlated, it is still possible to compromise between $O(\mathbf{N}_\alpha^2)$ computations and the limiting fully correlated case. In fact, this number can be reduced to $\mathbf{n}_\alpha < \mathbf{N}_\alpha$ by considering Hessian-vector products of the same form as Eq. 4.16. For each response, $r_k(\boldsymbol{\alpha}^0)$, $k = 1, \dots, \mathbf{N}_r$, the recommended steps are

- (1.) Rank the relative sensitivities $S_{ri}^k(\boldsymbol{\alpha}^0) \equiv \frac{\alpha_i^0}{r_k} \frac{\partial r_k(\boldsymbol{\alpha}^0)}{\partial \alpha_i}$ in decreasing order of absolute magnitudes $|S_{ri}^k(\boldsymbol{\alpha}^0)|$; this ranking will indicate the most important parameters α_i in contribution to response $r_k(\boldsymbol{\alpha}^0)$;
- (2.) Compute the quantities $c_{ii}^k \equiv \{S_{ri}^k(\boldsymbol{\alpha}^0) \sigma_{ri}\}$, where σ_{ri} denotes the relative standard de-

variation of parameter α_i ; rank the c_{ii}^k in decreasing order of their absolute magnitudes; c_{ii}^k can be thought of as the “partial standard deviation of the response r_k stemming from uncertainties in the parameters α_i ”, and thus quantifies the first order contributions to $\text{var}(r_k)$;

- (3.) Based on the rankings of the partial standard deviations c_{ii}^k , rank the standard deviations σ_i in order of importance in contribution to $\text{var}(r_k)$, thus constructing the vector sequence of $(\sigma_1, \sigma_2, \dots, \sigma_{n_\alpha})$, where σ_{n_α} denotes a user-defined cutoff value that corresponds to a negligible (from the user’s perspective) contribution to $\text{var}(r_k)$;
- (4.) For each of the selected standard deviations in the sequence $(\sigma_1, \sigma_2, \dots, \sigma_{n_\alpha})$, construct the n_α -dimensional column vectors $\boldsymbol{\sigma}_1 \equiv (\sigma_1, 0, \dots, 0), \dots, \boldsymbol{\sigma}_i \equiv (0, \dots, \sigma_i, \dots, 0), \dots, \boldsymbol{\sigma}_{n_\alpha} \equiv (0, \dots, \sigma_{n_\alpha})$, and use each of these, in turn, in conjunction with one adjoint model computation, to obtain the n_α -dimensional vector $\mathbf{t}^{ki} \equiv (t_1^{ki}, \dots, t_{n_\alpha}^{ki})^T$ defined as

$$\begin{aligned} \mathbf{t}^{ki} &\equiv (t_1^{ki}, \dots, t_{n_\alpha}^{ki})^T \equiv \left(\frac{\partial^2 r_k(\boldsymbol{\alpha}^0)}{\partial \alpha_1 \partial \alpha_i} \sigma_i, \dots, \frac{\partial^2 r_k(\boldsymbol{\alpha}^0)}{\partial \alpha_{n_\alpha} \partial \alpha_i} \sigma_i \right)^T \\ &= \nabla^2 r_k(\boldsymbol{\alpha}^0) \boldsymbol{\sigma}_i \cong \frac{\nabla_\alpha [r_k(\boldsymbol{\alpha}^0 + b \boldsymbol{\sigma}_i)] - \nabla_\alpha [r_k(\boldsymbol{\alpha}^0)]}{b}; \quad k = 1, \dots, n_\alpha; \end{aligned} \quad (4.18)$$

- (5.) For each $i = 1, \dots, n_\alpha$, multiply the first component, t_1^{ki} , of the vector $\mathbf{t}^{ki} \equiv (t_1^{ki}, \dots, t_{n_\alpha}^{ki})^T$ obtained in Eq. 4.18 by the correlation coefficient ρ_{i1} , the second component of this vector by the correlation coefficient ρ_{i2} , etc., until the last component $t_{n_\alpha}^{ki}$, which is to be multiplied by ρ_{in_α} , in order to construct the sequence of vectors

$$\left(t_1^{ki} \rho_{i1}, \dots, t_{n_\alpha}^{ki} \rho_{in_\alpha} \right)^T = \left(\frac{\partial^2 r_k(\boldsymbol{\alpha}^0)}{\partial \alpha_1 \partial \alpha_i} \sigma_i \rho_{i1}, \dots, \frac{\partial^2 r_k(\boldsymbol{\alpha}^0)}{\partial \alpha_{n_\alpha} \partial \alpha_i} \sigma_i \rho_{in_\alpha} \right)^T; \quad i = 1, \dots, n_\alpha; \quad (4.19)$$

- (6.) Sum the corresponding components of the vectors in Eq. 4.19 to construct the column

vector

$$\left(\sum_{i=1}^{n_\alpha} t_1^{ki} \rho_{i1}, \dots, \sum_{i=1}^{n_\alpha} t_{n_\alpha}^{ki} \rho_{in_\alpha} \right)^T = \left(\sum_{i=1}^{n_\alpha} \frac{\partial^2 r_k(\boldsymbol{\alpha}^0)}{\partial \alpha_1 \partial \alpha_i} \sigma_i \rho_{i1}, \dots, \sum_{i=1}^{n_\alpha} \frac{\partial^2 r_k(\boldsymbol{\alpha}^0)}{\partial \alpha_{n_\alpha} \partial \alpha_i} \sigma_i \rho_{in_\alpha} \right)^T ; \quad (4.20)$$

(7.) Form the inner product of the above vector with the row vector $(\sigma_1, \sigma_2, \dots, \sigma_{n_\alpha})$ to obtain the sum of the retained first order contributions to $var(r_k)$, namely:

$$(\sigma_1, \sigma_2, \dots, \sigma_{n_\alpha}) \left(\sum_{i=1}^{n_\alpha} t_1^{ki} \rho_{i1}, \dots, \sum_{i=1}^{n_\alpha} t_{n_\alpha}^{ki} \rho_{in_\alpha} \right)^T = \sum_{i_1, i_2=1}^{n_\alpha} \frac{\partial^2 r_k(\boldsymbol{\alpha}^0)}{\partial \alpha_{i_1} \partial \alpha_{i_2}} \rho_{i_1 i_2} \sigma_{i_1} \sigma_{i_2}. \quad (4.21)$$

Thus, the sum $\sum_{i_1, i_2=1}^{n_\alpha} \frac{\partial^2 r_k(\boldsymbol{\alpha}^0)}{\partial \alpha_{i_1} \partial \alpha_{i_2}} \rho_{i_1 i_2} \sigma_{i_1} \sigma_{i_2}$, which comprises the major first order contributions to the variance $var(r_k)$ can be computed most efficiently by needing only $n_\alpha < N_\alpha$ adjoint model computations, as opposed to at least N_α^2 runs if only forward model computations were utilized.

Lastly, the second-order mixed-derivatives $\frac{\partial^2 r_k}{\partial \alpha_{i_1} \partial \alpha_{i_2}}$ of the response r_k can be computed by dividing each of the components of $\mathbf{t}^{ki} \equiv (t_1^{ki}, \dots, t_{n_\alpha}^{ki})^T$ through by σ_i as follows:

$$\left(\frac{t_1^{ki}}{\sigma_i}, \dots, \frac{t_{n_\alpha}^{ki}}{\sigma_i} \right)^T = \left(\frac{\partial^2 r_k(\boldsymbol{\alpha}^0)}{\partial \alpha_1 \partial \alpha_i}, \dots, \frac{\partial^2 r_k(\boldsymbol{\alpha}^0)}{\partial \alpha_{n_\alpha} \partial \alpha_i} \right)^T ; \quad i = 1, \dots, n_\alpha. \quad (4.22)$$

To iterate, the computational framework is a restatement of Cacuci [9]. The following results section illustrate the exercise of this framework on representative nuclear benchmark problems; see Chapter 3.

4.2.2 Results

4.2.2.1 Partial Standard Deviations and Sensitivities

Forward and adjoint homogeneous runs at nominal parameter values were completed for the Godiva and Jezebel benchmarks. All cases were run with SCALE's ENDF/BVII.0 44 group neutron library on a (x, y, z) mesh of (10, 10, 10) for a symmetric octant of the sphere. The

inner-iteration tolerance was set to 1e-11 while the outer iteration l_2 -norm tolerance for the flux and eigenvalue were set to 1e-10. For both experiments, four inhomogeneous adjoint runs were completed to compute the first order sensitivities, S_r^k , defined as

$$S_{ri}^k = \frac{\alpha_i^0}{r_k} \frac{\partial r_k(\boldsymbol{\alpha}^0)}{\partial \alpha_i}; \quad k = 1, \dots, 4, \quad i = 1, \dots, N_\alpha, \quad (4.23)$$

for the responses

$$\begin{aligned} r(\text{Np-237}) &= \frac{\langle \sigma_f^{\text{Np237}}, \phi \rangle_{\text{foil}}}{\langle \sigma_f^{\text{U235}}, \phi \rangle_{\text{foil}}}; & r(\text{Pu-239}) &= \frac{\langle \sigma_f^{\text{Pu239}}, \phi \rangle_{\text{foil}}}{\langle \sigma_f^{\text{U235}}, \phi \rangle_{\text{foil}}}; \\ r(\text{U-233}) &= \frac{\langle \sigma_f^{\text{U233}}, \phi \rangle_{\text{foil}}}{\langle \sigma_f^{\text{U235}}, \phi \rangle_{\text{foil}}}; & r(\text{U-238}) &= \frac{\langle \sigma_f^{\text{U238}}, \phi \rangle_{\text{foil}}}{\langle \sigma_f^{\text{U235}}, \phi \rangle_{\text{foil}}}, \end{aligned} \quad (4.24)$$

where the inner product space is defined over all energy and volume ΔV in the domain

$$\langle a, b \rangle_{\text{foil}} \equiv \int_{\Delta V} \int_0^\infty ab \, dE dV.$$

The ‘‘partial standard deviation of the response r_k stemming from uncertainties in the parameters α_i ’’ was computed as

$$c_{ii}^k = \left[S_{ri}^k \sigma_{ri} \right]; \quad k = 1, \dots, 4, \quad i = 1, \dots, N_\alpha, \quad (4.25)$$

where σ_{ri} represents the relative standard deviation of the i -th input parameter. All of the c_{ii}^k for a response k were ranked in absolute magnitude. Each corresponded to a particular isotope, reaction type and energy group for a particular material zone within the problem setup; see section 2.4.1.

Figure 4.3 shows all non-zero partial standard deviations for both Godiva and Jezebel. Each line represents a different response ranked from largest in magnitude to smallest. Figure 4.4 takes a closer look at the same data with a cutoff value of $1.0E - 4$.

As evident from Figure 4.4, for both Godiva and Jezebel, Uranium-238 and Neptunium-237

Godiva and Jezebel Partial Standard Deviation Rankings of Fission Rate Responses

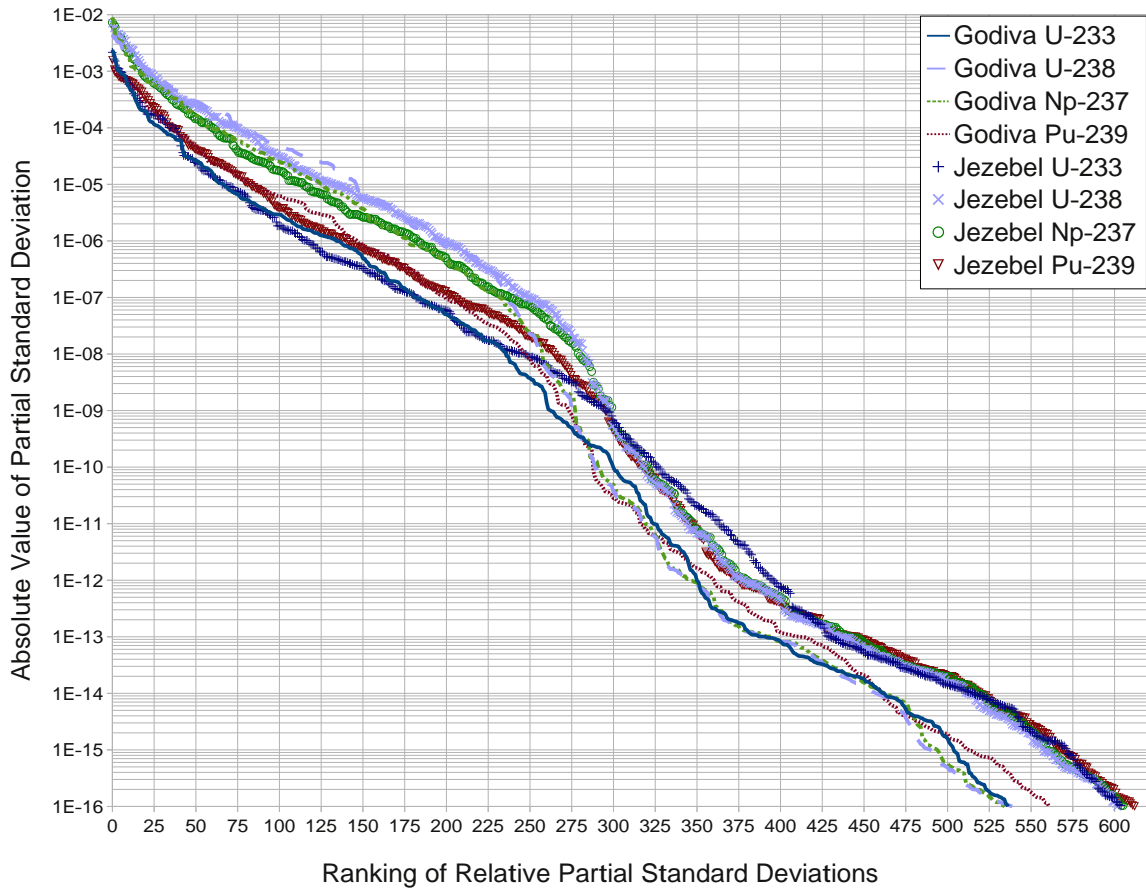


Figure 4.3: Combined plot of the absolute value of the partial standard deviations for both the Godiva and Jezebel Benchmarks.

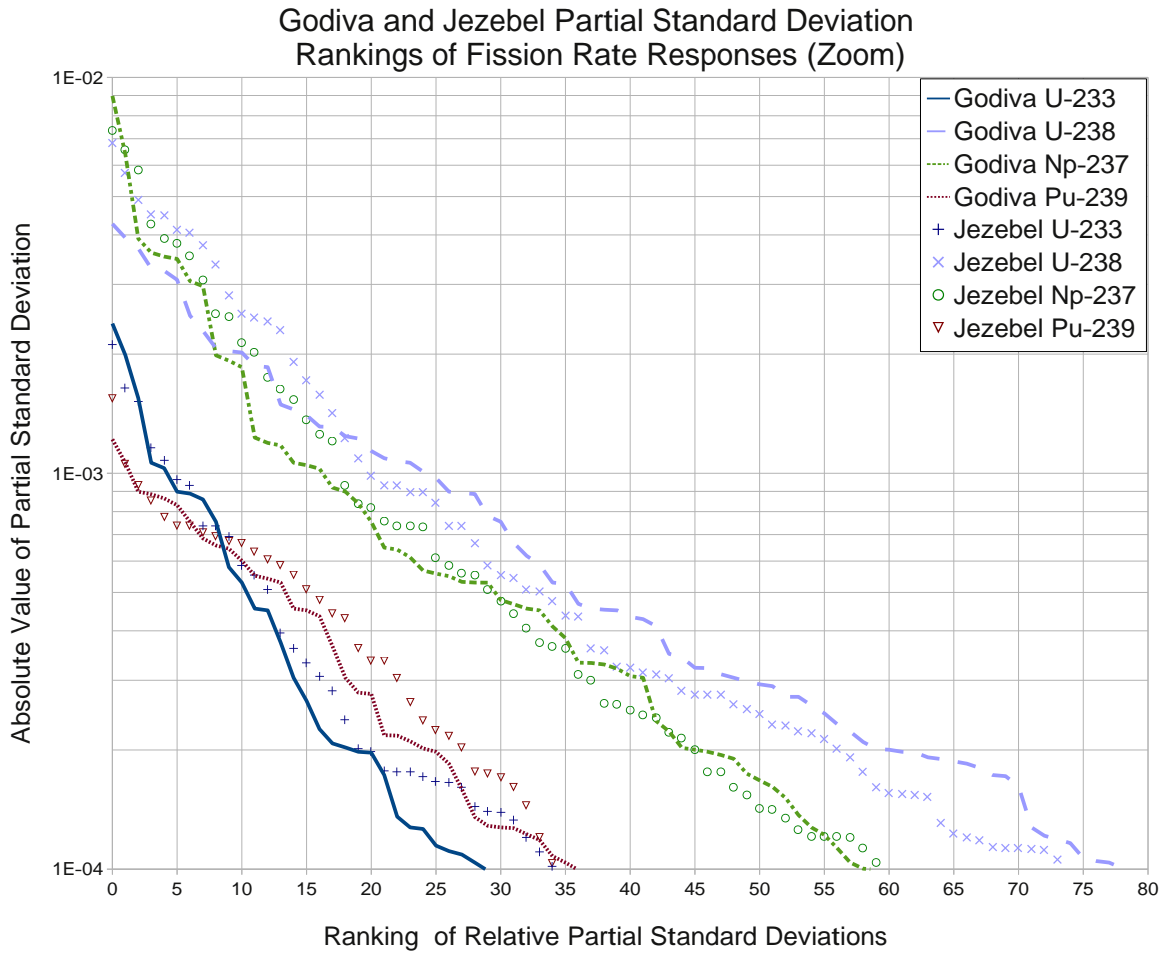


Figure 4.4: Combined plot of the absolute value of the partial standard deviations for both the Godiva and Jezebel Benchmarks. The plot has been focused on the largest contributing members above $1.0E - 4$.

responses maintain a higher partial standard deviation from the parameters than the Uranium-233 and Plutonium-239 responses until at least a value of $1.0E - 8$. To further expound on the partial standard deviations for each response, the tables below contain c_{ii}^k values specifically for the top five parameter contributions for both the Godiva and Jezebel experiments.

Table 4.1: Godiva c_{ii}^k rankings.

Rank	$r(Np237)$		$r(Pu239)$	
	ID	Value	ID	Value
1	$^{237}_{9}Np_{fission}^{foil}$	8.98074860e-03	$^{239}_{9}Pu_{fission}^{foil}$	1.21838694e-03
2	$^{237}_{8}Np_{fission}^{foil}$	6.40012073e-03	$^{235}_{9}U_{fission}^{foil}$	-1.06314222e-03
3	$^{237}_{7}Np_{fission}^{foil}$	3.91591596e-03	$^{235}_{10}U_{fission}^{foil}$	-8.98513677e-04
4	$^{235}_{9}U_{n,n'}^{fuel}$	-3.60836359e-03	$^{239}_{8}Pu_{fission}^{foil}$	8.84983144e-04
5	$^{237}_{3}Np_{fission}^{foil}$	3.52700603e-03	$^{235}_{9}U_{n,n'}^{fuel}$	-8.64052569e-04

Table 4.2: Godiva c_{ii}^k rankings (cont.).

Rank	$r(U233)$		$r(U238)$	
	ID	Value	ID	Value
1	$^{233}_{9}U_{fission}^{foil}$	2.38927158e-03	$^{235}_{9}U_{\chi}^{fuel}$	-4.26702153e-03
2	$^{233}_{10}U_{fission}^{foil}$	1.98826542e-03	$^{235}_{3}U_{\chi}^{fuel}$	3.93382674e-03
3	$^{233}_{8}U_{fission}^{foil}$	1.54844546e-03	$^{235}_{10}U_{n,\gamma}^{fuel}$	3.69938090e-03
4	$^{235}_{9}U_{fission}^{foil}$	-1.06314222e-03	$^{235}_{3}U_{n,n'}^{fuel}$	-3.29353255e-03
5	$^{233}_{7}U_{fission}^{foil}$	1.03040740e-03	$^{235}_{10}U_{\chi}^{fuel}$	-3.24708777e-03

Tables 4.1 and 4.2 represent the top five contributors for all four responses for the Godiva experiment. Tables 4.3 and 4.4 represent the top five contributors for all four responses for the Jezebel experiment.

To compliment the c_{ii}^k values, Tables 4.5, 4.6, 4.7 and 4.8 list the first and second-order

Table 4.3: Jezebel c_{ii}^k rankings.

Rank	$r(Np237)$		$r(Pu239)$	
	ID	Value	ID	Value
1	$^{237}_{9}Np_{\text{fission}}^{\text{foil}}$	7.33315223e-03	$^{239}_{9}Pu_{n,n}^{\text{fuel}}$	-1.54054310e-03
2	$^{239}_{9}Pu_{n,n}^{\text{fuel}}$	-6.55072408e-03	$^{239}_{9}Pu_{\text{fission}}^{\text{foil}}$	1.05471603e-03
3	$^{237}_{8}Np_{\text{fission}}^{\text{foil}}$	5.81786651e-03	$^{235}_{9}U_{\text{fission}}^{\text{foil}}$	-9.32122096e-04
4	$^{237}_{3}Np_{\text{fission}}^{\text{foil}}$	4.25585526e-03	$^{239}_{8}Pu_{\text{fission}}^{\text{foil}}$	8.52699649e-04
5	$^{239}_{8}Pu_{n,n}^{\text{fuel}}$	-3.91120319e-03	$^{239}_{10}Pu_{n,n}^{\text{fuel}}$	-7.73169360e-04

Table 4.4: Jezebel c_{ii}^k rankings (cont.).

Rank	$r(U233)$		$r(U238)$	
	ID	Value	ID	Value
1	$^{233}_{9}U_{\text{fission}}^{\text{foil}}$	2.10685867e-03	$^{239}_{3}Pu_{n,n}^{\text{fuel}}$	-6.81102811e-03
2	$^{233}_{10}U_{\text{fission}}^{\text{foil}}$	1.64037198e-03	$^{239}_{9}Pu_{n,n}^{\text{fuel}}$	-5.73917132e-03
3	$^{233}_{8}U_{\text{fission}}^{\text{foil}}$	1.51879057e-03	$^{239}_{7}Pu_{n,n}^{\text{fuel}}$	-4.89170810e-03
4	$^{233}_{3}U_{\text{fission}}^{\text{foil}}$	1.15678754e-03	$^{239}_{9}Pu_{\chi}^{\text{fuel}}$	-4.50779250e-03
5	$^{233}_{7}U_{\text{fission}}^{\text{foil}}$	1.07899369e-03	$^{239}_{6}Pu_{n,n}^{\text{fuel}}$	-4.47782959e-03

relative sensitivity values for the top five parameters based on the rankings of c_{ii}^k for the Godiva experiment. Tables 4.9, 4.10, 4.11 and 4.12 list the first and second-order relative sensitivity values for the top five parameters based on the rankings of c_{ii}^k for the Jezebel experiment.

In each table are identifications that resemble ${}^b A_e^d$. “A” represents the periodic element, “b” is the particular isotopic number of element “A”, “c” is the energy group number, “d” is the physical location of the parameter and “e” specifies the reaction type in question.

Table 4.5: Godiva $r(U233)$ first and second-order sensitivities.

1 st Order Sensitivities	Parameter ID	$^{233}\text{U}_{9\text{ fission}}^{\text{foil}}$	$^{233}\text{U}_{10\text{ fission}}^{\text{foil}}$	$^{233}\text{U}_{8\text{ fission}}^{\text{foil}}$	$^{235}\text{U}_{9\text{ fission}}^{\text{foil}}$	$^{233}\text{U}_{7\text{ fission}}^{\text{foil}}$
2.340e-01	$^{233}\text{U}_{9\text{ fission}}^{\text{foil}}$	1.419e-08	-3.853e-15	-3.317e-15	-5.101e-02	0.000e+00
1.925e-01	$^{233}\text{U}_{10\text{ fission}}^{\text{foil}}$	-3.431e-15	6.681e-07	0.000e+00	-4.197e-02	0.000e+00
1.519e-01	$^{233}\text{U}_{8\text{ fission}}^{\text{foil}}$	-3.432e-15	-3.856e-15	-4.594e-07	-3.313e-02	1.703e-15
-2.184e-01	$^{235}\text{U}_{9\text{ fission}}^{\text{foil}}$	-5.113e-02	-4.206e-02	-3.318e-02	9.533e-02	-2.211e-02
1.012e-01	$^{233}\text{U}_{7\text{ fission}}^{\text{foil}}$	-3.434e-15	-3.858e-15	0.000e+00	-2.209e-02	2.924e-07

Table 4.6: Godiva $r(U238)$ first and second-order sensitivities.

1 st Order Sensitivities	Parameter ID	$^{235}\text{U}_{9\chi}^{\text{fuel}}$	$^{235}\text{U}_{3\chi}^{\text{fuel}}$	$^{235}\text{U}_{10\text{ n},\gamma}^{\text{fuel}}$	$^{235}\text{U}_{3\text{ n},\text{n}'}^{\text{fuel}}$	$^{235}\text{U}_{10\chi}^{\text{fuel}}$
-1.654e-01	$^{235}\text{U}_{9\chi}^{\text{fuel}}$	5.670e-02	2.326e-03	-2.559e-03	1.151e-02	3.178e-02
1.254e-01	$^{235}\text{U}_{3\chi}^{\text{fuel}}$	2.421e-03	-3.610e-02	1.017e-03	-4.531e-02	1.648e-03
1.450e-02	$^{235}\text{U}_{10\text{ n},\gamma}^{\text{fuel}}$	-2.467e-03	9.685e-04	-1.619e-03	-1.665e-04	4.128e-03
-5.112e-02	$^{235}\text{U}_{3\text{ n},\text{n}'}^{\text{fuel}}$	1.115e-02	-4.435e-02	-1.668e-04	2.147e-02	6.255e-03
-9.374e-02	$^{235}\text{U}_{10\chi}^{\text{fuel}}$	3.170e-02	1.679e-03	4.182e-03	6.458e-03	1.773e-02

Table 4.7: Godiva $r(Np237)$ first and second-order sensitivities.

1 st Order Sensitivities	Parameter ID	$^{237}_{9}\text{Np}_{\text{fission}}^{\text{foil}}$	$^{237}_{8}\text{Np}_{\text{fission}}^{\text{foil}}$	$^{237}_{7}\text{Np}_{\text{fission}}^{\text{foil}}$	$^{235}_{9}\text{U}_{\text{n,n}}^{\text{fuel}}$	$^{237}_{3}\text{Np}_{\text{fission}}^{\text{foil}}$
1.948e-01	$^{237}_{9}\text{Np}_{\text{fission}}^{\text{foil}}$	-2.444e-07	0.000e+00	0.000e+00	-2.519e-02	0.000e+00
2.120e-01	$^{237}_{8}\text{Np}_{\text{fission}}^{\text{foil}}$	0.000e+00	5.578e-07	0.000e+00	-5.094e-03	2.427e-15
1.469e-01	$^{237}_{7}\text{Np}_{\text{fission}}^{\text{foil}}$	0.000e+00	0.000e+00	-4.375e-07	-3.485e-03	2.429e-15
-4.165e-02	$^{235}_{9}\text{U}_{\text{n,n}}^{\text{fuel}}$	-2.521e-02	-5.103e-03	-3.488e-03	1.210e-02	-3.190e-03
1.368e-01	$^{237}_{3}\text{Np}_{\text{fission}}^{\text{foil}}$	2.857e-15	0.000e+00	0.000e+00	-3.188e-03	2.833e-07

Table 4.8: Godiva $r(Pu239)$ first and second-order sensitivities.

1 st Order Sensitivities	Parameter ID	$^{239}_{9}\text{Pu}_{\text{fission}}^{\text{foil}}$	$^{235}_{9}\text{U}_{\text{fission}}^{\text{foil}}$	$^{235}_{10}\text{U}_{\text{fission}}^{\text{foil}}$	$^{239}_{8}\text{Pu}_{\text{fission}}^{\text{foil}}$	$^{235}_{9}\text{U}_{\text{n,n}}^{\text{fuel}}$
2.239e-01	$^{239}_{9}\text{Pu}_{\text{fission}}^{\text{foil}}$	-4.822e-08	-4.880e-02	-4.106e-02	0.000e+00	-2.895e-02
-2.184e-01	$^{235}_{9}\text{U}_{\text{fission}}^{\text{foil}}$	-4.891e-02	9.533e-02	8.020e-02	-3.560e-02	3.042e-02
-1.838e-01	$^{235}_{10}\text{U}_{\text{fission}}^{\text{foil}}$	-4.115e-02	8.022e-02	6.749e-02	-2.995e-02	-3.319e-02
1.630e-01	$^{239}_{8}\text{Pu}_{\text{fission}}^{\text{foil}}$	-3.283e-15	-3.554e-02	-2.990e-02	-1.934e-07	-3.919e-03
-9.935e-03	$^{235}_{9}\text{U}_{\text{n,n}}^{\text{fuel}}$	-2.897e-02	3.043e-02	-3.321e-02	-3.923e-03	2.752e-03

Table 4.9: Jezebel $r(U_{233})$ first and second-order sensitivities.

1 st Order Sensitivities	Parameter ID	$^{233}_{9}\text{U}_{\text{fission}}^{\text{foil}}$	$^{233}_{10}\text{U}_{\text{fission}}^{\text{foil}}$	$^{233}_{8}\text{U}_{\text{fission}}^{\text{foil}}$	$^{233}_{3}\text{U}_{\text{fission}}^{\text{foil}}$	$^{233}_{7}\text{U}_{\text{fission}}^{\text{foil}}$
2.064e-01	$^{233}_{9}\text{U}_{\text{fission}}^{\text{foil}}$	-3.268e-07	-1.938e-15	1.669e-15	-3.106e-15	-1.712e-15
1.587e-01	$^{233}_{10}\text{U}_{\text{fission}}^{\text{foil}}$	0.000e+00	-6.024e-07	0.000e+00	-3.108e-15	-1.713e-15
1.490e-01	$^{233}_{8}\text{U}_{\text{fission}}^{\text{foil}}$	0.000e+00	0.000e+00	-4.508e-07	0.000e+00	-1.713e-15
1.133e-01	$^{233}_{3}\text{U}_{\text{fission}}^{\text{foil}}$	0.000e+00	-1.940e-15	0.000e+00	1.382e-07	0.000e+00
1.060e-01	$^{233}_{7}\text{U}_{\text{fission}}^{\text{foil}}$	0.000e+00	-1.940e-15	1.670e-15	0.000e+00	3.062e-07

Table 4.10: Jezebel $r(U_{238})$ first and second-order sensitivities.

1 st Order Sensitivities	Parameter ID	$^{239}_{3}\text{Pu}_{n,n}^{\text{fuel}}$	$^{239}_{9}\text{Pu}_{n,n}^{\text{fuel}}$	$^{239}_{7}\text{Pu}_{n,n}^{\text{fuel}}$	$^{239}_{9}\text{Pu}_{\chi}^{\text{fuel}}$	$^{239}_{6}\text{Pu}_{n,n}^{\text{fuel}}$
-3.052e-02	$^{239}_{3}\text{Pu}_{n,n}^{\text{fuel}}$	5.674e-03	1.025e-04	3.302e-04	6.589e-03	4.783e-04
-1.767e-02	$^{239}_{9}\text{Pu}_{n,n}^{\text{fuel}}$	1.090e-04	3.104e-03	5.569e-05	-7.129e-03	7.891e-05
-2.497e-02	$^{239}_{7}\text{Pu}_{n,n}^{\text{fuel}}$	3.324e-04	5.247e-05	5.250e-03	5.343e-03	-7.069e-05
-1.490e-01	$^{239}_{9}\text{Pu}_{\chi}^{\text{fuel}}$	6.855e-03	-7.276e-03	5.556e-03	4.676e-02	5.291e-03
-2.424e-02	$^{239}_{6}\text{Pu}_{n,n}^{\text{fuel}}$	4.792e-04	7.444e-05	-7.187e-05	5.083e-03	4.627e-03

Table 4.11: Jezebel $r(Np237)$ first and second-order sensitivities.

1 st Order Sensitivities	Parameter ID	$^{237}_{9}\text{Np}_{\text{fission}}^{\text{foil}}$	$^{239}_{9}\text{Pu}_{\text{n,n}}^{\text{fuel}}$	$^{237}_{8}\text{Np}_{\text{fission}}^{\text{foil}}$	$^{237}_{3}\text{Np}_{\text{fission}}^{\text{foil}}$	$^{239}_{8}\text{Pu}_{\text{n,n}}^{\text{fuel}}$
1.591e-01	$^{237}_{9}\text{Np}_{\text{fission}}^{\text{foil}}$	-2.897e-07	-6.466e-03	-2.158e-15	-2.263e-15	1.014e-02
-2.015e-02	$^{239}_{9}\text{Pu}_{\text{n,n}}^{\text{fuel}}$	-6.450e-03	2.285e-03	-3.441e-03	-2.903e-03	-9.650e-04
1.926e-01	$^{237}_{8}\text{Np}_{\text{fission}}^{\text{foil}}$	0.000e+00	-3.428e-03	5.071e-07	0.000e+00	-1.668e-02
1.650e-01	$^{237}_{3}\text{Np}_{\text{fission}}^{\text{foil}}$	0.000e+00	-2.893e-03	-2.158e-15	3.416e-07	-2.285e-03
-1.504e-02	$^{239}_{8}\text{Pu}_{\text{n,n}}^{\text{fuel}}$	1.014e-02	-9.655e-04	-1.667e-02	-2.291e-03	2.561e-03

Table 4.12: Jezebel $r(Pu239)$ first and second-order sensitivities.

1 st Order Sensitivities	Parameter ID	$^{239}_{9}\text{Pu}_{\text{n,n}}^{\text{fuel}}$	$^{239}_{9}\text{Pu}_{\text{fission}}^{\text{foil}}$	$^{235}_{9}\text{U}_{\text{fission}}^{\text{foil}}$	$^{239}_{8}\text{Pu}_{\text{fission}}^{\text{foil}}$	$^{239}_{10}\text{Pu}_{\text{n,n}}^{\text{fuel}}$
-4.738e-03	$^{239}_{9}\text{Pu}_{\text{n,n}}^{\text{fuel}}$	4.680e-04	-7.859e-03	8.667e-03	-2.805e-03	-1.809e-04
1.939e-01	$^{239}_{9}\text{Pu}_{\text{fission}}^{\text{foil}}$	-7.878e-03	-1.661e-07	-3.706e-02	0.000e+00	-1.354e-03
-1.915e-01	$^{235}_{9}\text{U}_{\text{fission}}^{\text{foil}}$	8.686e-03	-3.713e-02	7.326e-02	-3.007e-02	1.734e-03
1.570e-01	$^{239}_{8}\text{Pu}_{\text{fission}}^{\text{foil}}$	-2.795e-03	-3.244e-15	-3.003e-02	-1.863e-07	-1.078e-03
-2.069e-03	$^{239}_{10}\text{Pu}_{\text{n,n}}^{\text{fuel}}$	-1.812e-04	-1.361e-03	1.740e-03	-1.082e-03	6.926e-05

The differencing parameter “ b ” from Eq. 4.18 was chosen such that the multiplication with the corresponding standard deviation resulted in a 1% perturbation of the representative cross section (α_i^0) that it was added to. As a result, asymmetries on the order of $O(b)$ may be present in the Hessian matrices. If b is chosen too small, the effect of the perturbation of a parameter within the code will not produce a measurable difference from the nominal case at α^0 . If a perturbation is chosen too large, nonlinear effects may be present in the perturbation and would bias the derivative result.

If desired, a central difference (or higher-order) scheme may be employed at the cost of further adjoint runs to obtain symmetries that are on the order of $O(b^2)$ (or better). Even with additional adjoint runs for higher precision Hessians, the cost of the overall computation still remains at $O(n_\alpha)$.

Tables 4.5 through 4.12, in general, indicate that the second-order sensitivities are significantly smaller than the corresponding first-order sensitivities. Despite there being a few cases where second-order derivatives are of the same order of magnitude as the first-order derivatives, quite a few are either several orders of magnitude smaller or zero to the precision of the computation.

The magnitude of the second-order derivatives indicates that the responses of each system behave nearly linearly as functions of their respective cross sections. For the experiments, Godiva and Jezebel, this behavior is to be expected.

4.2.2.2 Higher-Order Moments

With first- and second-order derivatives available, it is possible to utilize the equations in section 4.1 to compute the expectation value, covariance, skewness and kurtosis for each response.

The user-defined cutoff to determine how many second-order derivatives to compute for each response was set based on the partial standard deviations of that response. Tables 4.5 through 4.12 give the c_{ii}^k value for the top ranked parameter. Taking this value, for each response, and dropping it an order of magnitude set the chosen c_{ii}^k cutoff value. From this, Figure 4.4 may

be used to determine the number of adjoint runs to execute based on where the c_{ii}^k chosen cutoff value intersects the x-axis. One additional inhomogeneous adjoint run corresponds to one additional second-order derivative term computed as according to Eq. 4.18. Table 4.13 summarizes the necessary number of adjoint runs per response to incorporate all parameters at or above a particular c_{ii}^k cutoff value; in other words: values of \mathbf{n}_α .

Table 4.13: Number (\mathbf{n}_α) of second-order derivatives (and hence, inhomogeneous adjoint runs) to complete for both experiments Godiva and Jezebel as a function of response such that partial standard deviation rankings within an order of magnitude of the top value are incorporated into the higher-order moment results.

\mathbf{n}_α	$\mathbf{r}(U233)$	$\mathbf{r}(U238)$	$\mathbf{r}(Np237)$	$\mathbf{r}(Pu239)$
Godiva	15	41	18	32
Jezebel	18	27	23	31

Based on these set numbers of inhomogeneous adjoint runs, values are reported for the computed response, expectation value, relative covariances, skewness and excess kurtosis for each response for both Godiva and Jezebel. Tables 4.14 and 4.15 contains specifically the computed responses and expectation values. Tables 4.16 and 4.18 contain the first-order relative response covariance matrices for each system, i.e. “the sandwich equation”. Tables 4.17 and 4.19 contain the second-order relative response covariance matrices for each system, i.e. “the sandwich equation” plus higher-order nonlinear terms from Eq. 4.8.

Table 4.14: Computed responses and expectation values for each response in Godiva given the number of computed inhomogeneous adjoints in Table 4.13.

Godiva	$\mathbf{r}(U233)$	$\mathbf{r}(U238)$	$\mathbf{r}(Np237)$	$\mathbf{r}(Pu239)$
Computed Response	1.56145688	0.17132921	0.90951271	1.39511123
Expectation Value	1.56147871	0.17134588	0.90946001	1.39506648

Table 4.15: Computed responses and expectation values for each response in Jezebel given the number of computed inhomogeneous adjoints in Table 4.13.

Jezebel	$r(U233)$	$r(U238)$	$r(Np237)$	$r(Pu239)$
Computed Response	1.55237282	0.20331751	0.97610488	1.41226606
Expectation Value	1.55235515	0.20345702	0.97634541	1.41229669

Table 4.16: First-order computed response relative covariance matrix for Godiva.

Godiva	$r(U233)$	$r(U238)$	$r(Np237)$	$r(Pu239)$
$r(U233)$	1.13119870e-04	-3.30279777e-06	9.29934691e-06	1.56621806e-05
$r(U238)$	-3.30279777e-06	7.52809808e-04	3.45137120e-04	8.14593187e-05
$r(Np237)$	9.29934691e-06	3.45137120e-04	5.18198500e-03	5.45937331e-05
$r(Pu239)$	1.56621806e-05	8.14593187e-05	5.45937331e-05	4.78079800e-05

Table 4.17: second-order computed response relative covariance matrix for Godiva.

Godiva	$r(U233)$	$r(U238)$	$r(Np237)$	$r(Pu239)$
$r(U233)$	1.13119681e-04	-3.30415722e-06	9.30016120e-06	1.56626366e-05
$r(U238)$	-3.30415722e-06	7.52857179e-04	3.45179337e-04	8.14728750e-05
$r(Np237)$	9.30016120e-06	3.45179337e-04	5.18201713e-03	5.46018543e-05
$r(Pu239)$	1.56626366e-05	8.14728750e-05	5.46018543e-05	4.78103226e-05

Tables 4.20 and 4.21 provide skewness and excess kurtosis information on Godiva and Jezebel respectively. Recall that both skewness and excess kurtosis are centered about zero for a normal distribution.

Table 4.18: First-order computed response relative covariance matrix for Jezebel.

Jezebel	$\mathbf{r}(U233)$	$\mathbf{r}(U238)$	$\mathbf{r}(Np237)$	$\mathbf{r}(Pu239)$
$\mathbf{r}(U233)$	1.11889583e-04	-4.05258915e-05	-8.70107226e-06	1.19807031e-05
$\mathbf{r}(U238)$	-4.05258915e-05	1.51689841e-03	7.23297573e-04	1.57050707e-04
$\mathbf{r}(Np237)$	-8.70107226e-06	7.23297573e-04	5.53392779e-03	9.95219417e-05
$\mathbf{r}(Pu239)$	1.19807031e-05	1.57050707e-04	9.95219417e-05	5.78114151e-05

Table 4.19: second-order computed response relative covariance matrix for Jezebel.

Jezebel	$\mathbf{r}(U233)$	$\mathbf{r}(U238)$	$\mathbf{r}(Np237)$	$\mathbf{r}(Pu239)$
$\mathbf{r}(U233)$	1.11889893e-04	-4.05264964e-05	-8.70235351e-06	1.19802473e-05
$\mathbf{r}(U238)$	-4.05264964e-05	1.51670798e-03	7.23279197e-04	1.57064261e-04
$\mathbf{r}(Np237)$	-8.70235351e-06	7.23279197e-04	5.53395491e-03	9.95333110e-05
$\mathbf{r}(Pu239)$	1.19802473e-05	1.57064261e-04	9.95333110e-05	5.78141650e-05

Table 4.20: Skewness and excess kurtosis values for each response in Godiva given the number of computed inhomogeneous adjoints in Table 4.13.

Godiva	$\mathbf{r}(U233)$	$\mathbf{r}(U238)$	$\mathbf{r}(Np237)$	$\mathbf{r}(Pu239)$
Skewness	-3.76823853e-03	-9.91657776e-03	2.42068329e-03	1.68782435e-02
Excess Kurtosis	1.03025103e-05	7.17401534e-05	3.87752934e-06	1.26412266e-04

Table 4.21: Skewness and excess kurtosis values for each response in Jezebel given the number of computed inhomogeneous adjoints in Table 4.13.

Jezebel	$\mathbf{r}(U233)$	$\mathbf{r}(U238)$	$\mathbf{r}(Np237)$	$\mathbf{r}(Pu239)$
Skewness	3.32842837e-03	-4.20089068e-02	-9.63178691e-03	-5.98445813e-03
Excess Kurtosis	6.90929473e-06	1.65952748e-03	6.37390642e-05	3.16780628e-05

Next, information about the evolution of the expectation values, variances, skewnesses and kurtoses as n_α is increased from 0 to the values in Table 4.13 and beyond for each response is displayed graphically. Figure 4.5 and Figure 4.6 display the evolution of the normalized expectation value (which is Eq. 4.5 divided by the computed response) as more information is added via additional second-order derivatives. Figure 4.7 and Figure 4.8 show the change in variance (which is Eq. 4.9 divided by $(C_{rc})_{kk}$) as additional second-order derivatives are appended. Figure 4.9 and Figure 4.10 display the evolution of the skewness for each response as more information is added via additional second-order derivatives. Finally, Figure 4.11 and Figure 4.12 display the evolution of the excess kurtosis for each response as more information is added via additional second-order derivatives.

All figures confirm the relative linearity of both Godiva and Jezebel benchmark models. For normalized expectation value and normalized variance, there is little departure from 1.0; the value associated with a linear model. Where there was lower-order information for expectation value and variance, there was none for skewness and excess kurtosis. Each addition of a second-order derivative gives new information about these shape factors that help quantify the non-Gaussian properties of the probability distribution. While non-zero, the skewness and excess kurtosis also confirm little departure from a Gaussian.

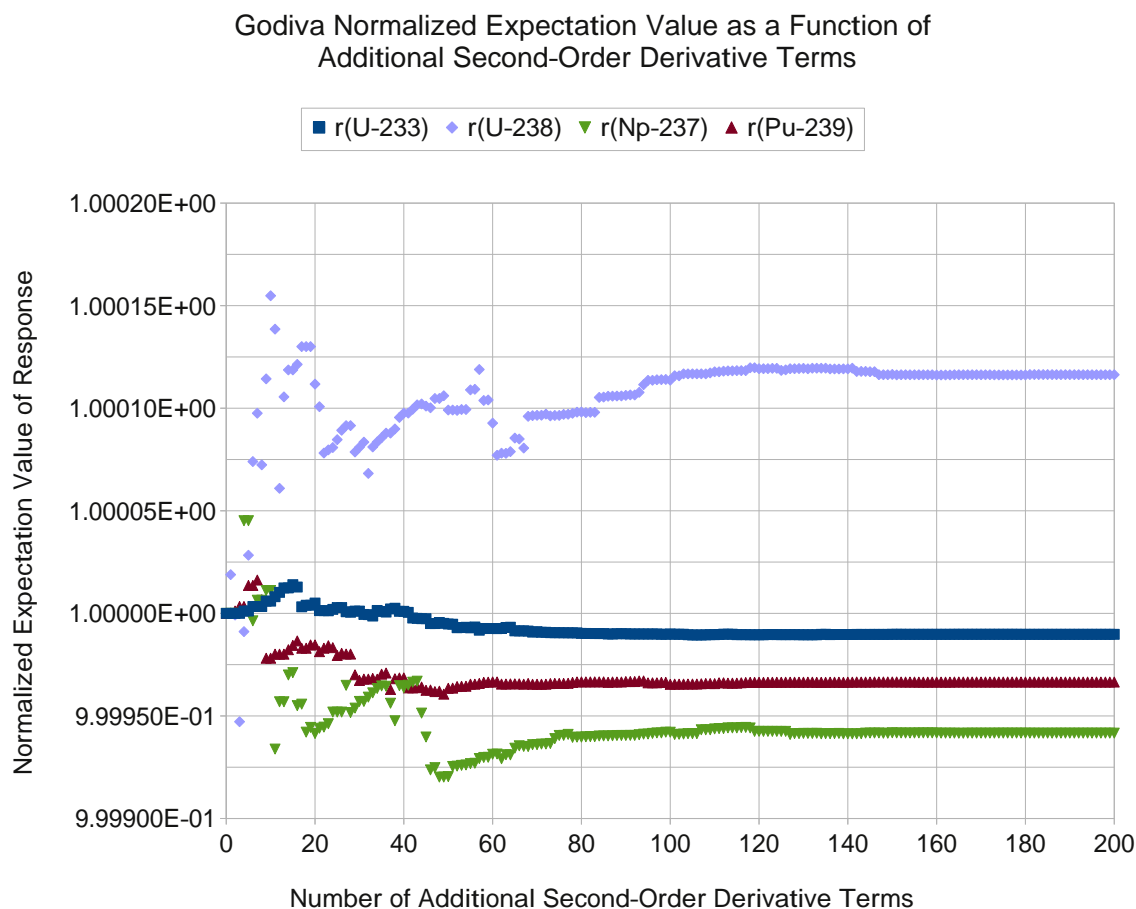


Figure 4.5: Normalized expectation values for Godiva as additional second-order derivative information is added by incrementing n_α as indicated by the parameter rankings via c_{ii}^k .

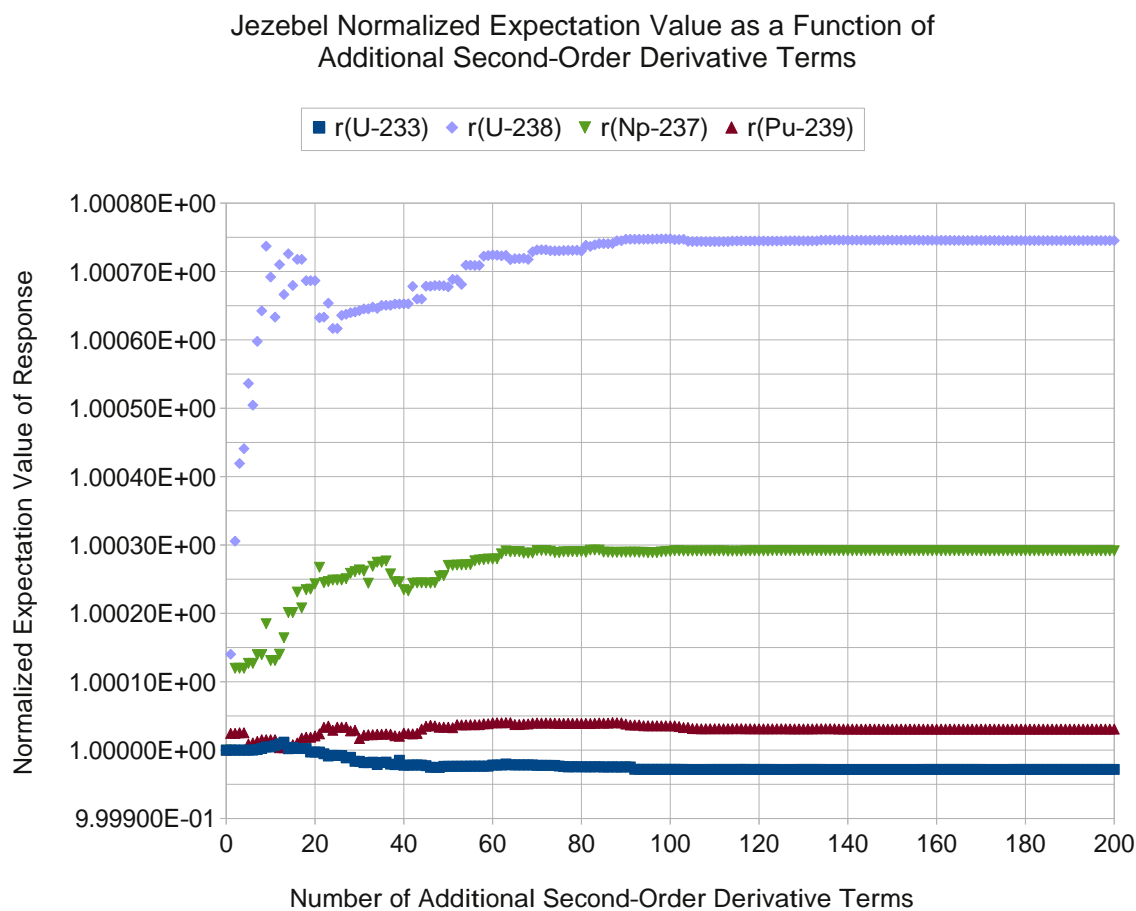


Figure 4.6: Normalized expectation values for Jezebel as additional second-order derivative information is added by incrementing n_α as indicated by the parameter rankings via c_{ii}^k .

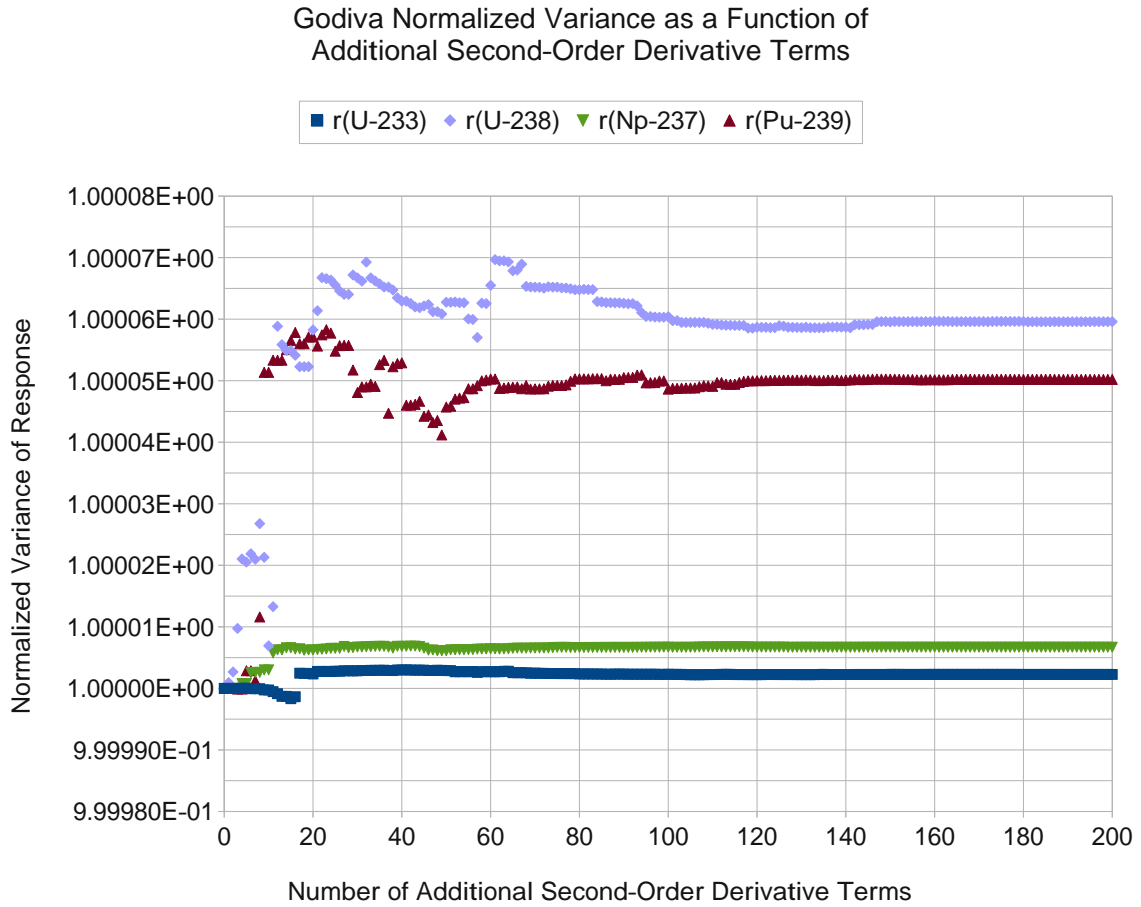


Figure 4.7: Normalized variances for Godiva as additional second-order derivative information is added by incrementing n_α as indicated by the parameter rankings via c_{ii}^k .

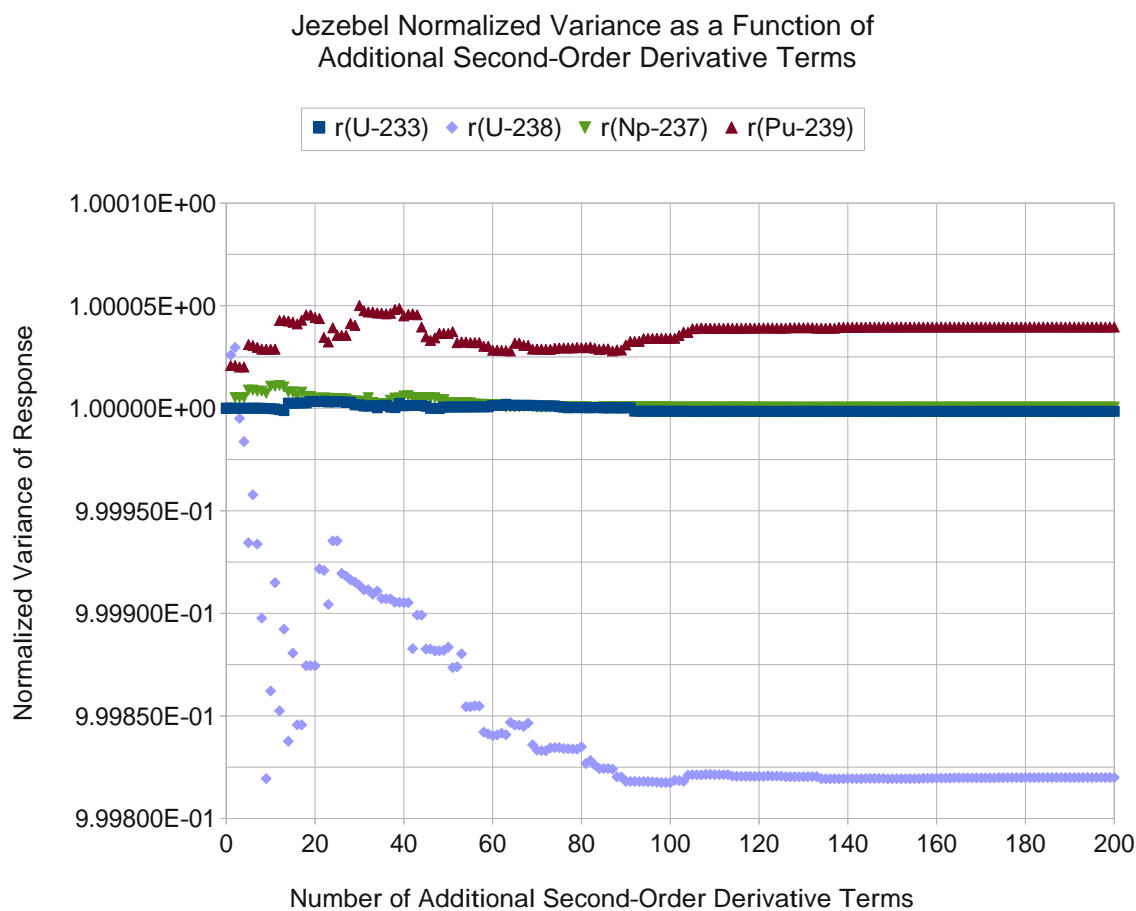


Figure 4.8: Normalized variances for Jezebel as additional second-order derivative information is added by incrementing n_α as indicated by the parameter rankings via c_{ii}^k .

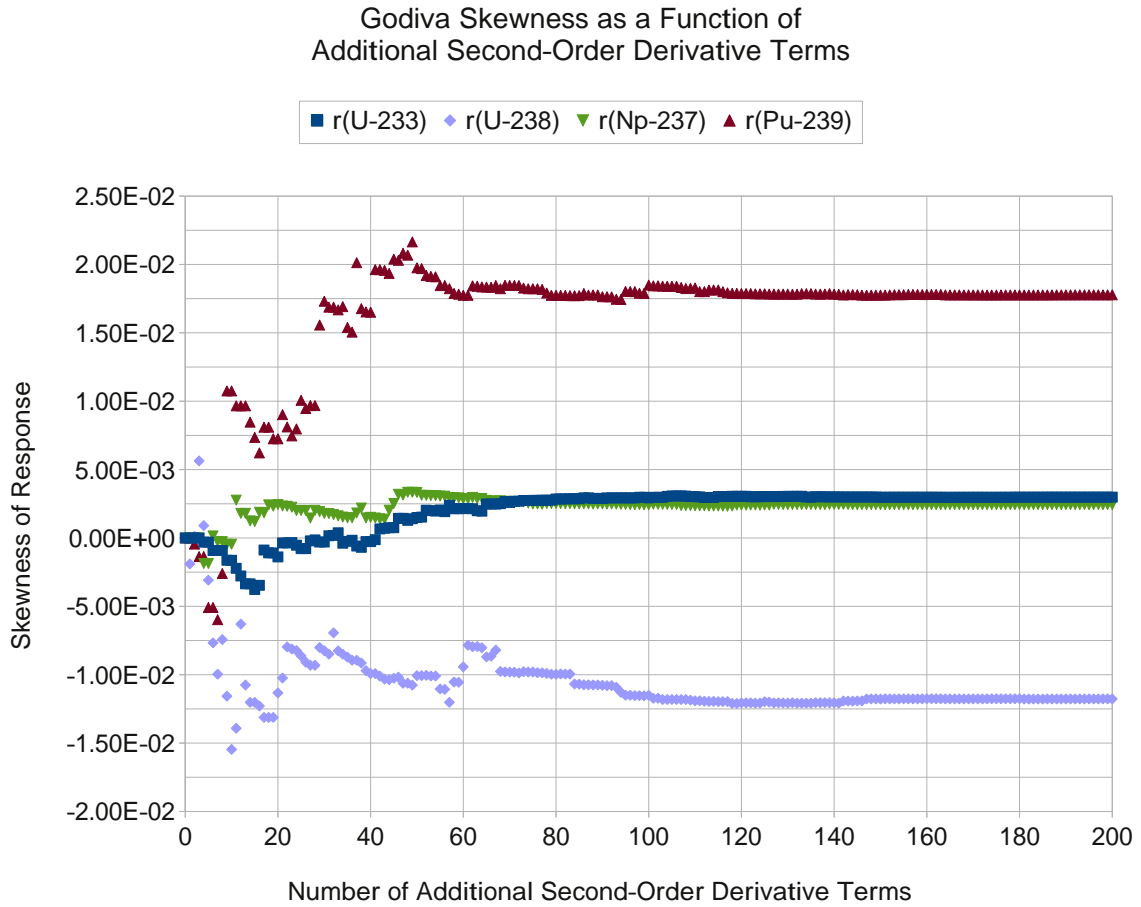


Figure 4.9: Skewness values for Godiva as additional second-order derivative information is added by incrementing n_α as indicated by the parameter rankings via c_{ii}^k .

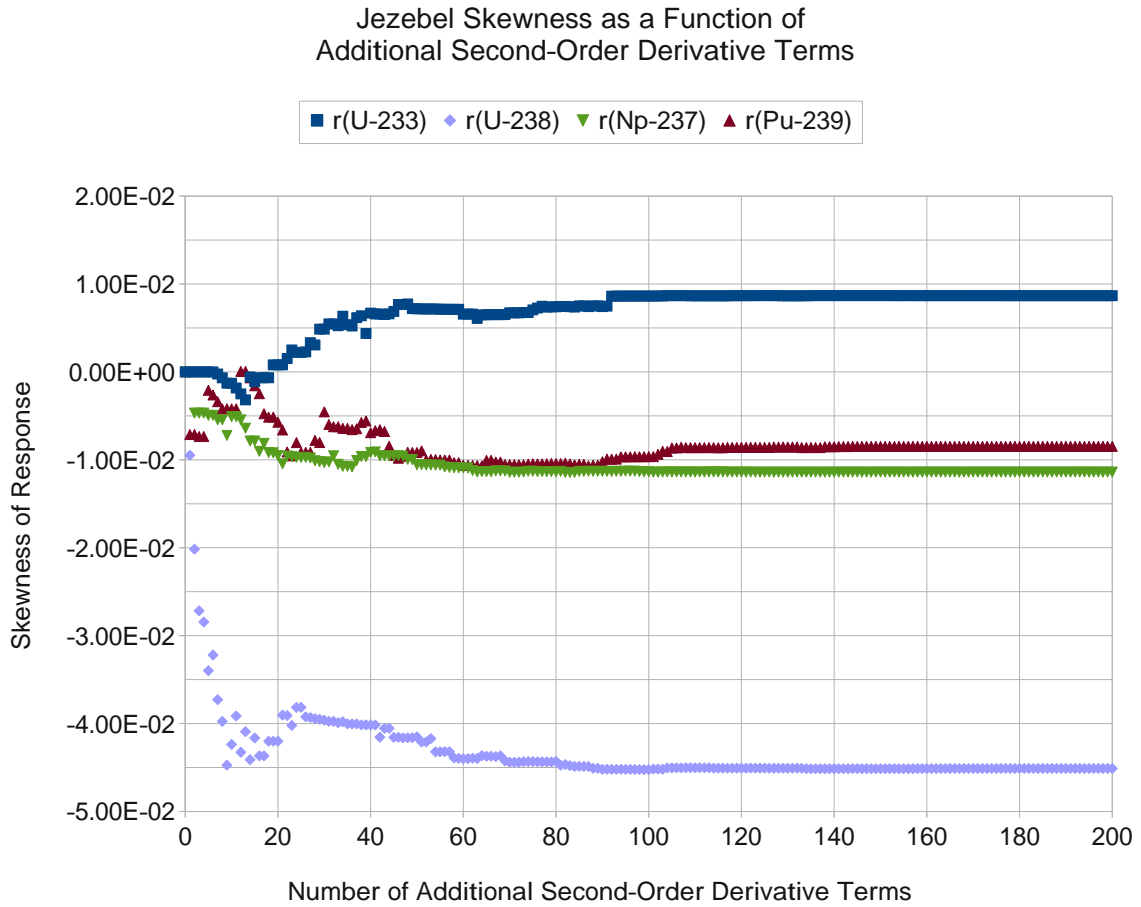


Figure 4.10: Skewness values for Jezebel as additional second-order derivative information is added by incrementing n_α as indicated by the parameter rankings via c_{ii}^k .

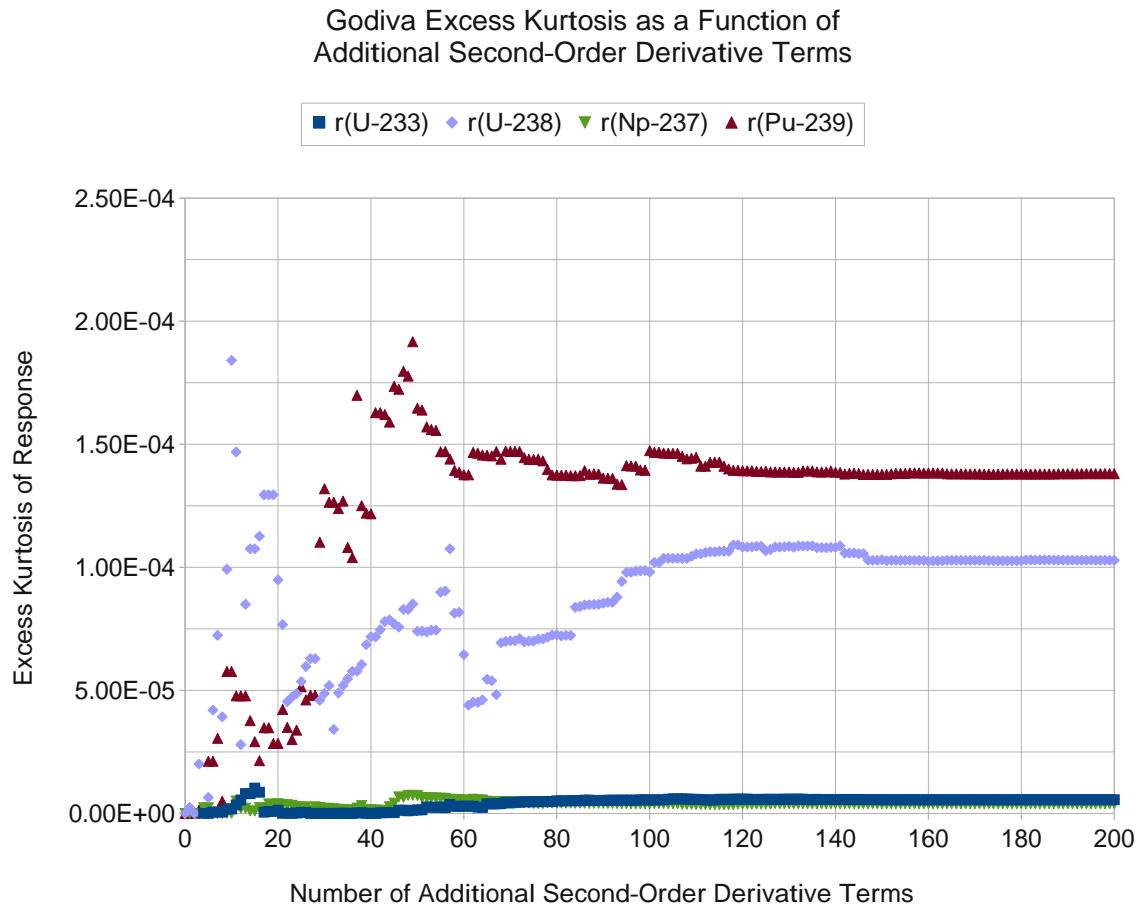


Figure 4.11: Excess kurtosis values for Godiva as additional second-order derivative information is added by incrementing n_α as indicated by the parameter rankings via c_{ii}^k .

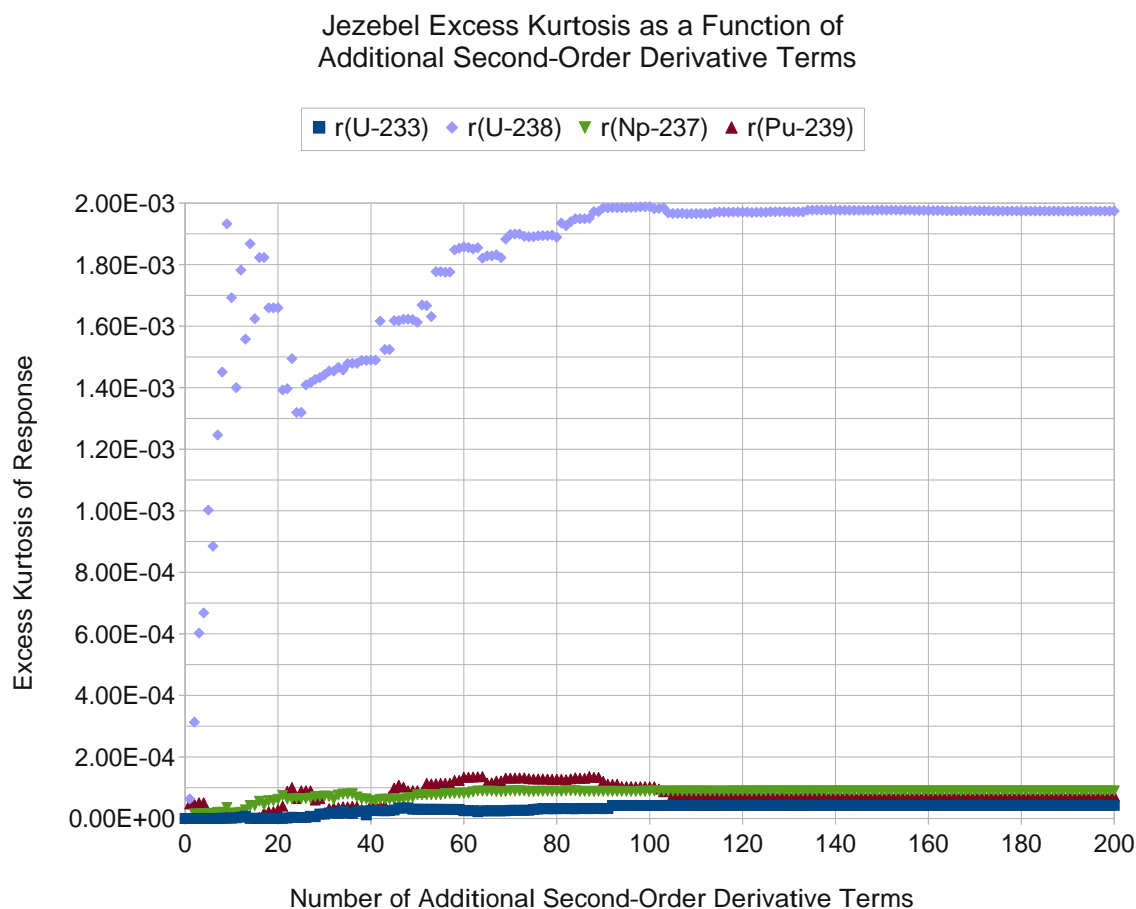


Figure 4.12: Excess kurtosis values for Jezebel as additional second-order derivative information is added by incrementing n_α as indicated by the parameter rankings via c_{ii}^k .

Chapter 5

Conclusions & Outlook

This work has presented several advances in the field of data assimilation and predictive model calibration, and has illustrated the significance and applicability of these advances by using the experimental results from the Lady Godiva, Jezebel and LCT critical assemblies, to calibrate cross-sections within the neutron transport code Denovo to obtain best-estimate predictions for these reactor physics problems. An important aspect of the novel contributions presented in this work is the development of highly parallel and scalable algorithms for application of data adjustment and assimilation to large (peta)- scale systems, thereby significantly extending the practical feasibility and applicability of predictive model calibration activities. As shown in Chapter 2, these new algorithms also include mathematical verification procedures for identifying non-physical covariance matrices, as well as quantifying the consistency of computational and experimental information. Very importantly, the new consistency verification criteria introduced in Chapter 2 have identified unphysical deficiencies in the 44-group evaluated covariance files of the widely used ORNL’s SCALE code package.

The significant impact of the above algorithmic advances has been demonstrated in Chapter 3 by using the neutron transport code Denovo, a highly parallel (over ten thousand processors) code that runs on ORNL’s leadership-class computer Jaguar. Denovo is interfaced through the software module “Lemon” to the module “best_pred” to perform efficiently first-order data

assimilation and calibration of model parameters. Both lemon and best-pred were developed as part of this work, and have been demonstrated to be scalable from a desktop PC to the 2.3 peta-FLOP Jaguar. The experiments used for data assimilation were: Lady Godiva (a bare sphere containing 94 wt% ^{235}U), Jezebel (a critical assembly containing ^{239}Pu), and the “LEU-COMP- THERM-008” (shorthand: LCT) assembly (which models a 3×3 array of Pressurized Water Reactor fuel assemblies comprising 4808 fuel rods and 153 water holes). Noteworthy new results in this dissertation are also obtained by using the remarkable efficiency of the “adjoint sensitivity analysis procedure for operator-type responses”, originally developed by Cacuci in 1981, to compute the sensitivities (derivatives) of the spatially dependent (as opposed to point-values of) neutron fluxes to cross sections for Lady Godiva. For all of these illustrative examples, the newly developed algorithms have performed robustly, very efficiently and accurately, for computing response sensitivities, propagating cross section covariances to obtain uncertainties in computed responses, combining computational with experimental uncertainties within the data assimilation procedure and, finally, obtaining best-estimate predictions with a correspondingly calibrated Denovo.

Chapter 4 of the dissertation presents expressions for computing the skewness and kurtosis of response distributions, to be used for quantifying non-Gaussian features of computed response distributions. Evaluation of these expressions requires the prior computation of the second-order mixed-derivatives of responses with respect to parameters. These second-order derivatives are computationally demanding to compute for large-scale problems, since, for N_α parameters, the current computational procedures require $O(N_\alpha^2)$ large-scale computations for each scalar response. Using a novel method based on the work of Cacuci [9], the second-order mixed derivatives of responses to parameters are computed in $O(N_\alpha)$. The first- and second-order response derivatives are computed explicitly for Godiva and Jezebel for reaction-rate responses. Most of the second-order derivatives are at least one order of magnitude smaller than the corresponding first-order ones, confirming the expectation that the flux behaves almost linearly as a function of most cross sections. For each response, the number of computations of second-order derivatives

was limited to the most significant parameters (cross sections) by using an indicator comprising, for each parameter, the product of the first-order sensitivity and the corresponding standard deviation. This indicator actually quantifies the partial contribution made by each parameter to the leading (i.e., first-order) term of the respective responses variance. By ranking these indicators in descending order of their absolute magnitude, the number of computations of the second-order derivatives was drastically reduced without affecting significantly the contributions involving second-order derivatives to the responses expectation values, variances, skewness, and kurtosis. These novel results are depicted graphically in Chapter 4, and they show that, also as expected, if the cross-sections are considered to be Normally distributed, their rather small uncertainties and small second-order derivatives cause the reaction-rate responses to be almost Normally-distributed, as would be expected in view of the central limit theorem. Only the ^{238}U reaction-rate response displays a small asymmetry (negative skewness) and peaked-ness (slightly positive excess kurtosis).

Although the work presented in this dissertation significantly advances the current state-of-the-art methods and algorithms for predictive model calibration, it nevertheless represents only a first step within a program to develop a new, fourth-order data assimilation and predictive model calibration procedure, which would incorporate the results obtained in this work. Immediate extensions of the work presented in this dissertation would be to provide a Chebyshev-basis, in addition to the Fourier cosine basis, for computing sensitivities of operator-type responses to parameters. Using Chebyshev polynomials would further reduce the number of required adjoint computations for a pre-determined accuracy criterion, since these polynomials satisfy a minimax principle and can be fitted exactly at points deemed especially important by the user. Furthermore, we plan to analyze several multi-physics benchmarks, going beyond the relatively simple reactor physics benchmarks that served as test-beds for the new algorithms presented in this work. Defining and developing best-practices procedures for handling large sets of covariance matrices for data assimilation would also be an important step forward, since such procedures are lacking at this time.

The results obtained in this dissertation represent first-of-a-kind computations of response skewness and kurtosis, thus enabling a quantitative assessment of non-Gaussian features of predicted responses (results). In particular, the illustrative results presented for the Godiva and Jezebel benchmarks show that the response skewness and kurtosis are relatively small, thus quantitatively confirming the intuitive feeling (based on the presumed applicability of the central limit theorem) that simple reactor physics problems involving small cross section uncertainties tend to produce reaction-rate responses that are nearly Normally distributed. Finally, yet importantly, the algorithmic advances and results presented in this work represent a fundamental first step towards developing a high-order predictive model calibration procedure capable of Bayesian combination of non-Gaussian model parameter features with non-Gaussian experimental distributions. Such developments are currently underway, and their successful completion is expected to enable more accurate predictions of “best-estimate results” including corresponding predicted non-Gaussian features, for large (peta- and exa-) scale systems.

A particularly important open issue is the estimation of the validation domain of the physics underlying the models of interest, which requires estimation of contours of constant uncertainty in the high-dimensional space that characterizes the application of interest. In practice, this involves the identification of areas where the predictive estimation of uncertainty meets specified requirements for the performance, reliability, or safety of the system of interest. Developing predictive experimentally validated “best-estimate” numerical models is particularly important for designing new technologies and facilities based on novel processes, while striving to avoid, as much as possible, the costly and lengthy procedures of building representative mock-up experiments which might confirm –but would not necessarily explain– the predictions of simulation tools. For example, assessing and predicting the performance of nuclear reactor fuels and materials under irradiation currently relies on very expensive and time-consuming confirmatory mockup experiments (e.g., multiyear irradiations); the corresponding computational predictive tools are crude, so improvements in this regard have very high potential payoff. A similar situation exists in reactor safety analyses, where validation has been restricted to either

mockup or component-level experimental comparison, with little predictive capability. The specific applications of the new mathematical methodologies to massively parallel multi-scale reactor physics modules will readily benefit both the fields of radiation imaging and therapy, as well as the simulation-based design, assessment, and licensing of nuclear energy systems.

REFERENCES

- [1] E. Anderson, Z. Bai, and C. Bischof. *LAPACK Users' Guide*, volume 9. Society for Industrial Mathematics, 1999.
- [2] J. Barhen, MA Bjerke, DG Cacuci, CB Mullins, and GG Wagschal. Uncertainty Analysis of Time-Dependent Nonlinear Systems: Theory and Application to Transient Thermal Hydraulics. *Nucl. Sci. Eng.:(United States)*, 81(1), 1982.
- [3] L.S. Blackford, A. Cleary, J. Choi, E. D'Azevedo, J. Demmel, I. Dhillon, J. Dongarra, S. Hammarling, G. Henry, A. Petitet, et al. *ScaLAPACK Users' Guide*, volume 4. Society for Industrial Mathematics, 1997.
- [4] J.B. Briggs, L. Scott, A. Nouri, et al. The International Criticality Safety Benchmark Evaluation Project. *Nuclear science and engineering*, 145(1):1–10, 2003.
- [5] CC Byers. Cross Sections of Various Materials in the Godiva and Jezebel Critical Assemblies. *Nuclear Sci. and Eng.*, 8, 1960.
- [6] D.G. Cacuci. Sensitivity Theory for Nonlinear Systems. I. Nonlinear Functional Analysis Approach. *Journal of Mathematical Physics*, 22:2794, 1981.
- [7] D.G. Cacuci. Sensitivity Theory for Nonlinear Systems. II. Extensions to Additional Classes of Responses. *Journal of Mathematical Physics*, 22:2803, 1981.
- [8] D.G. Cacuci. *Sensitivity and Uncertainty Analysis: Theory*, volume 1. CRC Press, 2003.
- [9] D.G. Cacuci. Integration of Experimental and Computational Data for Optimal Predictions in Nonlinear Systems: I. Model Validation. *Nuclear science and engineering*, 2011. Publication Pending.
- [10] D.G. Cacuci and M. Ionescu-Bujor. Best-Estimate Model Calibration and Prediction Through Experimental Data Assimilation I: Mathematical Framework. *Nuclear science and engineering*, 165(1):18–44, 2010.
- [11] DG Cacuci, MI Navon, and M. Ionescu-Bujor. Computational Methods for Data Analysis and Assimilation, 2007.
- [12] G. Cecchini, U. Farinelli, A. Gandini, and M. Salvatores. Analysis of Integral Data for Few-Group Parameter Evaluation of Fast Reactors. Technical report, Italy. Comitato Nazionale per l'Energia Nucleare, Rome, 1964.
- [13] MB Chadwick, P. Oblozinsky, M. Herman, NM Greene, RD McKnight, DL Smith, PG Young, RE MacFarlane, GM Hale, SC Frankle, et al. ENDF/B-VII.0: Next Generation Evaluated Nuclear Data Library for Nuclear Science and Technology. *Nuclear Data Sheets*, 107(12):2931–3060, 2006.

- [14] JB Dragt, JWM Dekker, H. Gruppelaar, and AJ Janssen. Methods of Adjustment and Error Evaluation of Neutron Capture Cross Sections: Application to Fission Product Nuclides. *Nucl. Sci. Eng.:(United States)*, 62(1), 1977.
- [15] R. T. Evans and D. G. Cacuci. Development and Implementation of Sensitivity Analysis Computational Capabilities in the Denovo Code System. *Nuclear Sci. and Eng.*, 2012. Publication Pending.
- [16] T.M. Evans, A.S. Stafford, R.N. Slaybaugh, and K.T. Clarno. Denovo: A New Three-Dimensional Parallel Discrete Ordinates Code in SCALE. *Nuclear technology*, 171(2):171–200, 2010.
- [17] S.C. Frankle and J.F. Briesmeister. Spectral Measurements in Critical Assemblies: MCNP Specifications and Calculated Results. Technical report, Los Alamos National Lab., Los Alamos, NM (US), 1999.
- [18] A. Gandini. Implicit and Explicit Higher Order Perturbation Methods for Nuclear Reactor Analysis. *Nucl. Sci. Eng.:(United States)*, 67(3), 1978.
- [19] A. Gandini and M. Petilli. AMARA: a Code Using the Lagrange’s Multipliers Method for Nuclear Data Adjustment. Technical report, Comitato Nazionale per l’Energia Nucleare, Rome (Italy), 1973.
- [20] E. Greenspan. New Developments in Sensitivity Theory. *Advances in nuclear science and technology*, 14, 1982.
- [21] GE Hansen and HC Paxton. Reevaluated Critical Specification of some Los Alamos Fast-Neutron Systems. Technical report, Los Alamos Scientific Lab., N. Mex., 1969.
- [22] M.A. Heroux and J.M. Willenbring. *Trilinos Users’ Guide*. United States. Dept. of Energy, 2003.
- [23] M. Humi, JJ Wagschal, and Y. Yeivin. Multi-Group Constants from Integral Data. Technical report, Hebrew Univ., Jerusalem, 1964.
- [24] I.C.F. Ipsen and C.D. Meyer. The Idea Behind Krylov Methods. *American Mathematical Monthly*, 105(10):889–899, 1998.
- [25] GA Jarvis, GA Linenberger, JD Orndoff, and HC Paxton. Two Plutonium-Metal Critical Assemblies. *Nuclear Sci. and Eng.*, 8, 1960.
- [26] H. KUROI and H. MITANI. Adjustment to Cross Section Data to Fit Integral Experiments by Least Squares Method. *Journal of Nuclear Science and Technology*, 12(11):663–680, 1975.
- [27] W.A. Lahoz, B. Khatatov, R. Ménard, and SpringerLink (Service en ligne). *Data assimilation: Making Sense of Observations*. Springer, 2010.

- [28] NM Larson, LC Leal, H. Derrien, G. Arbanas, RO Sayer, and D. Wiarda. A Systematic Description of the Generation of Covariance Matrices. In *PHYSOR-2006: ANS Topical Meeting on Reactor Physics*, pages 10–14, 2006.
- [29] J.M. Lewis, S. Lakshmivarahan, and S.K. Dhall. *Dynamic Data Assimilation: a Least Squares Approach*, volume 104. Cambridge Univ Pr, 2006.
- [30] RC Little, T. Kawano, GD Hale, MT Pigni, M. Herman, P. Oblozinski, ML Williams, ME Dunn, G. Arbanas, D. Wiarda, et al. Low-fidelity Covariance Project. *Nuclear Data Sheets*, 109(12):2828–2833, 2008.
- [31] RE MacFarlane and AC Kahler. Methods for Processing ENDF/B-VII with NJOY. *Nuclear Data Sheets*, 111(12):2739–2890, 2010.
- [32] C.D. Meyer. *Matrix Analysis and Applied Linear Algebra*. Society for Industrial and Applied Mathematics, Philadelphia, 2000.
- [33] Oak Ridge National Laboratory. *Scale: A Comprehensive Modeling and Simulation Suite for Nuclear Safety Analysis and Design, ORNL/TM-2005/39, Version 6.1*, 2011. Available from Radiation Safety Information Computational Center at Oak Ridge National Laboratory as CCC-785.
- [34] JL Rowlands, CJ Dean, JD MacDougall, and RW Smith. Production and Performance of the Adjusted Cross-Section Set FGL5. Technical report, Atomic Energy Establishment, Winfrith, Eng., 1973.
- [35] D.L. Smith. Evaluated Nuclear Data Covariances: The Journey From ENDF/B-VII.0 to ENDF/B-VII.1. *Nuclear Data Sheets*, 112(12):3037–3053, 2011.
- [36] LN Usachev. Perturbation Theory for the Breeding Ratio and for Other Number Ratios Pertaining to Various Reactor Processes. *Journal of Nuclear Energy. Parts A/B. Reactor Science and Technology*, 18(10):571–583, 1964.
- [37] CR Weisbin, EM Oblow, JH Marable, RW Peelle, and JL Lucius. Application of Sensitivity and Uncertainty Methodology to Fast Reactor Integral Experiment Analysis. *Nucl. Sci. Eng.:(United States)*, 66(3), 1978.

APPENDICES

Appendix A

KENO Input Specifications

A.1 Godiva

SCALE version 6.1 typical input listing:

```
=mavric parm=(nodose , forinput )
```

```
GODIVA V7-27 20 20 20
```

```
v7-27
```

```
read comp
```

```
U-234 1 0 0.00049184 end
```

```
U-235 1 0 0.044994 end
```

```
U-238 1 0 0.0024984 end
```

```
U-235 2 0 1.0 end
```

```
U-238 3 0 1.0 end
```

```
U-233 4 0 1.0 end
```

```
Np-237 5 0 1.0 end
```

```
Pu-239 6 0 1.0 end
```

```
Mn-55 7 0 1.0 end
```

```
Cu-63 8 0 1.0 end
```

```
Nb-93 9 0 1.0 end
```

```
end comp
```

```
read geom
```

```
global unit 999
```

```
sphere 10 8.7407
```

```
media 1 1 10
boundary 10
end geom
read definitions
  gridGeometry 1
    xlinear 20 -8.7407 8.7407
    ylinear 20 -8.7407 8.7407
    zlinear 20 -8.7407 8.7407
  end gridGeometry
end definitions
read sources
  src 1
    strength=100
    neutrons
    sphere 0.0
  end src
end sources
read importanceMap
  gridGeometryid=1
  mmsubcells=1
  mmtolerance=0.1
end importanceMap
end data
end
```

A.2 Jezebel

SCALE version 6.1 typical input listing:

```
=mavric parm=(nodose,forinp)
JEZEBEL V5-44 20 20 20
v5-44
read comp
pu-239 1 0 0.037047 end
pu-240 1 0 0.0017512 end
pu-241 1 0 0.00011674 end
ga      1 0 0.0013752 end

U-235 2 0 1.0 end
U-238 3 0 1.0 end
U-233 4 0 1.0 end
Np-237 5 0 1.0 end
Pu-239 6 0 1.0 end
end comp
read geom
global unit 999
sphere 10 6.38493
media 1 1 10
boundary 10
end geom
read definitions
  gridGeometry 1
    xlinear 20 0 6.38493
    ylinear 20 0 6.38493
    zlinear 20 0 6.38493
  end gridGeometry
end definitions
read sources
  src 1
  strength=100
  neutrons
  sphere 0
  end src
end sources
```

```
read importanceMap
  gridGeometryid=1
  mmsubcells=1
  mmtolerance=0.1
end importanceMap
end data
end
```

A.3 LEU-THERM-COMP-008

SCALE version 6.1 typical input listing (computer generated):

```
=mavric parm=(adjinp)
bw27-XI2: LEU-COMP-THERM-008 case 2; Core XI, Loading 2; 27-group xsecs
v7-27
read comp
h      1  0.0  6.6737e-2  end
o      1  0.0  3.3369e-2  end
b-10   1  0.0  1.4821e-5  end
b-11   1  0.0  5.9657e-5  end
u-234  2  0.0  4.5689e-6  end
u-235  2  0.0  5.6868e-4  end
u-238  2  0.0  2.2268e-2  end
o      2  0.0  4.5683e-2  end
b-10   2  0.0  2.6055e-7  end
mg     3  0.0  6.2072e-4  end
al     3  0.0  5.3985e-2  end
si     3  0.0  3.2230e-4  end
ti     3  0.0  4.7263e-5  end
cr     3  0.0  5.8029e-5  end
mn     3  0.0  4.1191e-5  end
fe     3  0.0  1.8910e-4  end
cu     3  0.0  5.9353e-5  end
u-234  4  0.0  4.5689e-6  end
u-235  4  0.0  5.6868e-4  end
u-238  4  0.0  2.2268e-2  end
o      4  0.0  4.5683e-2  end
b-10   4  0.0  2.6055e-7  end
u-234  5  0.0  4.5689e-6  end
u-235  5  0.0  5.6868e-4  end
u-238  5  0.0  2.2268e-2  end
o      5  0.0  4.5683e-2  end
b-10   5  0.0  2.6055e-7  end
u-234  6  0.0  4.5689e-6  end
u-235  6  0.0  5.6868e-4  end
u-238  6  0.0  2.2268e-2  end
o      6  0.0  4.5683e-2  end
```

b-10	6	0.0	2.6055e-7	end
u-234	7	0.0	4.5689e-6	end
u-235	7	0.0	5.6868e-4	end
u-238	7	0.0	2.2268e-2	end
o	7	0.0	4.5683e-2	end
b-10	7	0.0	2.6055e-7	end
h	8	0.0	6.6737e-2	end
o	8	0.0	3.3369e-2	end
b-10	8	0.0	1.4821e-5	end
b-11	8	0.0	5.9657e-5	end
mg	9	0.0	6.2072e-4	end
al	9	0.0	5.3985e-2	end
si	9	0.0	3.2230e-4	end
ti	9	0.0	4.7263e-5	end
cr	9	0.0	5.8029e-5	end
mn	9	0.0	4.1191e-5	end
fe	9	0.0	1.8910e-4	end
cu	9	0.0	5.9353e-5	end
h	10	0.0	6.6737e-2	end
o	10	0.0	3.3369e-2	end
b-10	10	0.0	1.4821e-5	end
b-11	10	0.0	5.9657e-5	end
mg	11	0.0	6.2072e-4	end
al	11	0.0	5.3985e-2	end
si	11	0.0	3.2230e-4	end
ti	11	0.0	4.7263e-5	end
cr	11	0.0	5.8029e-5	end
mn	11	0.0	4.1191e-5	end
fe	11	0.0	1.8910e-4	end
cu	11	0.0	5.9353e-5	end
h	12	0.0	6.6737e-2	end
o	12	0.0	3.3369e-2	end
b-10	12	0.0	1.4821e-5	end
b-11	12	0.0	5.9657e-5	end
mg	13	0.0	6.2072e-4	end
al	13	0.0	5.3985e-2	end
si	13	0.0	3.2230e-4	end
ti	13	0.0	4.7263e-5	end
cr	13	0.0	5.8029e-5	end

```

mn      13    0.0    4.1191e-5    end
fe      13    0.0    1.8910e-4    end
cu      13    0.0    5.9353e-5    end
h       14    0.0    6.6737e-2    end
o       14    0.0    3.3369e-2    end
b-10   14    0.0    1.4821e-5    end
b-11   14    0.0    5.9657e-5    end
mg      15    0.0    6.2072e-4    end
al      15    0.0    5.3985e-2    end
si      15    0.0    3.2230e-4    end
ti      15    0.0    4.7263e-5    end
cr      15    0.0    5.8029e-5    end
mn      15    0.0    4.1191e-5    end
fe      15    0.0    1.8910e-4    end
cu      15    0.0    5.9353e-5    end
end comp
read cell
latticecell squarepitch pitch=1.63576 1 fuel=1.02972 2 cladd=1.20599 3 end
latticecell squarepitch pitch=1.63576 8 fuel=1.02972 4 cladd=1.20599 9 end
centrm data dan2pitch(4)=0.18052      end centrm
latticecell squarepitch pitch=1.63576 10 fuel=1.02972 5 cladd=1.20599 11 end
centrm data dan2pitch(5)=0.17204      end centrm
latticecell squarepitch pitch=1.63576 12 fuel=1.02972 6 cladd=1.20599 13 end
centrm data dan2pitch(6)=0.15142      end centrm
latticecell squarepitch pitch=1.63576 14 fuel=1.02972 7 cladd=1.20599 15 end
centrm data dan2pitch(7)=0.14294      end centrm
end cell
read geometry
unit      1
com='fuel rods—unperturbed lattice'
cylinder  1
          5.148580E-01  1.633240E+02  0.000000E+00
          origin  x=  0.000000E+00  y=  0.000000E+00
media     2    1      1
          vol=  3.786553E+05
cylinder  2
          6.029960E-01  1.633240E+02  0.000000E+00
          origin  x=  0.000000E+00  y=  0.000000E+00
media     3    1      2  -1

```



```

                                vol= 1.407400E+05
cuboid      3
            8.178800E-01 -8.178800E-01 8.178800E-01
            -8.178800E-01 1.633240E+02 0.000000E+00
media      1  1      3 -2 -1
                                vol= 6.972344E+05
boundary   3
unit       2
com=^fuel rods with 1 kitty-cornered water hole^
cylinder   1
            5.148580E-01 1.633240E+02 0.000000E+00
            origin x= 0.000000E+00 y= 0.000000E+00
media      4  1      1
                                vol= 4.406764E+04
cylinder   2
            6.029960E-01 1.633240E+02 0.000000E+00
            origin x= 0.000000E+00 y= 0.000000E+00
media      3  1      2 -1
                                vol= 1.637922E+04
cuboid      3
            8.178800E-01 -8.178800E-01 8.178800E-01
            -8.178800E-01 1.633240E+02 0.000000E+00
media      1  1      3 -2 -1
                                vol= 8.114366E+04
boundary   3
unit       3
com=^fuel rods with 2 kitty-cornered water holes^
cylinder   1
            5.148580E-01 1.633240E+02 0.000000E+00
            origin x= 0.000000E+00 y= 0.000000E+00
media      5  1      1
                                vol= 9.792810E+03
cylinder   2
            6.029960E-01 1.633240E+02 0.000000E+00
            origin x= 0.000000E+00 y= 0.000000E+00
media      3  1      2 -1
                                vol= 3.639827E+03
cuboid      3
            8.178800E-01 -8.178800E-01 8.178800E-01

```

```

-8.178800E-01  1.633240E+02  0.000000E+00
media  1  1  3  -2  -1
      vol=  1.803192E+04
boundary  3
unit  4
com=^fuel rods with 1 adjacent water hole^
cylinder  1
      5.148580E-01  1.633240E+02  0.000000E+00
      origin  x=  0.000000E+00  y=  0.000000E+00
media  6  1  1
      vol=  6.365326E+04
cylinder  2
      6.029960E-01  1.633240E+02  0.000000E+00
      origin  x=  0.000000E+00  y=  0.000000E+00
media  3  1  2  -1
      vol=  2.365887E+04
cuboid  3
      8.178800E-01  -8.178800E-01  8.178800E-01
      -8.178800E-01  1.633240E+02  0.000000E+00
media  1  1  3  -2  -1
      vol=  1.172075E+05
boundary  3
unit  5
com=^fuel rods with 1 adjacent and 1 kitty-cornered water hole^
cylinder  1
      5.148580E-01  1.633240E+02  0.000000E+00
      origin  x=  0.000000E+00  y=  0.000000E+00
media  7  1  1
      vol=  1.958562E+04
cylinder  2
      6.029960E-01  1.633240E+02  0.000000E+00
      origin  x=  0.000000E+00  y=  0.000000E+00
media  3  1  2  -1
      vol=  7.279653E+03
cuboid  3
      8.178800E-01  -8.178800E-01  8.178800E-01
      -8.178800E-01  1.633240E+02  0.000000E+00
media  1  1  3  -2  -1
      vol=  3.606385E+04

```

```

boundary      3
unit          8
com=^water hole^
cuboid        1
              8.178800E-01 -8.178800E-01 8.178800E-01
              -8.178800E-01 1.633240E+02 0.000000E+00
media         1 1 1
              vol= 6.686219E+04
boundary      1
unit          14
com=^15 x 15 fuel assembly lattice^
cuboid        1
              2.453640E+01 0.000000E+00 2.453640E+01
              0.000000E+00 1.633240E+02 0.000000E+00
array         1 1
              place 1 1 1 8.17880E-01 8.17880E-01 0.00000E+00
boundary      1
unit          15
com=^61 x 8 x 1 driver fuel array^
cuboid        1
              4.979068E+01 -4.979068E+01 6.443040E+00
              -6.443040E+00 8.166200E+01 -8.166200E+01
array         2 1
              place 1 1 1 -4.90728E+01 -5.72516E+00 -8.16620E+01
boundary      1
unit          16
com=^41 x 5 x 1 driver fuel array^
cuboid        1
              3.343308E+01 -3.343308E+01 3.989400E+00
              -3.989400E+00 8.166200E+01 -8.166200E+01
array         3 1
              place 1 1 1 -3.27152E+01 -3.27152E+00 -8.16620E+01
boundary      1
unit          17
com=^21 x 5 x 1 driver fuel array^
cuboid        1
              1.707548E+01 -1.707548E+01 3.989400E+00
              -3.989400E+00 8.166200E+01 -8.166200E+01
array         4 1

```

```

        place 1 1 1   -1.63576E+01   -3.27152E+00   -8.16620E+01
boundary    1
unit        18
com=8 x 45 x 1 driver fuel array^
cuboid     1
        6.443040E+00  -6.443040E+00  3.670460E+01
        -3.670460E+01  8.166200E+01  -8.166200E+01
array      5      1
        place 1 1 1   -5.72516E+00   -3.598672E+01   -8.16620E+01
boundary    1
unit        19
com=5 x 41 x 1 driver fuel array^
cuboid     1
        3.989400E+00  -3.989400E+00  3.343308E+01
        -3.343308E+01  8.166200E+01  -8.166200E+01
array      6      1
        place 1 1 1   -3.27152E+00   -3.27152E+01   -8.16620E+01
boundary    1
unit        20
com=5 x 21 x 1 driver fuel array^
cuboid     1
        3.989400E+00  -3.989400E+00  1.707548E+01
        -1.707548E+01  8.166200E+01  -8.166200E+01
array      7      1
        place 1 1 1   -3.27152E+00   -1.63576E+01   -8.16620E+01
boundary    1
unit        21
com=fuel rods with right side shaved for hole
cylinder   1
        5.148580E-01  1.633240E+02  0.000000E+00
        origin  x= 0.000000E+00  y= 0.000000E+00
media      2      1      1
        vol= 3.073854E+04
cylinder   2
        6.029960E-01  1.633240E+02  0.000000E+00
        origin  x= 0.000000E+00  y= 0.000000E+00
media      3      1      2  -1
        vol= 1.142501E+04
cuboid     3

```

```

7.178800E-01 -8.178800E-01 8.178800E-01
-8.178800E-01 1.633240E+02 0.000000E+00
media 1 1 3 -2 -1
vol= 5.056241E+04
boundary 3
unit 22
com=^fuel rods with left side shaved for hole^
cylinder 1
5.148580E-01 1.633240E+02 0.000000E+00
origin x= 0.000000E+00 y= 0.000000E+00
media 2 1 1
vol= 3.073854E+04
cylinder 2
6.029960E-01 1.633240E+02 0.000000E+00
origin x= 0.000000E+00 y= 0.000000E+00
media 3 1 2 -1
vol= 1.142501E+04
cuboid 3
8.178800E-01 -7.178800E-01 8.178800E-01
-8.178800E-01 1.633240E+02 0.000000E+00
media 1 1 3 -2 -1
vol= 5.056241E+04
boundary 3
unit 23
com=^fuel rods with upper side shaved for hole^
cylinder 1
5.148580E-01 1.633240E+02 0.000000E+00
origin x= 0.000000E+00 y= 0.000000E+00
media 2 1 1
vol= 3.509090E+04
cylinder 2
6.029960E-01 1.633240E+02 0.000000E+00
origin x= 0.000000E+00 y= 0.000000E+00
media 3 1 2 -1
vol= 1.304271E+04
cuboid 3
8.178800E-01 -8.178800E-01 7.178800E-01
-8.178800E-01 1.633240E+02 0.000000E+00
media 1 1 3 -2 -1

```

```

                                vol= 5.772169E+04
boundary      3
unit          24
com=^fuel rods with lower side shaved for hole^
cylinder     1
              5.148580E-01  1.633240E+02  0.000000E+00
              origin  x= 0.000000E+00  y= 0.000000E+00
media        2  1  1
              vol= 3.509090E+04
cylinder     2
              6.029960E-01  1.633240E+02  0.000000E+00
              origin  x= 0.000000E+00  y= 0.000000E+00
media        3  1  2  -1
              vol= 1.304271E+04
cuboid       3
              8.178800E-01  -8.178800E-01  8.178800E-01
              -7.178800E-01  1.633240E+02  0.000000E+00
media        1  1  3  -2  -1
              vol= 5.772169E+04
boundary      3
unit          25
com=^fuel rods with right and lower sides shaved for hole^
cylinder     1
              5.148580E-01  1.633240E+02  0.000000E+00
              origin  x= 0.000000E+00  y= 0.000000E+00
media        2  1  1
              vol= 1.632135E+03
cylinder     2
              6.029960E-01  1.633240E+02  0.000000E+00
              origin  x= 0.000000E+00  y= 0.000000E+00
media        3  1  2  -1
              vol= 6.066378E+02
cuboid       3
              7.178800E-01  -8.178800E-01  8.178800E-01
              -7.178800E-01  1.633240E+02  0.000000E+00
media        1  1  3  -2  -1
              vol= 2.383738E+03
boundary      3
unit          26

```

```

com=^fuel rods with left and lower sides shaved for hole^
cylinder 1
      5.148580E-01  1.633240E+02  0.000000E+00
      origin  x=  0.000000E+00  y=  0.000000E+00
media 2 1 1
      vol=  1.632135E+03
cylinder 2
      6.029960E-01  1.633240E+02  0.000000E+00
      origin  x=  0.000000E+00  y=  0.000000E+00
media 3 1 2 -1
      vol=  6.066378E+02
cuboid 3
      8.178800E-01  -7.178800E-01  8.178800E-01
      -7.178800E-01  1.633240E+02  0.000000E+00
media 1 1 3 -2 -1
      vol=  2.383738E+03
boundary 3
unit 27
com=^fuel rods with right and upper sides shaved for hole^
cylinder 1
      5.148580E-01  1.633240E+02  0.000000E+00
      origin  x=  0.000000E+00  y=  0.000000E+00
media 2 1 1
      vol=  1.632135E+03
cylinder 2
      6.029960E-01  1.633240E+02  0.000000E+00
      origin  x=  0.000000E+00  y=  0.000000E+00
media 3 1 2 -1
      vol=  6.066378E+02
cuboid 3
      7.178800E-01  -8.178800E-01  7.178800E-01
      -8.178800E-01  1.633240E+02  0.000000E+00
media 1 1 3 -2 -1
      vol=  2.383738E+03
boundary 3
unit 28
com=^fuel rods with left and upper sides shaved for hole^
cylinder 1
      5.148580E-01  1.633240E+02  0.000000E+00

```

```

origin x= 0.000000E+00 y= 0.000000E+00
media 2 1 1
vol= 1.632135E+03
cylinder 2
6.029960E-01 1.633240E+02 0.000000E+00
origin x= 0.000000E+00 y= 0.000000E+00
media 3 1 2 -1
vol= 6.066378E+02
cuboid 3
8.178800E-01 -7.178800E-01 7.178800E-01
-8.178800E-01 1.633240E+02 0.000000E+00
media 1 1 3 -2 -1
vol= 2.383738E+03
boundary 3
global
unit 999
cuboid 1
3.680460E+01 -3.680460E+01 3.680460E+01
-3.680460E+01 8.166200E+01 -8.166200E+01
array 8 1
place 1 1 1 -3.68046E+01 -3.68046E+01 -8.16620E+01
cylinder 2
7.620000E+01 8.166200E+01 -8.166200E+01
origin x= 0.000000E+00 y= 0.000000E+00
media 1 1 2 -1
vol= 8.396215E+05
hole 15 origin x= 0.000000E+00 y= -4.334764E+01 z= 0.000000E+00
hole 16 origin x= 0.000000E+00 y= -5.398008E+01 z= 0.000000E+00
hole 17 origin x= 0.000000E+00 y= -6.215888E+01 z= 0.000000E+00
hole 18 origin x= -4.334764E+01 y= 0.000000E+00 z= 0.000000E+00
hole 19 origin x= -5.398008E+01 y= 0.000000E+00 z= 0.000000E+00
hole 20 origin x= -6.215888E+01 y= 0.000000E+00 z= 0.000000E+00
hole 15 origin x= 0.000000E+00 y= 4.334764E+01 z= 0.000000E+00
hole 16 origin x= 0.000000E+00 y= 5.398008E+01 z= 0.000000E+00
hole 17 origin x= 0.000000E+00 y= 6.215888E+01 z= 0.000000E+00
hole 18 origin x= 4.334764E+01 y= 0.000000E+00 z= 0.000000E+00
hole 19 origin x= 5.398008E+01 y= 0.000000E+00 z= 0.000000E+00
hole 20 origin x= 6.215888E+01 y= 0.000000E+00 z= 0.000000E+00
boundary 2

```



```

end geometry
read array
ara=1 nux=15 nuy=15 nuz=1 fill
1 1 1 1 1 1 1 1 1 1 1 1 1 1 1
1 1 1 1 2 4 2 1 2 4 2 1 1 1 1
1 1 2 4 5 8 4 1 4 8 5 4 2 1 1
1 1 4 8 5 4 2 1 2 4 5 8 4 1 1
1 2 5 5 3 4 2 1 2 4 3 5 5 2 1
1 4 8 4 4 8 4 1 4 8 4 4 8 4 1
1 2 4 2 2 4 3 4 3 4 2 2 4 2 1
1 1 1 1 1 1 4 8 4 1 1 1 1 1 1
1 2 4 2 2 4 3 4 3 4 2 2 4 2 1
1 4 8 4 4 8 4 1 4 8 4 4 8 4 1
1 2 5 5 3 4 2 1 2 4 3 5 5 2 1
1 1 4 8 5 4 2 1 2 4 5 8 4 1 1
1 1 2 4 5 8 4 1 4 8 5 4 2 1 1
1 1 1 1 2 4 2 1 2 4 2 1 1 1 1
1 1 1 1 1 1 1 1 1 1 1 1 1 1 1
end fill
ara=2 nux=61 nuy=8 nuz=1 fill 26 59r24 25 22 59r1 21 5q61 28 59r23 27
end fill
ara=3 nux=41 nuy=5 nuz=1 fill 26 39r24 25 22 39r1 21 2q41 28 39r23 27
end fill
ara=4 nux=21 nuy=5 nuz=1 fill 26 19r24 25 22 19r1 21 2q21 28 19r23 27
end fill
ara=5 nux=8 nuy=45 nuz=1 fill 26 6r24 25 22 6r1 21 42q8 28 6r23 27
end fill
ara=6 nux=5 nuy=41 nuz=1 fill 26 3r24 25 22 3r1 21 38q5 28 3r23 27
end fill
ara=7 nux=5 nuy=21 nuz=1 fill 26 3r24 25 22 3r1 21 18q5 28 3r23 27
end fill
ara=8 nux=3 nuy=3 nuz=1 fill f14 end fill
end array
read definitions
  gridGeometry 1
    xlinear 340 -85 85
    ylinear 340 -85 85
    zlinear 340 -85 85
  end gridGeometry

```

```

location 1
    position 0.001 0 0
end location
response 1
    specialDose=9029
end response
distribution 1
    special="wattSpectrum" parameters 1 3 end
end distribution
end definitions
read sources
    src 1
        strength=1.0
        neutrons
        sphere 0.0
        edistributionid=1
    end src
end sources
read importanceMap
    gridGeometryid=1
    adjointSource 1
        locationID=1
        responseID=1
    end adjointSource
    mmsubcells=2
end importanceMap
end data
end

```

Appendix B

Detailed Higher Order Derivations

B.1 Third Central Moment

Continuing from second order work via Eq. 4.7, multiply by $[r_m - E(r_m)]$

$$\begin{aligned}
& [r_k - E(r_k)][r_l - E(r_l)][r_m - E(r_m)] = \\
& \sum_{i_1, i_2, i_3=1}^{N_\alpha} \frac{\partial r_k}{\partial \alpha_{i_1}} \frac{\partial r_l}{\partial \alpha_{i_2}} \frac{\partial r_m}{\partial \alpha_{i_3}} \Big|_{\alpha^0} \delta \alpha_{i_1} \delta \alpha_{i_2} \delta \alpha_{i_3} \\
& + \frac{1}{2} \sum_{i_1, i_2, i_3, i_4=1}^{N_\alpha} \frac{\partial r_k}{\partial \alpha_{i_1}} \frac{\partial r_l}{\partial \alpha_{i_2}} \frac{\partial^2 r_m}{\partial \alpha_{i_3} \partial \alpha_{i_4}} \Big|_{\alpha^0} \delta \alpha_{i_1} \delta \alpha_{i_2} \delta \alpha_{i_3} \delta \alpha_{i_4} \\
& - \frac{1}{2} \sum_{i_1, i_2, i_3, i_4=1}^{N_\alpha} \frac{\partial r_k}{\partial \alpha_{i_1}} \frac{\partial r_l}{\partial \alpha_{i_2}} \frac{\partial^2 r_m}{\partial \alpha_{i_3} \partial \alpha_{i_4}} \Big|_{\alpha^0} \delta \alpha_{i_1} \delta \alpha_{i_2} \text{cov}(\alpha_{i_3}, \alpha_{i_4}) \\
& + \frac{1}{2} \sum_{i_1, i_2, i_3, i_4=1}^{N_\alpha} \frac{\partial r_k}{\partial \alpha_{i_1}} \frac{\partial^2 r_l}{\partial \alpha_{i_2} \partial \alpha_{i_3}} \frac{\partial r_m}{\partial \alpha_{i_4}} \Big|_{\alpha^0} \delta \alpha_{i_1} \delta \alpha_{i_2} \delta \alpha_{i_3} \delta \alpha_{i_4} \\
& + \frac{1}{4} \sum_{i_1, i_2, i_3, i_4, i_5=1}^{N_\alpha} \frac{\partial r_k}{\partial \alpha_{i_1}} \frac{\partial^2 r_l}{\partial \alpha_{i_2} \partial \alpha_{i_3}} \frac{\partial^2 r_m}{\partial \alpha_{i_4} \partial \alpha_{i_5}} \Big|_{\alpha^0} \delta \alpha_{i_1} \delta \alpha_{i_2} \delta \alpha_{i_3} \delta \alpha_{i_4} \delta \alpha_{i_5} \\
& - \frac{1}{4} \sum_{i_1, i_2, i_3, i_4, i_5=1}^{N_\alpha} \frac{\partial r_k}{\partial \alpha_{i_1}} \frac{\partial^2 r_l}{\partial \alpha_{i_2} \partial \alpha_{i_3}} \frac{\partial^2 r_m}{\partial \alpha_{i_4} \partial \alpha_{i_5}} \Big|_{\alpha^0} \delta \alpha_{i_1} \delta \alpha_{i_2} \delta \alpha_{i_3} \text{cov}(\alpha_{i_4}, \alpha_{i_5})
\end{aligned}$$

$$\begin{aligned}
& -\frac{1}{4} \sum_{i_1, i_2, i_3, i_4, i_5=1}^{N_\alpha} \frac{\partial^2 r_k}{\partial \alpha_{i_1} \partial \alpha_{i_2}} \frac{\partial^2 r_l}{\partial \alpha_{i_3} \partial \alpha_{i_4}} \frac{\partial r_m}{\partial \alpha_{i_5}} \Big|_{\alpha^0} \delta \alpha_{i_1} \delta \alpha_{i_2} \text{cov}(\alpha_{i_3}, \alpha_{i_4}) \delta \alpha_{i_5} \\
& -\frac{1}{8} \sum_{i_1, i_2, i_3, i_4, i_5, i_6=1}^{N_\alpha} \frac{\partial^2 r_k}{\partial \alpha_{i_1} \partial \alpha_{i_2}} \frac{\partial^2 r_l}{\partial \alpha_{i_3} \partial \alpha_{i_4}} \frac{\partial^2 r_m}{\partial \alpha_{i_5} \partial \alpha_{i_6}} \Big|_{\alpha^0} \delta \alpha_{i_1} \delta \alpha_{i_2} \text{cov}(\alpha_{i_3}, \alpha_{i_4}) \delta \alpha_{i_5} \delta \alpha_{i_6} \\
& +\frac{1}{8} \sum_{i_1, i_2, i_3, i_4, i_5, i_6=1}^{N_\alpha} \frac{\partial^2 r_k}{\partial \alpha_{i_1} \partial \alpha_{i_2}} \frac{\partial^2 r_l}{\partial \alpha_{i_3} \partial \alpha_{i_4}} \frac{\partial^2 r_m}{\partial \alpha_{i_5} \partial \alpha_{i_6}} \Big|_{\alpha^0} \delta \alpha_{i_1} \delta \alpha_{i_2} \text{cov}(\alpha_{i_3}, \alpha_{i_4}) \text{cov}(\alpha_{i_5}, \alpha_{i_6}) \\
& -\frac{1}{4} \sum_{i_1, i_2, i_3, i_4, i_5=1}^{N_\alpha} \frac{\partial^2 r_k}{\partial \alpha_{i_1} \partial \alpha_{i_2}} \frac{\partial^2 r_l}{\partial \alpha_{i_3} \partial \alpha_{i_4}} \frac{\partial r_m}{\partial \alpha_{i_5}} \Big|_{\alpha^0} \text{cov}(\alpha_{i_1}, \alpha_{i_2}) \delta \alpha_{i_3} \delta \alpha_{i_4} \delta \alpha_{i_5} \\
& -\frac{1}{8} \sum_{i_1, i_2, i_3, i_4, i_5, i_6=1}^{N_\alpha} \frac{\partial^2 r_k}{\partial \alpha_{i_1} \partial \alpha_{i_2}} \frac{\partial^2 r_l}{\partial \alpha_{i_3} \partial \alpha_{i_4}} \frac{\partial^2 r_m}{\partial \alpha_{i_5} \partial \alpha_{i_6}} \Big|_{\alpha^0} \text{cov}(\alpha_{i_1}, \alpha_{i_2}) \delta \alpha_{i_3} \delta \alpha_{i_4} \delta \alpha_{i_5} \delta \alpha_{i_6} \\
& +\frac{1}{8} \sum_{i_1, i_2, i_3, i_4, i_5, i_6=1}^{N_\alpha} \frac{\partial^2 r_k}{\partial \alpha_{i_1} \partial \alpha_{i_2}} \frac{\partial^2 r_l}{\partial \alpha_{i_3} \partial \alpha_{i_4}} \frac{\partial^2 r_m}{\partial \alpha_{i_5} \partial \alpha_{i_6}} \Big|_{\alpha^0} \text{cov}(\alpha_{i_1}, \alpha_{i_2}) \delta \alpha_{i_3} \delta \alpha_{i_4} \text{cov}(\alpha_{i_5}, \alpha_{i_6}) \\
& +\frac{1}{4} \sum_{i_1, i_2, i_3, i_4, i_5=1}^{N_\alpha} \frac{\partial^2 r_k}{\partial \alpha_{i_1} \partial \alpha_{i_2}} \frac{\partial^2 r_l}{\partial \alpha_{i_3} \partial \alpha_{i_4}} \frac{\partial r_m}{\partial \alpha_{i_5}} \Big|_{\alpha^0} \text{cov}(\alpha_{i_1}, \alpha_{i_2}) \text{cov}(\alpha_{i_3}, \alpha_{i_4}) \delta \alpha_{i_5} \\
& +\frac{1}{8} \sum_{i_1, i_2, i_3, i_4, i_5, i_6=1}^{N_\alpha} \frac{\partial^2 r_k}{\partial \alpha_{i_1} \partial \alpha_{i_2}} \frac{\partial^2 r_l}{\partial \alpha_{i_3} \partial \alpha_{i_4}} \frac{\partial^2 r_m}{\partial \alpha_{i_5} \partial \alpha_{i_6}} \Big|_{\alpha^0} \text{cov}(\alpha_{i_1}, \alpha_{i_2}) \text{cov}(\alpha_{i_3}, \alpha_{i_4}) \delta \alpha_{i_5} \delta \alpha_{i_6} \\
& -\frac{1}{8} \sum_{i_1, i_2, i_3, i_4, i_5, i_6=1}^{N_\alpha} \frac{\partial^2 r_k}{\partial \alpha_{i_1} \partial \alpha_{i_2}} \frac{\partial^2 r_l}{\partial \alpha_{i_3} \partial \alpha_{i_4}} \frac{\partial^2 r_m}{\partial \alpha_{i_5} \partial \alpha_{i_6}} \Big|_{\alpha^0} \text{cov}(\alpha_{i_1}, \alpha_{i_2}) \text{cov}(\alpha_{i_3}, \alpha_{i_4}) \text{cov}(\alpha_{i_5}, \alpha_{i_6}).
\end{aligned}$$

Note that the sums have been consolidated into one symbol even though they still represent up to six independent sums. Next, each of the 27 terms may be multiplied by the unknown probability distribution $p(\boldsymbol{\alpha}, \mathbf{r})$, integrated over all input parameter space and all constants factored out of the integrands. For convenience, the two following definitions will be used to simplify notation

$$\mu_{1,1,1}(\alpha_{i_1}, \alpha_{i_2}, \alpha_{i_3}) \equiv \int_{D_\alpha} \delta \alpha_{i_1} \delta \alpha_{i_2} \delta \alpha_{i_3} p(\boldsymbol{\alpha}, \mathbf{r}) d\boldsymbol{\alpha} \quad (\text{B.1})$$

$$\mu_{1,1,1,1}(\alpha_{i_1}, \alpha_{i_2}, \alpha_{i_3}, \alpha_{i_4}) \equiv \int_{D_{\alpha}} \delta\alpha_{i_1} \delta\alpha_{i_2} \delta\alpha_{i_3} \delta\alpha_{i_4} p(\alpha, \mathbf{r}) d\alpha \quad (\text{B.2})$$

Fifth and sixth order moments will arise once the integration is carried out. Any term that is higher than fourth order is set to zero.

$$\begin{aligned} & E([r_k - E(r_k)][r_l - E(r_l)][r_m - E(r_m)]) = \\ & \sum_{i_1, i_2, i_3=1}^{N_{\alpha}} \frac{\partial r_k}{\partial \alpha_{i_1}} \frac{\partial r_l}{\partial \alpha_{i_2}} \frac{\partial r_m}{\partial \alpha_{i_3}} \Big|_{\alpha^0} \mu_{1,1,1}(\alpha_{i_1}, \alpha_{i_2}, \alpha_{i_3}) \\ & + \frac{1}{2} \sum_{i_1, i_2, i_3, i_4=1}^{N_{\alpha}} \frac{\partial r_k}{\partial \alpha_{i_1}} \frac{\partial r_l}{\partial \alpha_{i_2}} \frac{\partial^2 r_m}{\partial \alpha_{i_3} \partial \alpha_{i_4}} \Big|_{\alpha^0} \mu_{1,1,1,1}(\alpha_{i_1}, \alpha_{i_2}, \alpha_{i_3}, \alpha_{i_4}) \\ & - \frac{1}{2} \sum_{i_1, i_2, i_3, i_4=1}^{N_{\alpha}} \frac{\partial r_k}{\partial \alpha_{i_1}} \frac{\partial r_l}{\partial \alpha_{i_2}} \frac{\partial^2 r_m}{\partial \alpha_{i_3} \partial \alpha_{i_4}} \Big|_{\alpha^0} \text{cov}(\alpha_{i_1}, \alpha_{i_2}) \text{cov}(\alpha_{i_3}, \alpha_{i_4}) \\ & + \frac{1}{2} \sum_{i_1, i_2, i_3, i_4=1}^{N_{\alpha}} \frac{\partial r_k}{\partial \alpha_{i_1}} \frac{\partial^2 r_l}{\partial \alpha_{i_2} \partial \alpha_{i_3}} \frac{\partial r_m}{\partial \alpha_{i_4}} \Big|_{\alpha^0} \mu_{1,1,1,1}(\alpha_{i_1}, \alpha_{i_2}, \alpha_{i_3}, \alpha_{i_4}) \\ & + 0 \\ & - \frac{1}{4} \sum_{i_1, i_2, i_3, i_4, i_5=1}^{N_{\alpha}} \frac{\partial r_k}{\partial \alpha_{i_1}} \frac{\partial^2 r_l}{\partial \alpha_{i_2} \partial \alpha_{i_3}} \frac{\partial^2 r_m}{\partial \alpha_{i_4} \partial \alpha_{i_5}} \Big|_{\alpha^0} \mu_{1,1,1}(\alpha_{i_1}, \alpha_{i_2}, \alpha_{i_3}) \text{cov}(\alpha_{i_4}, \alpha_{i_5}) \\ & - \frac{1}{2} \sum_{i_1, i_2, i_3, i_4=1}^{N_{\alpha}} \frac{\partial r_k}{\partial \alpha_{i_1}} \frac{\partial^2 r_l}{\partial \alpha_{i_2} \partial \alpha_{i_3}} \frac{\partial r_m}{\partial \alpha_{i_4}} \Big|_{\alpha^0} \text{cov}(\alpha_{i_1}, \alpha_{i_4}) \text{cov}(\alpha_{i_2}, \alpha_{i_3}) \\ & - \frac{1}{4} \sum_{i_1, i_2, i_3, i_4, i_5=1}^{N_{\alpha}} \frac{\partial r_k}{\partial \alpha_{i_1}} \frac{\partial^2 r_l}{\partial \alpha_{i_2} \partial \alpha_{i_3}} \frac{\partial^2 r_m}{\partial \alpha_{i_4} \partial \alpha_{i_5}} \Big|_{\alpha^0} \mu_{1,1,1}(\alpha_{i_1}, \alpha_{i_4}, \alpha_{i_5}) \text{cov}(\alpha_{i_2}, \alpha_{i_3}) \\ & + 0 \end{aligned}$$

$$\begin{aligned}
& + \frac{1}{2} \sum_{i_1, i_2, i_3, i_4=1}^{N_\alpha} \frac{\partial r_l}{\partial \alpha_{i_1}} \frac{\partial^2 r_k}{\partial \alpha_{i_2} \partial \alpha_{i_3}} \frac{\partial r_m}{\partial \alpha_{i_4}} \Big|_{\alpha^0} \mu_{1,1,1,1}(\alpha_{i_1}, \alpha_{i_2}, \alpha_{i_3}, \alpha_{i_4}) \\
& + 0 \\
& - \frac{1}{4} \sum_{i_1, i_2, i_3, i_4, i_5=1}^{N_\alpha} \frac{\partial r_l}{\partial \alpha_{i_1}} \frac{\partial^2 r_k}{\partial \alpha_{i_2} \partial \alpha_{i_3}} \frac{\partial^2 r_m}{\partial \alpha_{i_4} \partial \alpha_{i_5}} \Big|_{\alpha^0} \mu_{1,1,1}(\alpha_{i_1}, \alpha_{i_2}, \alpha_{i_3}) \text{cov}(\alpha_{i_4}, \alpha_{i_5}) \\
& - \frac{1}{2} \sum_{i_1, i_2, i_3, i_4=1}^{N_\alpha} \frac{\partial r_l}{\partial \alpha_{i_1}} \frac{\partial^2 r_k}{\partial \alpha_{i_2} \partial \alpha_{i_3}} \frac{\partial r_m}{\partial \alpha_{i_4}} \Big|_{\alpha^0} \text{cov}(\alpha_{i_1}, \alpha_{i_4}) \text{cov}(\alpha_{i_2}, \alpha_{i_3}) \\
& - \frac{1}{4} \sum_{i_1, i_2, i_3, i_4, i_5=1}^{N_\alpha} \frac{\partial r_l}{\partial \alpha_{i_1}} \frac{\partial^2 r_k}{\partial \alpha_{i_2} \partial \alpha_{i_3}} \frac{\partial^2 r_m}{\partial \alpha_{i_4} \partial \alpha_{i_5}} \Big|_{\alpha^0} \mu_{1,1,1}(\alpha_{i_1}, \alpha_{i_4}, \alpha_{i_5}) \text{cov}(\alpha_{i_2}, \alpha_{i_3}) \\
& + 0 \\
& + 0 \\
& - \frac{1}{8} \sum_{i_1, i_2, i_3, i_4, i_5, i_6=1}^{N_\alpha} \frac{\partial^2 r_k}{\partial \alpha_{i_1} \partial \alpha_{i_2}} \frac{\partial^2 r_l}{\partial \alpha_{i_3} \partial \alpha_{i_4}} \frac{\partial^2 r_m}{\partial \alpha_{i_5} \partial \alpha_{i_6}} \Big|_{\alpha^0} \mu_{1,1,1,1}(\alpha_{i_1}, \alpha_{i_2}, \alpha_{i_3}, \alpha_{i_4}) \text{cov}(\alpha_{i_5}, \alpha_{i_6}) \\
& - \frac{1}{4} \sum_{i_1, i_2, i_3, i_4, i_5=1}^{N_\alpha} \frac{\partial^2 r_k}{\partial \alpha_{i_1} \partial \alpha_{i_2}} \frac{\partial^2 r_l}{\partial \alpha_{i_3} \partial \alpha_{i_4}} \frac{\partial r_m}{\partial \alpha_{i_5}} \Big|_{\alpha^0} \mu_{1,1,1}(\alpha_{i_1}, \alpha_{i_2}, \alpha_{i_5}) \text{cov}(\alpha_{i_3}, \alpha_{i_4}) \\
& - \frac{1}{8} \sum_{i_1, i_2, i_3, i_4, i_5, i_6=1}^{N_\alpha} \frac{\partial^2 r_k}{\partial \alpha_{i_1} \partial \alpha_{i_2}} \frac{\partial^2 r_l}{\partial \alpha_{i_3} \partial \alpha_{i_4}} \frac{\partial^2 r_m}{\partial \alpha_{i_5} \partial \alpha_{i_6}} \Big|_{\alpha^0} \mu_{1,1,1,1}(\alpha_{i_1}, \alpha_{i_2}, \alpha_{i_5}, \alpha_{i_6}) \text{cov}(\alpha_{i_3}, \alpha_{i_4}) \\
& + \frac{1}{8} \sum_{i_1, i_2, i_3, i_4, i_5, i_6=1}^{N_\alpha} \frac{\partial^2 r_k}{\partial \alpha_{i_1} \partial \alpha_{i_2}} \frac{\partial^2 r_l}{\partial \alpha_{i_3} \partial \alpha_{i_4}} \frac{\partial^2 r_m}{\partial \alpha_{i_5} \partial \alpha_{i_6}} \Big|_{\alpha^0} \text{cov}(\alpha_{i_1}, \alpha_{i_2}) \text{cov}(\alpha_{i_3}, \alpha_{i_4}) \text{cov}(\alpha_{i_5}, \alpha_{i_6})
\end{aligned}$$

$$\begin{aligned}
& -\frac{1}{4} \sum_{i_1, i_2, i_3, i_4, i_5=1}^{N_\alpha} \frac{\partial^2 r_k}{\partial \alpha_{i_1} \partial \alpha_{i_2}} \frac{\partial^2 r_l}{\partial \alpha_{i_3} \partial \alpha_{i_4}} \frac{\partial r_m}{\partial \alpha_{i_5}} \Big|_{\alpha^0} \text{cov}(\alpha_{i_1}, \alpha_{i_2}) \mu_{1,1,1}(\alpha_{i_3}, \alpha_{i_4}, \alpha_{i_5}) \\
& -\frac{1}{8} \sum_{i_1, i_2, i_3, i_4, i_5, i_6=1}^{N_\alpha} \frac{\partial^2 r_k}{\partial \alpha_{i_1} \partial \alpha_{i_2}} \frac{\partial^2 r_l}{\partial \alpha_{i_3} \partial \alpha_{i_4}} \frac{\partial^2 r_m}{\partial \alpha_{i_5} \partial \alpha_{i_6}} \Big|_{\alpha^0} \text{cov}(\alpha_{i_1}, \alpha_{i_2}) \mu_{1,1,1,1}(\alpha_{i_3}, \alpha_{i_4}, \alpha_{i_5}, \alpha_{i_6}) \\
& +\frac{1}{8} \sum_{i_1, i_2, i_3, i_4, i_5, i_6=1}^{N_\alpha} \frac{\partial^2 r_k}{\partial \alpha_{i_1} \partial \alpha_{i_2}} \frac{\partial^2 r_l}{\partial \alpha_{i_3} \partial \alpha_{i_4}} \frac{\partial^2 r_m}{\partial \alpha_{i_5} \partial \alpha_{i_6}} \Big|_{\alpha^0} \text{cov}(\alpha_{i_1}, \alpha_{i_2}) \text{cov}(\alpha_{i_3}, \alpha_{i_4}) \text{cov}(\alpha_{i_5}, \alpha_{i_6}) \\
& +0 \\
& +\frac{1}{8} \sum_{i_1, i_2, i_3, i_4, i_5, i_6=1}^{N_\alpha} \frac{\partial^2 r_k}{\partial \alpha_{i_1} \partial \alpha_{i_2}} \frac{\partial^2 r_l}{\partial \alpha_{i_3} \partial \alpha_{i_4}} \frac{\partial^2 r_m}{\partial \alpha_{i_5} \partial \alpha_{i_6}} \Big|_{\alpha^0} \text{cov}(\alpha_{i_1}, \alpha_{i_2}) \text{cov}(\alpha_{i_3}, \alpha_{i_4}) \text{cov}(\alpha_{i_5}, \alpha_{i_6}) \\
& -\frac{1}{8} \sum_{i_1, i_2, i_3, i_4, i_5, i_6=1}^{N_\alpha} \frac{\partial^2 r_k}{\partial \alpha_{i_1} \partial \alpha_{i_2}} \frac{\partial^2 r_l}{\partial \alpha_{i_3} \partial \alpha_{i_4}} \frac{\partial^2 r_m}{\partial \alpha_{i_5} \partial \alpha_{i_6}} \Big|_{\alpha^0} \text{cov}(\alpha_{i_1}, \alpha_{i_2}) \text{cov}(\alpha_{i_3}, \alpha_{i_4}) \text{cov}(\alpha_{i_5}, \alpha_{i_6}).
\end{aligned}$$

Collect on highest order common terms

$$\begin{aligned}
& E([r_k - E(r_k)][r_l - E(r_l)][r_m - E(r_m)]) = \\
& +\frac{1}{2} \sum_{i_1, i_2, i_3, i_4=1}^{N_\alpha} \frac{\partial r_k}{\partial \alpha_{i_1}} \frac{\partial r_l}{\partial \alpha_{i_2}} \frac{\partial^2 r_m}{\partial \alpha_{i_3} \partial \alpha_{i_4}} \Big|_{\alpha^0} \mu_{1,1,1,1}(\alpha_{i_1}, \alpha_{i_2}, \alpha_{i_3}, \alpha_{i_4}) \\
& +\frac{1}{2} \sum_{i_1, i_2, i_3, i_4=1}^{N_\alpha} \frac{\partial r_k}{\partial \alpha_{i_1}} \frac{\partial^2 r_l}{\partial \alpha_{i_2} \partial \alpha_{i_3}} \frac{\partial r_m}{\partial \alpha_{i_4}} \Big|_{\alpha^0} \mu_{1,1,1,1}(\alpha_{i_1}, \alpha_{i_2}, \alpha_{i_3}, \alpha_{i_4}) \\
& +\frac{1}{2} \sum_{i_1, i_2, i_3, i_4=1}^{N_\alpha} \frac{\partial r_l}{\partial \alpha_{i_1}} \frac{\partial^2 r_k}{\partial \alpha_{i_2} \partial \alpha_{i_3}} \frac{\partial r_m}{\partial \alpha_{i_4}} \Big|_{\alpha^0} \mu_{1,1,1,1}(\alpha_{i_1}, \alpha_{i_2}, \alpha_{i_3}, \alpha_{i_4})
\end{aligned}$$

$$\begin{aligned}
& -\frac{1}{8} \sum_{i_1, i_2, i_3, i_4, i_5, i_6=1}^{N_\alpha} \frac{\partial^2 r_k}{\partial \alpha_{i_1} \partial \alpha_{i_2}} \frac{\partial^2 r_l}{\partial \alpha_{i_3} \partial \alpha_{i_4}} \frac{\partial^2 r_m}{\partial \alpha_{i_5} \partial \alpha_{i_6}} \Big|_{\alpha^0} \mu_{1,1,1,1}(\alpha_{i_1}, \alpha_{i_2}, \alpha_{i_3}, \alpha_{i_4}) \text{cov}(\alpha_{i_5}, \alpha_{i_6}) \\
& -\frac{1}{8} \sum_{i_1, i_2, i_3, i_4, i_5, i_6=1}^{N_\alpha} \frac{\partial^2 r_k}{\partial \alpha_{i_1} \partial \alpha_{i_2}} \frac{\partial^2 r_l}{\partial \alpha_{i_3} \partial \alpha_{i_4}} \frac{\partial^2 r_m}{\partial \alpha_{i_5} \partial \alpha_{i_6}} \Big|_{\alpha^0} \mu_{1,1,1,1}(\alpha_{i_1}, \alpha_{i_2}, \alpha_{i_5}, \alpha_{i_6}) \text{cov}(\alpha_{i_3}, \alpha_{i_4}) \\
& -\frac{1}{8} \sum_{i_1, i_2, i_3, i_4, i_5, i_6=1}^{N_\alpha} \frac{\partial^2 r_k}{\partial \alpha_{i_1} \partial \alpha_{i_2}} \frac{\partial^2 r_l}{\partial \alpha_{i_3} \partial \alpha_{i_4}} \frac{\partial^2 r_m}{\partial \alpha_{i_5} \partial \alpha_{i_6}} \Big|_{\alpha^0} \mu_{1,1,1,1}(\alpha_{i_3}, \alpha_{i_4}, \alpha_{i_5}, \alpha_{i_6}) \text{cov}(\alpha_{i_1}, \alpha_{i_2}) \\
& + \sum_{i_1, i_2, i_3=1}^{N_\alpha} \frac{\partial r_k}{\partial \alpha_{i_1}} \frac{\partial r_l}{\partial \alpha_{i_2}} \frac{\partial r_m}{\partial \alpha_{i_3}} \Big|_{\alpha^0} \mu_{1,1,1}(\alpha_{i_1}, \alpha_{i_2}, \alpha_{i_3})
\end{aligned}$$

$$\begin{aligned}
& -\frac{1}{4} \sum_{i_1, i_2, i_3, i_4, i_5=1}^{N_\alpha} \frac{\partial r_k}{\partial \alpha_{i_1}} \frac{\partial^2 r_l}{\partial \alpha_{i_2} \partial \alpha_{i_3}} \frac{\partial^2 r_m}{\partial \alpha_{i_4} \partial \alpha_{i_5}} \Big|_{\alpha^0} \mu_{1,1,1}(\alpha_{i_1}, \alpha_{i_4}, \alpha_{i_5}) \text{cov}(\alpha_{i_2}, \alpha_{i_3}) \\
& -\frac{1}{4} \sum_{i_1, i_2, i_3, i_4, i_5=1}^{N_\alpha} \frac{\partial r_k}{\partial \alpha_{i_1}} \frac{\partial^2 r_l}{\partial \alpha_{i_2} \partial \alpha_{i_3}} \frac{\partial^2 r_m}{\partial \alpha_{i_4} \partial \alpha_{i_5}} \Big|_{\alpha^0} \mu_{1,1,1}(\alpha_{i_1}, \alpha_{i_2}, \alpha_{i_3}) \text{cov}(\alpha_{i_4}, \alpha_{i_5}) \\
& -\frac{1}{4} \sum_{i_1, i_2, i_3, i_4, i_5=1}^{N_\alpha} \frac{\partial r_l}{\partial \alpha_{i_1}} \frac{\partial^2 r_k}{\partial \alpha_{i_2} \partial \alpha_{i_3}} \frac{\partial^2 r_m}{\partial \alpha_{i_4} \partial \alpha_{i_5}} \Big|_{\alpha^0} \mu_{1,1,1}(\alpha_{i_1}, \alpha_{i_2}, \alpha_{i_3}) \text{cov}(\alpha_{i_4}, \alpha_{i_5}) \\
& -\frac{1}{4} \sum_{i_1, i_2, i_3, i_4, i_5=1}^{N_\alpha} \frac{\partial r_l}{\partial \alpha_{i_1}} \frac{\partial^2 r_k}{\partial \alpha_{i_2} \partial \alpha_{i_3}} \frac{\partial^2 r_m}{\partial \alpha_{i_4} \partial \alpha_{i_5}} \Big|_{\alpha^0} \mu_{1,1,1}(\alpha_{i_1}, \alpha_{i_4}, \alpha_{i_5}) \text{cov}(\alpha_{i_2}, \alpha_{i_3}) \\
& -\frac{1}{4} \sum_{i_1, i_2, i_3, i_4, i_5=1}^{N_\alpha} \frac{\partial^2 r_k}{\partial \alpha_{i_1} \partial \alpha_{i_2}} \frac{\partial^2 r_l}{\partial \alpha_{i_3} \partial \alpha_{i_4}} \frac{\partial r_m}{\partial \alpha_{i_5}} \Big|_{\alpha^0} \mu_{1,1,1}(\alpha_{i_1}, \alpha_{i_2}, \alpha_{i_5}) \text{cov}(\alpha_{i_3}, \alpha_{i_4}) \\
& -\frac{1}{4} \sum_{i_1, i_2, i_3, i_4, i_5=1}^{N_\alpha} \frac{\partial^2 r_k}{\partial \alpha_{i_1} \partial \alpha_{i_2}} \frac{\partial^2 r_l}{\partial \alpha_{i_3} \partial \alpha_{i_4}} \frac{\partial r_m}{\partial \alpha_{i_5}} \Big|_{\alpha^0} \mu_{1,1,1}(\alpha_{i_3}, \alpha_{i_4}, \alpha_{i_5}) \text{cov}(\alpha_{i_1}, \alpha_{i_2})
\end{aligned}$$

$$\begin{aligned}
& -\frac{1}{2} \sum_{i_1, i_2, i_3, i_4=1}^{N_\alpha} \frac{\partial r_k}{\partial \alpha_{i_1}} \frac{\partial^2 r_l}{\partial \alpha_{i_2} \partial \alpha_{i_3}} \frac{\partial r_m}{\partial \alpha_{i_4}} \Big|_{\alpha^0} \text{cov}(\alpha_{i_1}, \alpha_{i_4}) \text{cov}(\alpha_{i_2}, \alpha_{i_3}) \\
& -\frac{1}{2} \sum_{i_1, i_2, i_3, i_4=1}^{N_\alpha} \frac{\partial r_k}{\partial \alpha_{i_1}} \frac{\partial r_l}{\partial \alpha_{i_2}} \frac{\partial^2 r_m}{\partial \alpha_{i_3} \partial \alpha_{i_4}} \Big|_{\alpha^0} \text{cov}(\alpha_{i_1}, \alpha_{i_2}) \text{cov}(\alpha_{i_3}, \alpha_{i_4}) \\
& -\frac{1}{2} \sum_{i_1, i_2, i_3, i_4=1}^{N_\alpha} \frac{\partial r_l}{\partial \alpha_{i_1}} \frac{\partial^2 r_k}{\partial \alpha_{i_2} \partial \alpha_{i_3}} \frac{\partial r_m}{\partial \alpha_{i_4}} \Big|_{\alpha^0} \text{cov}(\alpha_{i_1}, \alpha_{i_4}) \text{cov}(\alpha_{i_2}, \alpha_{i_3}) \\
& +\frac{1}{8} \sum_{i_1, i_2, i_3, i_4, i_5, i_6=1}^{N_\alpha} \frac{\partial^2 r_k}{\partial \alpha_{i_1} \partial \alpha_{i_2}} \frac{\partial^2 r_l}{\partial \alpha_{i_3} \partial \alpha_{i_4}} \frac{\partial^2 r_m}{\partial \alpha_{i_5} \partial \alpha_{i_6}} \Big|_{\alpha^0} \text{cov}(\alpha_{i_1}, \alpha_{i_2}) \text{cov}(\alpha_{i_3}, \alpha_{i_4}) \text{cov}(\alpha_{i_5}, \alpha_{i_6}) \\
& +\frac{1}{8} \sum_{i_1, i_2, i_3, i_4, i_5, i_6=1}^{N_\alpha} \frac{\partial^2 r_k}{\partial \alpha_{i_1} \partial \alpha_{i_2}} \frac{\partial^2 r_l}{\partial \alpha_{i_3} \partial \alpha_{i_4}} \frac{\partial^2 r_m}{\partial \alpha_{i_5} \partial \alpha_{i_6}} \Big|_{\alpha^0} \text{cov}(\alpha_{i_1}, \alpha_{i_2}) \text{cov}(\alpha_{i_3}, \alpha_{i_4}) \text{cov}(\alpha_{i_5}, \alpha_{i_6}) \\
& +\frac{1}{8} \sum_{i_1, i_2, i_3, i_4, i_5, i_6=1}^{N_\alpha} \frac{\partial^2 r_k}{\partial \alpha_{i_1} \partial \alpha_{i_2}} \frac{\partial^2 r_l}{\partial \alpha_{i_3} \partial \alpha_{i_4}} \frac{\partial^2 r_m}{\partial \alpha_{i_5} \partial \alpha_{i_6}} \Big|_{\alpha^0} \text{cov}(\alpha_{i_1}, \alpha_{i_2}) \text{cov}(\alpha_{i_3}, \alpha_{i_4}) \text{cov}(\alpha_{i_5}, \alpha_{i_6}) \\
& -\frac{1}{8} \sum_{i_1, i_2, i_3, i_4, i_5, i_6=1}^{N_\alpha} \frac{\partial^2 r_k}{\partial \alpha_{i_1} \partial \alpha_{i_2}} \frac{\partial^2 r_l}{\partial \alpha_{i_3} \partial \alpha_{i_4}} \frac{\partial^2 r_m}{\partial \alpha_{i_5} \partial \alpha_{i_6}} \Big|_{\alpha^0} \text{cov}(\alpha_{i_1}, \alpha_{i_2}) \text{cov}(\alpha_{i_3}, \alpha_{i_4}) \text{cov}(\alpha_{i_5}, \alpha_{i_6})
\end{aligned}$$

Neglecting parameter cross-correlations that are higher than second order *and* are multiplied by second order derivatives reduces all $\mu_{1,1,1}(\alpha_{i_1}, \alpha_{i_2}, \alpha_{i_3})$'s and $\mu_{1,1,1,1}(\alpha_{i_1}, \alpha_{i_2}, \alpha_{i_3}, \alpha_{i_4})$'s to simply third (unnormalized skewness) and fourth (unnormalized kurtosis) order central moments $\mu_3(\alpha_{i_1})$ and $\mu_4(\alpha_{i_1})$ except for one term; namely:

$$\sum_{i_1, i_2, i_3=1}^{N_\alpha} \frac{\partial r_k}{\partial \alpha_{i_1}} \frac{\partial r_l}{\partial \alpha_{i_2}} \frac{\partial r_m}{\partial \alpha_{i_3}} \Big|_{\alpha^0} \mu_{1,1,1}(\alpha_{i_1}, \alpha_{i_2}, \alpha_{i_3}). \quad (\text{B.3})$$

In this term, there are non-negligible cases when indices match, for example, $\alpha_{i_1} = \alpha_{i_2}$. For $\mu_{1,1,1}(\alpha_{i_1}, \alpha_{i_2}, \alpha_{i_3})$, this gives the following possibilities:

$$\mu_{1,1,1}(\alpha_{i_1}, \alpha_{i_2}, \alpha_{i_3}) \rightarrow \begin{cases} \mu_{1,1,1}(\alpha_{i_1}, \alpha_{i_2}, \alpha_{i_3}) & \text{when no indices match,} \\ \mu_{2,1}(\alpha_{i_1}, \alpha_{i_2}) & \text{when any two indices match,} \\ \mu_3(\alpha_{i_1}) & \text{when all three indices match.} \end{cases} \quad (\text{B.4})$$

Splitting the summation into two distinct pieces for $\mu_3(\alpha_{i_1})$ and everything else yields

$$\sum_{i_1, i_2, i_3=1}^{N_\alpha} \frac{\partial r_k}{\partial \alpha_{i_1}} \frac{\partial r_l}{\partial \alpha_{i_2}} \frac{\partial r_m}{\partial \alpha_{i_3}} \Big|_{\alpha^0} \mu_{1,1,1}(\alpha_{i_1}, \alpha_{i_2}, \alpha_{i_3}) = \sum_{i_1=1}^{N_\alpha} \frac{\partial r_k}{\partial \alpha_{i_1}} \frac{\partial r_l}{\partial \alpha_{i_1}} \frac{\partial r_m}{\partial \alpha_{i_1}} \Big|_{\alpha^0} \mu_3(\alpha_{i_1}) + \sum_{\substack{i_1, i_2, i_3=1 \\ i_1 \neq i_2 \neq i_3}}^{N_\alpha} \frac{\partial r_k}{\partial \alpha_{i_1}} \frac{\partial r_l}{\partial \alpha_{i_2}} \frac{\partial r_m}{\partial \alpha_{i_3}} \Big|_{\alpha^0} \mu_{1,1,1}(\alpha_{i_1}, \alpha_{i_2}, \alpha_{i_3}). \quad (\text{B.5})$$

Now, setting $r_k = r_l = r_m$ and suppressing the “evaluated at α^0 ” notation gives

$$\begin{aligned}
& E([r_k - E(r_k)]^3) = \\
& + \frac{3}{2} \sum_{i_1=1}^{N_\alpha} \left(\frac{\partial r_k}{\partial \alpha_{i_1}} \right)^2 \left(\frac{\partial^2 r_k}{\partial \alpha_{i_1}^2} \right) \mu_4(\alpha_{i_1}) \\
& - \frac{3}{8} \sum_{i_1, i_2, i_3=1}^{N_\alpha} \left(\frac{\partial^2 r_k}{\partial \alpha_{i_1}^2} \right) \left(\frac{\partial^2 r_k}{\partial \alpha_{i_2} \partial \alpha_{i_3}} \right) \mu_4(\alpha_{i_1}) \text{cov}(\alpha_{i_2}, \alpha_{i_3}) \\
& + \sum_{i_1=1}^{N_\alpha} \left(\frac{\partial r_k}{\partial \alpha_{i_1}} \right)^3 \mu_3(\alpha_{i_1}) \\
& + \sum_{\substack{i_1, i_2, i_3=1 \\ i_1 \neq i_2 \neq i_3}}^{N_\alpha} \left(\frac{\partial r_k}{\partial \alpha_{i_1}} \right) \left(\frac{\partial r_k}{\partial \alpha_{i_2}} \right) \left(\frac{\partial r_k}{\partial \alpha_{i_3}} \right) \mu_{1,1,1}(\alpha_{i_1}, \alpha_{i_2}, \alpha_{i_3}) \\
& - \frac{3}{2} \sum_{i_1, i_2, i_3=1}^{N_\alpha} \left(\frac{\partial r_k}{\partial \alpha_{i_1}} \right) \left(\frac{\partial^2 r_k}{\partial \alpha_{i_1}^2} \right) \left(\frac{\partial^2 r_k}{\partial \alpha_{i_2} \partial \alpha_{i_3}} \right) \mu_3(\alpha_{i_1}) \text{cov}(\alpha_{i_2}, \alpha_{i_3}) \\
& - \frac{3}{2} \sum_{i_1, i_2, i_3, i_4=1}^{N_\alpha} \left(\frac{\partial r_k}{\partial \alpha_{i_1}} \right) \left(\frac{\partial^2 r_k}{\partial \alpha_{i_2} \partial \alpha_{i_3}} \right) \left(\frac{\partial r_k}{\partial \alpha_{i_4}} \right) \text{cov}(\alpha_{i_1}, \alpha_{i_4}) \text{cov}(\alpha_{i_2}, \alpha_{i_3}) \\
& + \frac{1}{4} \left(\sum_{i_1, i_2=1}^{N_\alpha} \left(\frac{\partial^2 r_k}{\partial \alpha_{i_1} \partial \alpha_{i_2}} \right) \text{cov}(\alpha_{i_1}, \alpha_{i_2}) \right)^3. \tag{B.6}
\end{aligned}$$

Lastly, factor like terms to give the third order central moment

$$\begin{aligned}
E([r_k - E(r_k)]^3) = & \\
& \frac{1}{2} \sum_{i_1=1}^{N_\alpha} \left(\frac{\partial^2 r_k}{\partial \alpha_{i_1}^2} \right) \mu_4(\alpha_{i_1}) \left[3 \left(\frac{\partial r_k}{\partial \alpha_{i_1}} \right)^2 - \frac{3}{4} \left(\frac{\partial^2 r_k}{\partial \alpha_{i_1}^2} \right) \sum_{i_2, i_3=1}^{N_\alpha} \left(\frac{\partial^2 r_k}{\partial \alpha_{i_2} \partial \alpha_{i_3}} \right) \text{cov}(\alpha_{i_2}, \alpha_{i_3}) \right] \\
& + \sum_{i_1=1}^{N_\alpha} \left(\frac{\partial r_k}{\partial \alpha_{i_1}} \right) \mu_3(\alpha_{i_1}) \left[\left(\frac{\partial r_k}{\partial \alpha_{i_1}} \right)^2 - \frac{3}{2} \left(\frac{\partial^2 r_k}{\partial \alpha_{i_1}^2} \right) \sum_{i_2, i_3=1}^{N_\alpha} \left(\frac{\partial^2 r_k}{\partial \alpha_{i_2} \partial \alpha_{i_3}} \right) \text{cov}(\alpha_{i_2}, \alpha_{i_3}) \right] \\
& + \sum_{\substack{i_1, i_2, i_3=1 \\ i_1 \neq i_2 \neq i_3}}^{N_\alpha} \left(\frac{\partial r_k}{\partial \alpha_{i_1}} \right) \left(\frac{\partial r_k}{\partial \alpha_{i_2}} \right) \left(\frac{\partial r_k}{\partial \alpha_{i_3}} \right) \mu_{1,1,1}(\alpha_{i_1}, \alpha_{i_2}, \alpha_{i_3}) \\
& - \frac{3}{2} \left[\sum_{i_1, i_2=1}^{N_\alpha} \left(\frac{\partial r_k}{\partial \alpha_{i_1}} \right) \left(\frac{\partial r_k}{\partial \alpha_{i_2}} \right) \Big|_{\alpha^0} \text{cov}(\alpha_{i_1}, \alpha_{i_2}) \right] \left[\sum_{i_3, i_4=1}^{N_\alpha} \left(\frac{\partial^2 r_k}{\partial \alpha_{i_3} \partial \alpha_{i_4}} \right) \text{cov}(\alpha_{i_3}, \alpha_{i_4}) \right] \\
& + \frac{1}{4} \left(\sum_{i_1, i_2=1}^{N_\alpha} \left(\frac{\partial^2 r_k}{\partial \alpha_{i_1} \partial \alpha_{i_2}} \right) \text{cov}(\alpha_{i_1}, \alpha_{i_2}) \right)^3. \tag{B.7}
\end{aligned}$$

$$\begin{aligned}
& -\frac{1}{8} \sum_{i_1, i_2, i_3, i_4, i_5, i_6, i_7=1}^{N_\alpha} \frac{\partial^2 r_k}{\partial \alpha_{i_1} \partial \alpha_{i_2}} \frac{\partial^2 r_l}{\partial \alpha_{i_3} \partial \alpha_{i_4}} \frac{\partial r_m}{\partial \alpha_{i_5}} \frac{\partial^2 r_n}{\partial \alpha_{i_6} \partial \alpha_{i_7}} \Big|_{\alpha^0} \text{cov}(\alpha_{i_1}, \alpha_{i_2}) \text{cov}(\alpha_{i_3}, \alpha_{i_4}) \delta \alpha_{i_5} \text{cov}(\alpha_{i_6}, \alpha_{i_7}) \\
& -\frac{1}{16} \sum_{\substack{i_1, i_2, i_3, i_4 \\ i_5, i_6, i_7, i_8=1}}^{N_\alpha} \frac{\partial^2 r_k}{\partial \alpha_{i_1} \partial \alpha_{i_2}} \frac{\partial^2 r_l}{\partial \alpha_{i_3} \partial \alpha_{i_4}} \frac{\partial^2 r_m}{\partial \alpha_{i_5} \partial \alpha_{i_6}} \frac{\partial^2 r_n}{\partial \alpha_{i_7} \partial \alpha_{i_8}} \Big|_{\alpha^0} \text{cov}(\alpha_{i_1}, \alpha_{i_2}) \text{cov}(\alpha_{i_3}, \alpha_{i_4}) \delta \alpha_{i_5} \delta \alpha_{i_6} \text{cov}(\alpha_{i_7}, \alpha_{i_8}) \\
& +\frac{1}{16} \sum_{\substack{i_1, i_2, i_3, i_4=1 \\ i_5, i_6, i_7, i_8}}^{N_\alpha} \frac{\partial^2 r_k}{\partial \alpha_{i_1} \partial \alpha_{i_2}} \frac{\partial^2 r_l}{\partial \alpha_{i_3} \partial \alpha_{i_4}} \frac{\partial^2 r_m}{\partial \alpha_{i_5} \partial \alpha_{i_6}} \frac{\partial^2 r_n}{\partial \alpha_{i_7} \partial \alpha_{i_8}} \Big|_{\alpha^0} \text{cov}(\alpha_{i_1}, \alpha_{i_2}) \text{cov}(\alpha_{i_3}, \alpha_{i_4}) \text{cov}(\alpha_{i_5}, \alpha_{i_6}) \text{cov}(\alpha_{i_7}, \alpha_{i_8})
\end{aligned}$$

Next, each of the 81 terms may be multiplied by the unknown probability distribution $p(\boldsymbol{\alpha}, \boldsymbol{r})$, integrated over all input parameter space and all constants factored out of the integrands. Fifth, sixth, seventh and eighth order moments will arise once the integration is carried out. Any term that is higher than fourth order is set to zero.

$$\begin{aligned}
& E([r_k - E(r_k)][r_l - E(r_l)][r_m - E(r_m)][r_n - E(r_n)]) = \\
& \sum_{i_1, i_2, i_3, i_4=1}^{N_\alpha} \frac{\partial r_k}{\partial \alpha_{i_1}} \frac{\partial r_l}{\partial \alpha_{i_2}} \frac{\partial r_m}{\partial \alpha_{i_3}} \frac{\partial r_n}{\partial \alpha_{i_4}} \Big|_{\alpha^0} \mu_{1,1,1,1}(\alpha_{i_1}, \alpha_{i_2}, \alpha_{i_3}, \alpha_{i_4}) \\
& +0 \\
& -\frac{1}{2} \sum_{i_1, i_2, i_3, i_4, i_5=1}^{N_\alpha} \frac{\partial r_k}{\partial \alpha_{i_1}} \frac{\partial r_l}{\partial \alpha_{i_2}} \frac{\partial^2 r_m}{\partial \alpha_{i_3} \partial \alpha_{i_4}} \frac{\partial r_n}{\partial \alpha_{i_5}} \Big|_{\alpha^0} \mu_{1,1,1}(\alpha_{i_1}, \alpha_{i_2}, \alpha_{i_5}) \text{cov}(\alpha_{i_3}, \alpha_{i_4}) \\
& +0 \\
& +0 \\
& -\frac{1}{4} \sum_{i_1, i_2, i_3, i_4, i_5, i_6=1}^{N_\alpha} \frac{\partial r_k}{\partial \alpha_{i_1}} \frac{\partial^2 r_l}{\partial \alpha_{i_2} \partial \alpha_{i_3}} \frac{\partial^2 r_m}{\partial \alpha_{i_4} \partial \alpha_{i_5}} \frac{\partial r_n}{\partial \alpha_{i_6}} \Big|_{\alpha^0} \mu_{1,1,1,1}(\alpha_{i_1}, \alpha_{i_2}, \alpha_{i_3}, \alpha_{i_6}) \text{cov}(\alpha_{i_4}, \alpha_{i_5}) \\
& -\frac{1}{2} \sum_{i_1, i_2, i_3, i_4, i_5=1}^{N_\alpha} \frac{\partial r_k}{\partial \alpha_{i_1}} \frac{\partial^2 r_l}{\partial \alpha_{i_2} \partial \alpha_{i_3}} \frac{\partial r_m}{\partial \alpha_{i_4}} \frac{\partial r_n}{\partial \alpha_{i_5}} \Big|_{\alpha^0} \mu_{1,1,1}(\alpha_{i_1}, \alpha_{i_4}, \alpha_{i_5}) \text{cov}(\alpha_{i_2}, \alpha_{i_3}) \\
& -\frac{1}{4} \sum_{i_1, i_2, i_3, i_4, i_5, i_6=1}^{N_\alpha} \frac{\partial r_k}{\partial \alpha_{i_1}} \frac{\partial^2 r_l}{\partial \alpha_{i_2} \partial \alpha_{i_3}} \frac{\partial^2 r_m}{\partial \alpha_{i_4} \partial \alpha_{i_5}} \frac{\partial r_n}{\partial \alpha_{i_6}} \Big|_{\alpha^0} \mu_{1,1,1,1}(\alpha_{i_1}, \alpha_{i_4}, \alpha_{i_5}, \alpha_{i_6}) \text{cov}(\alpha_{i_2}, \alpha_{i_3}) \\
& +\frac{1}{4} \sum_{i_1, i_2, i_3, i_4, i_5, i_6=1}^{N_\alpha} \frac{\partial r_k}{\partial \alpha_{i_1}} \frac{\partial^2 r_l}{\partial \alpha_{i_2} \partial \alpha_{i_3}} \frac{\partial^2 r_m}{\partial \alpha_{i_4} \partial \alpha_{i_5}} \frac{\partial r_n}{\partial \alpha_{i_6}} \Big|_{\alpha^0} \text{cov}(\alpha_{i_1}, \alpha_{i_6}) \text{cov}(\alpha_{i_2}, \alpha_{i_3}) \text{cov}(\alpha_{i_4}, \alpha_{i_5})
\end{aligned}$$

+0

+0

$$-\frac{1}{4} \sum_{i_1, i_2, i_3, i_4, i_5, i_6=1}^{N_\alpha} \frac{\partial r_k}{\partial \alpha_{i_1}} \frac{\partial r_l}{\partial \alpha_{i_2}} \frac{\partial^2 r_m}{\partial \alpha_{i_3} \partial \alpha_{i_4}} \frac{\partial^2 r_n}{\partial \alpha_{i_5} \partial \alpha_{i_6}} \Big|_{\alpha^0} \mu_{1,1,1,1}(\alpha_{i_1}, \alpha_{i_2}, \alpha_{i_5}, \alpha_{i_6}) \text{cov}(\alpha_{i_3}, \alpha_{i_4})$$

+0

+0

-0

$$-\frac{1}{4} \sum_{i_1, i_2, i_3, i_4, i_5, i_6=1}^{N_\alpha} \frac{\partial r_k}{\partial \alpha_{i_1}} \frac{\partial^2 r_l}{\partial \alpha_{i_2} \partial \alpha_{i_3}} \frac{\partial r_m}{\partial \alpha_{i_4}} \frac{\partial^2 r_n}{\partial \alpha_{i_5} \partial \alpha_{i_6}} \Big|_{\alpha^0} \mu_{1,1,1,1}(\alpha_{i_1}, \alpha_{i_4}, \alpha_{i_5}, \alpha_{i_6}) \text{cov}(\alpha_{i_2}, \alpha_{i_3})$$

-0

$$+\frac{1}{8} \sum_{i_1, i_2, i_3, i_4, i_5, i_6, i_7=1}^{N_\alpha} \frac{\partial r_k}{\partial \alpha_{i_1}} \frac{\partial^2 r_l}{\partial \alpha_{i_2} \partial \alpha_{i_3}} \frac{\partial^2 r_m}{\partial \alpha_{i_4} \partial \alpha_{i_5}} \frac{\partial^2 r_n}{\partial \alpha_{i_6} \partial \alpha_{i_7}} \Big|_{\alpha^0} \mu_{1,1,1}(\alpha_{i_1}, \alpha_{i_6}, \alpha_{i_7}) \text{cov}(\alpha_{i_2}, \alpha_{i_3}) \text{cov}(\alpha_{i_4}, \alpha_{i_5})$$

+0

+0

-0

$$-\frac{1}{4} \sum_{i_1, i_2, i_3, i_4, i_5, i_6=1}^{N_\alpha} \frac{\partial r_l}{\partial \alpha_{i_1}} \frac{\partial^2 r_k}{\partial \alpha_{i_2} \partial \alpha_{i_3}} \frac{\partial r_m}{\partial \alpha_{i_4}} \frac{\partial^2 r_n}{\partial \alpha_{i_5} \partial \alpha_{i_6}} \Big|_{\alpha^0} \mu_{1,1,1,1}(\alpha_{i_1}, \alpha_{i_4}, \alpha_{i_5}, \alpha_{i_6}) \text{cov}(\alpha_{i_2}, \alpha_{i_3})$$

-0

$$+\frac{1}{8} \sum_{i_1, i_2, i_3, i_4, i_5, i_6, i_7=1}^{N_\alpha} \frac{\partial r_l}{\partial \alpha_{i_1}} \frac{\partial^2 r_k}{\partial \alpha_{i_2} \partial \alpha_{i_3}} \frac{\partial^2 r_m}{\partial \alpha_{i_4} \partial \alpha_{i_5}} \frac{\partial^2 r_n}{\partial \alpha_{i_6} \partial \alpha_{i_7}} \Big|_{\alpha^0} \mu_{1,1,1}(\alpha_{i_1}, \alpha_{i_6}, \alpha_{i_7}) \text{cov}(\alpha_{i_2}, \alpha_{i_3}) \text{cov}(\alpha_{i_4}, \alpha_{i_5})$$

+0

+0

-0

$$\begin{aligned}
& + \frac{1}{8} \sum_{\substack{i_1, i_2, i_3, i_4, i_5, i_6, i_7=1 \\ N_\alpha}} \frac{\partial^2 r_k}{\partial \alpha_{i_1} \partial \alpha_{i_2}} \frac{\partial^2 r_l}{\partial \alpha_{i_3} \partial \alpha_{i_4}} \frac{\partial r_m}{\partial \alpha_{i_5}} \frac{\partial^2 r_n}{\partial \alpha_{i_6} \partial \alpha_{i_7}} \Big|_{\alpha^0} \text{cov}(\alpha_{i_1}, \alpha_{i_2}) \mu_{1,1,1}(\alpha_{i_3}, \alpha_{i_4}, \alpha_{i_5}) \text{cov}(\alpha_{i_6}, \alpha_{i_7}) \\
& + \frac{1}{16} \sum_{\substack{i_1, i_2, i_3, i_4 \\ i_5, i_6, i_7, i_8=1 \\ N_\alpha}} \frac{\partial^2 r_k}{\partial \alpha_{i_1} \partial \alpha_{i_2}} \frac{\partial^2 r_l}{\partial \alpha_{i_3} \partial \alpha_{i_4}} \frac{\partial^2 r_m}{\partial \alpha_{i_5} \partial \alpha_{i_6}} \frac{\partial^2 r_n}{\partial \alpha_{i_7} \partial \alpha_{i_8}} \Big|_{\alpha^0} \text{cov}(\alpha_{i_1}, \alpha_{i_2}) \mu_{1,1,1,1}(\alpha_{i_3}, \alpha_{i_4}, \alpha_{i_5}, \alpha_{i_6}) \text{cov}(\alpha_{i_7}, \alpha_{i_8}) \\
& - \frac{1}{16} \sum_{\substack{i_1, i_2, i_3, i_4=1 \\ i_5, i_6, i_7, i_8 \\ N_\alpha}} \frac{\partial^2 r_k}{\partial \alpha_{i_1} \partial \alpha_{i_2}} \frac{\partial^2 r_l}{\partial \alpha_{i_3} \partial \alpha_{i_4}} \frac{\partial^2 r_m}{\partial \alpha_{i_5} \partial \alpha_{i_6}} \frac{\partial^2 r_n}{\partial \alpha_{i_7} \partial \alpha_{i_8}} \Big|_{\alpha^0} \text{cov}(\alpha_{i_1}, \alpha_{i_2}) \text{cov}(\alpha_{i_3}, \alpha_{i_4}) \text{cov}(\alpha_{i_5}, \alpha_{i_6}) \text{cov}(\alpha_{i_7}, \alpha_{i_8}) \\
& - 0 \\
& - \frac{1}{16} \sum_{\substack{i_1, i_2, i_3, i_4=1 \\ i_5, i_6, i_7, i_8 \\ N_\alpha}} \frac{\partial^2 r_k}{\partial \alpha_{i_1} \partial \alpha_{i_2}} \frac{\partial^2 r_l}{\partial \alpha_{i_3} \partial \alpha_{i_4}} \frac{\partial^2 r_m}{\partial \alpha_{i_5} \partial \alpha_{i_6}} \frac{\partial^2 r_n}{\partial \alpha_{i_7} \partial \alpha_{i_8}} \Big|_{\alpha^0} \text{cov}(\alpha_{i_1}, \alpha_{i_2}) \text{cov}(\alpha_{i_3}, \alpha_{i_4}) \text{cov}(\alpha_{i_5}, \alpha_{i_6}) \text{cov}(\alpha_{i_7}, \alpha_{i_8}) \\
& + \frac{1}{16} \sum_{\substack{i_1, i_2, i_3, i_4=1 \\ i_5, i_6, i_7, i_8 \\ N_\alpha}} \frac{\partial^2 r_k}{\partial \alpha_{i_1} \partial \alpha_{i_2}} \frac{\partial^2 r_l}{\partial \alpha_{i_3} \partial \alpha_{i_4}} \frac{\partial^2 r_m}{\partial \alpha_{i_5} \partial \alpha_{i_6}} \frac{\partial^2 r_n}{\partial \alpha_{i_7} \partial \alpha_{i_8}} \Big|_{\alpha^0} \text{cov}(\alpha_{i_1}, \alpha_{i_2}) \text{cov}(\alpha_{i_3}, \alpha_{i_4}) \text{cov}(\alpha_{i_5}, \alpha_{i_6}) \text{cov}(\alpha_{i_7}, \alpha_{i_8})
\end{aligned}$$

Collect on highest order common terms

$$\sum_{i_1, i_2, i_3, i_4=1}^{N_\alpha} \frac{\partial r_k}{\partial \alpha_{i_1}} \frac{\partial r_l}{\partial \alpha_{i_2}} \frac{\partial r_m}{\partial \alpha_{i_3}} \frac{\partial r_n}{\partial \alpha_{i_4}} \Big|_{\alpha^0} \mu_{1,1,1,1}(\alpha_{i_1}, \alpha_{i_2}, \alpha_{i_3}, \alpha_{i_4})$$

Neglecting parameter cross-correlations that are higher than second order *and* are multiplied by second order derivatives reduces all $\mu_{1,1,1}(\alpha_{i_1}, \alpha_{i_2}, \alpha_{i_3})$'s and $\mu_{1,1,1,1}(\alpha_{i_1}, \alpha_{i_2}, \alpha_{i_3}, \alpha_{i_4})$'s to simply third (unnormalized skewness) and fourth (unnormalized kurtosis) order central moments $\mu_3(\alpha_{i_1})$ and $\mu_4(\alpha_{i_1})$ except for one term; namely:

$$\sum_{i_1, i_2, i_3, i_4=1}^{N_\alpha} \left. \frac{\partial r_k}{\partial \alpha_{i_1}} \frac{\partial r_l}{\partial \alpha_{i_2}} \frac{\partial r_m}{\partial \alpha_{i_3}} \frac{\partial r_n}{\partial \alpha_{i_4}} \right|_{\alpha^0} \mu_{1,1,1,1}(\alpha_{i_1}, \alpha_{i_2}, \alpha_{i_3}, \alpha_{i_4}) \quad (\text{B.8})$$

In this term, there are non-negligible cases when indices match, for example, $\alpha_{i_1} = \alpha_{i_2} = \alpha_{i_4}$.

For $\mu_{1,1,1,1}(\alpha_{i_1}, \alpha_{i_2}, \alpha_{i_3}, \alpha_{i_4})$, this gives the following possibilities:

$$\mu_{1,1,1,1}(\alpha_{i_1}, \alpha_{i_2}, \alpha_{i_3}, \alpha_{i_4}) \rightarrow \begin{cases} \mu_{1,1,1,1}(\alpha_{i_1}, \alpha_{i_2}, \alpha_{i_3}, \alpha_{i_4}) & \text{when no indices match,} \\ \mu_{2,1,1}(\alpha_{i_1}, \alpha_{i_2}, \alpha_{i_3}) & \text{when any two indices match,} \\ \mu_{2,2}(\alpha_{i_1}, \alpha_{i_2}) & \text{when any two sets of two indices match,} \\ \mu_{3,1}(\alpha_{i_1}, \alpha_{i_2}) & \text{when any three indices match,} \\ \mu_4(\alpha_{i_1}) & \text{when all four indices match.} \end{cases} \quad (\text{B.9})$$

Splitting the summation into two distinct pieces for $\mu_4(\alpha_{i_1})$ and everything else yields

$$\begin{aligned} & \sum_{i_1, i_2, i_3, i_4=1}^{N_\alpha} \left. \frac{\partial r_k}{\partial \alpha_{i_1}} \frac{\partial r_l}{\partial \alpha_{i_2}} \frac{\partial r_m}{\partial \alpha_{i_3}} \frac{\partial r_n}{\partial \alpha_{i_4}} \right|_{\alpha^0} \mu_{1,1,1,1}(\alpha_{i_1}, \alpha_{i_2}, \alpha_{i_3}, \alpha_{i_4}) = \\ & \sum_{i_1=1}^{N_\alpha} \left. \frac{\partial r_k}{\partial \alpha_{i_1}} \frac{\partial r_l}{\partial \alpha_{i_1}} \frac{\partial r_m}{\partial \alpha_{i_1}} \frac{\partial r_n}{\partial \alpha_{i_1}} \right|_{\alpha^0} \mu_4(\alpha_{i_1}) + \\ & \sum_{\substack{i_1, i_2, i_3, i_4=1 \\ i_1 \neq i_2 \neq i_3 \neq i_4}}^{N_\alpha} \left. \frac{\partial r_k}{\partial \alpha_{i_1}} \frac{\partial r_l}{\partial \alpha_{i_2}} \frac{\partial r_m}{\partial \alpha_{i_3}} \frac{\partial r_n}{\partial \alpha_{i_4}} \right|_{\alpha^0} \mu_{1,1,1,1}(\alpha_{i_1}, \alpha_{i_2}, \alpha_{i_3}, \alpha_{i_4}). \end{aligned} \quad (\text{B.10})$$

Now, setting $r_k = r_l = r_m = r_n$ and suppressing the “evaluated at α^0 ” notation gives

$$\begin{aligned}
& E([r_k - E(r_k)]^4) = \\
& \sum_{i_1=1}^{N_\alpha} \left(\frac{\partial r_k}{\partial \alpha_{i_1}} \right)^4 \mu_4(\alpha_{i_1}) \\
& + \sum_{\substack{i_1, i_2, i_3, i_4=1 \\ i_1 \neq i_2 \neq i_3 \neq i_4}}^{N_\alpha} \left(\frac{\partial r_k}{\partial \alpha_{i_1}} \right) \left(\frac{\partial r_k}{\partial \alpha_{i_2}} \right) \left(\frac{\partial r_k}{\partial \alpha_{i_3}} \right) \left(\frac{\partial r_k}{\partial \alpha_{i_4}} \right) \mu_{1,1,1,1}(\alpha_{i_1}, \alpha_{i_2}, \alpha_{i_3}, \alpha_{i_4}) \\
& - 3 \sum_{i_1, i_2, i_3=1}^{N_\alpha} \left(\frac{\partial r_k}{\partial \alpha_{i_1}} \right)^2 \left(\frac{\partial^2 r_k}{\partial \alpha_{i_1}^2} \right) \left(\frac{\partial^2 r_k}{\partial \alpha_{i_2} \partial \alpha_{i_3}} \right) \mu_4(\alpha_{i_1}) \text{cov}(\alpha_{i_2}, \alpha_{i_3}) \\
& + \frac{3}{8} \sum_{i_1, i_2, i_3, i_4, i_5=1}^{N_\alpha} \left(\frac{\partial^2 r_k}{\partial \alpha_{i_1}^2} \right)^2 \left(\frac{\partial^2 r_k}{\partial \alpha_{i_2} \partial \alpha_{i_3}} \right) \left(\frac{\partial^2 r_k}{\partial \alpha_{i_4} \partial \alpha_{i_5}} \right) \mu_4(\alpha_{i_1}) \text{cov}(\alpha_{i_2}, \alpha_{i_3}) \text{cov}(\alpha_{i_4}, \alpha_{i_5}) \\
& - 2 \sum_{i_1, i_2, i_3=1}^{N_\alpha} \left(\frac{\partial r_k}{\partial \alpha_{i_1}} \right)^3 \left(\frac{\partial^2 r_k}{\partial \alpha_{i_2} \partial \alpha_{i_3}} \right) \mu_3(\alpha_{i_1}) \text{cov}(\alpha_{i_2}, \alpha_{i_3}) \\
& + \frac{3}{2} \sum_{i_1, i_2, i_3, i_4, i_5, i_6, i_7=1}^{N_\alpha} \left(\frac{\partial r_k}{\partial \alpha_{i_1}} \right) \left(\frac{\partial^2 r_k}{\partial \alpha_{i_1}^2} \right) \left(\frac{\partial^2 r_k}{\partial \alpha_{i_2} \partial \alpha_{i_3}} \right) \left(\frac{\partial^2 r_k}{\partial \alpha_{i_4} \partial \alpha_{i_5}} \right) \mu_3(\alpha_{i_1}) \text{cov}(\alpha_{i_2}, \alpha_{i_3}) \text{cov}(\alpha_{i_4}, \alpha_{i_5}) \\
& + \frac{3}{2} \sum_{i_1, i_2, i_3, i_4, i_5, i_6=1}^{N_\alpha} \left(\frac{\partial r_k}{\partial \alpha_{i_1}} \right) \left(\frac{\partial^2 r_k}{\partial \alpha_{i_2} \partial \alpha_{i_3}} \right) \left(\frac{\partial^2 r_k}{\partial \alpha_{i_4} \partial \alpha_{i_5}} \right) \left(\frac{\partial r_k}{\partial \alpha_{i_6}} \right) \text{cov}(\alpha_{i_1}, \alpha_{i_6}) \text{cov}(\alpha_{i_2}, \alpha_{i_3}) \text{cov}(\alpha_{i_4}, \alpha_{i_5}) \\
& - \frac{3}{16} \sum_{\substack{i_1, i_2, i_3, i_4=1 \\ i_5, i_6, i_7, i_8}}^{N_\alpha} \left(\frac{\partial^2 r_k}{\partial \alpha_{i_1} \partial \alpha_{i_2}} \right) \left(\frac{\partial^2 r_k}{\partial \alpha_{i_3} \partial \alpha_{i_4}} \right) \left(\frac{\partial^2 r_k}{\partial \alpha_{i_5} \partial \alpha_{i_6}} \right) \left(\frac{\partial^2 r_k}{\partial \alpha_{i_7} \partial \alpha_{i_8}} \right) \times \\
& \quad \text{cov}(\alpha_{i_1}, \alpha_{i_2}) \text{cov}(\alpha_{i_3}, \alpha_{i_4}) \text{cov}(\alpha_{i_5}, \alpha_{i_6}) \text{cov}(\alpha_{i_7}, \alpha_{i_8})
\end{aligned} \tag{B.11}$$

Lastly, factor like terms to give the fourth order central moment

$$\begin{aligned}
\mu_4(r_k) &= E([r_k - E(r_k)]^4) = \\
&\sum_{i_1=1}^{N_\alpha} \mu_4(\alpha_{i_1}) \left\{ \left(\frac{\partial r_k}{\partial \alpha_{i_1}} \right)^4 + \frac{3}{8} \left(\frac{\partial^2 r_k}{\partial \alpha_{i_1}^2} \right)^2 \left[\sum_{i_2, i_3=1}^{N_\alpha} \left(\frac{\partial^2 r_k}{\partial \alpha_{i_2} \partial \alpha_{i_3}} \right) \text{cov}(\alpha_{i_2}, \alpha_{i_3}) \right]^2 \right. \\
&\quad \left. - 3 \left(\frac{\partial r_k}{\partial \alpha_{i_1}} \right)^2 \left(\frac{\partial^2 r_k}{\partial \alpha_{i_1}^2} \right) \left[\sum_{i_2, i_3=1}^{N_\alpha} \left(\frac{\partial^2 r_k}{\partial \alpha_{i_2} \partial \alpha_{i_3}} \right) \text{cov}(\alpha_{i_2}, \alpha_{i_3}) \right] \right\} \\
&+ \sum_{\substack{i_1, i_2, i_3, i_4=1 \\ i_1 \neq i_2 \neq i_3 \neq i_4}}^{N_\alpha} \left(\frac{\partial r_k}{\partial \alpha_{i_1}} \right) \left(\frac{\partial r_k}{\partial \alpha_{i_2}} \right) \left(\frac{\partial r_k}{\partial \alpha_{i_3}} \right) \left(\frac{\partial r_k}{\partial \alpha_{i_4}} \right) \mu_{1,1,1,1}(\alpha_{i_1}, \alpha_{i_2}, \alpha_{i_3}, \alpha_{i_4}) \\
&+ \sum_{i_1=1}^{N_\alpha} \left(\frac{\partial r_k}{\partial \alpha_{i_1}} \right) \mu_3(\alpha_{i_1}) \left[\sum_{i_2, i_3=1}^{N_\alpha} \left(\frac{\partial^2 r_k}{\partial \alpha_{i_2} \partial \alpha_{i_3}} \right) \text{cov}(\alpha_{i_2}, \alpha_{i_3}) \right] \times \\
&\quad \left\{ \frac{3}{2} \left(\frac{\partial^2 r_k}{\partial \alpha_{i_1}^2} \right) \left[\sum_{i_2, i_3=1}^{N_\alpha} \left(\frac{\partial^2 r_k}{\partial \alpha_{i_2} \partial \alpha_{i_3}} \right) \text{cov}(\alpha_{i_2}, \alpha_{i_3}) \right] - 2 \left(\frac{\partial r_k}{\partial \alpha_{i_1}} \right)^2 \right\} \\
&+ \frac{3}{2} \left[\sum_{i_1, i_2=1}^{N_\alpha} \left(\frac{\partial r_k}{\partial \alpha_{i_1}} \right) \left(\frac{\partial r_k}{\partial \alpha_{i_2}} \right) \text{cov}(\alpha_{i_1}, \alpha_{i_2}) \right] \left[\sum_{i_3, i_4=1}^{N_\alpha} \left(\frac{\partial^2 r_k}{\partial \alpha_{i_3} \partial \alpha_{i_4}} \right) \text{cov}(\alpha_{i_3}, \alpha_{i_4}) \right]^2 \\
&- \frac{3}{16} \left[\sum_{i_1, i_2=1}^{N_\alpha} \left(\frac{\partial^2 r_k}{\partial \alpha_{i_1} \partial \alpha_{i_2}} \right) \text{cov}(\alpha_{i_1}, \alpha_{i_2}) \right]^4
\end{aligned}$$